Optimizing Drug Delivery: Characterization of DLin-KC2-DMA/Distearoylphosphatidylserine by ^{31}P and ^{2}H NMR Spectroscopy

by

Siyun (Linda) Wang

B.Sc., University of Lethbridge, 2011

Thesis Submitted in Partial Fulfillment of the
Requirements for the Degree of
Master of Science

in the
Department of Molecular Biology and Biochemistry
Faculty of Science

SIMON FRASER UNIVERSITY

Fall 2013

Approval

Name: **Siyun (Linda) Wang**

Degree: **Master of Science**

Title of Thesis: ***Optimizing Drug Delivery: Characterization of DLin-KC2-DMA/Distearoylphosphatiylserine by ^{31}P and ^{2}H NMR Spectroscopy***

Examining Committee: **Chair:** Esther Verheyen
Professor

Jenifer Thewalt
Senior Supervisor
Professor

Rosemary B. Cornell
Supervisor
Professor

Pieter R. Cullis
Supervisor
Professor
Department of Biochemistry
University of British Columbia

Martin Zuckermann
Internal Examiner
Adjunct/Professor
Department of Physics

Date Defended/Approved: December 10th, 2013

Partial Copyright License

Abstract

Lipid nanoparticles (LNPs) are used to deliver siRNA to hepatocytes via endocytosis and subsequent endosomal release. With 99% of the LNPs taken up by the cell via endocytosis, only 1% of the siRNA is actually released into the cell cytosol. To improve the effectiveness of LNPs association with and disruption of endosomal membranes, the biophysical properties of a model system composed of 1:1 molar ratio of anionic lipid 1,2-distearoyl(d70)-*sn*-glycero-3-[phospho-L-serine] (DSPS-d70) and the cationic lipid DLin-KC2-DMA are characterized by ^{2}H and ^{31}P NMR spectroscopy. The bilayer to inverted hexagonal (H_{II}) phase transition of the model system was shown to be influenced by temperature, pH and salt concentration. The order parameter profiles are obtained, revealing the extent of acyl chain movement of DSPS-d70 in bilayer and H_{II} phases. The results help provide insights into computational simulation and eventually optimized LNPs design.

Keywords: Lipid nanoparticles; drug delivery; inverted hexagonal (H_{II}); phase transition; ^{2}H NMR spectroscopy

To my parents, for your encouragement and support

Acknowledgements

I would like to thank my senior supervisor Dr. Jenifer Thewalt for introducing me to the lipid research field and providing me the precious opportunity to work on this lipid project combining molecular biology and biochemistry knowledge with spectroscopy methods. Your expertise in both MBB and Physics field guide me through this project. Thank you for creating a great working environment and your patience, wise and support.

I would like to thank Dr. Pieter R. Cullis for the initial planning of the project. Your expertise in the lipid field for therapeutic drug delivery has greatly inspired me. I appreciated the suggestions given after presentations and the valuable email input during the busy schedules. Thank you and the lab for designing and synthesizing the lipid DLin-KC2-DMA and giving us as a gift and allow me preparing samples in the lab.

I greatly appreciated Dr. Ismail M. Hafez for his help while I was at UBC. It was very kind of him sharing his lipid preparation protocol and the training on the sample preparation. Thank you for the valuable discussions and your ideas has always inspired me.

Thank you to my committee member Dr. Rosemary B. Cornell for teaching me the biomembrane course and share your expertise and knowledge in the lipid field. Thank you for your valuable discussions on the project in all the committee meetings throughout my graduate program.

Thank you to the Thewalt lab members Sherry Leung and Mehran Shaghaghi for the help they provided in the lab and valuable discussions at lab meetings.

Thank you to Dr. Martin Zuckermann for participating in the group meetings and discussions and updating us new paper in the field.

I would like to thank summer undergraduate NSERC student Jason Wang for helping on the salt concentration study and editing of the writings.

Thank you to Dr. Elana Brief for proof reading of the thesis.

I would like to thank our collaborator Dr. Peter D. Tieleman for purchasing the deuterated lipid and discussion on the project.

Thank you to NMR facility manager Dr. Andrew Lewis for guidance and help while I work on the ^{31}P NMR experiment.

Thanks to the Department of Molecular Biology and Biochemistry in Simon Fraser University for awarding me the graduate student fellowship.

Thank you to my parents Mingchun Zhang and Jing Wang for their love, encouragement and support. Thanks to my friends for your support and keep me enthusiastic while I am completing the project.

Table of Contents

Approval ii
Partial Copyright License iii
Abstract iv
Dedication v
Acknowledgements vi
Table of Contents viii
List of Figures xi
List of Equations xiii
List of Tables xiii
List of Acronyms xiv

Chapter 1. Introduction 1
1.1. Lipid Nanoparticles and Drug Delivery Systems 1
1.2. Liposomes 2
1.3. Liposome preparation techniques 3
1.3.1. Sonication 3
1.3.2. Extrusion 4
1.3.3. Active Drug Trapping Techniques: pH gradient 5
1.4. Microfluidics and LNP development 6
1.5. Current Model of the LNP and the Proposed Drug Delivery Mechanism 7
1.6. Lipid Polymorphism 11
1.6.1. Early shape theory 11
1.6.2. Lipid Phases 12
1.6.3. Lipid Phase Transitions of a Model Lipid System 13
1.6.4. Factors that Influence Lipid Phase Transitions 14
1.7. The Model Membrane Chosen for This Study 14
1.7.1. Anionic Lipid: PS 15
1.7.2. Cationic Lipid: XTC2 16
1.7.3. PS and XTC2 model membrane 18
1.7.4. Project Objective 18

Chapter 2. Nuclear Magnetic Resonance Theory and Its Application to Study Lipid Biomembranes 19
2.1. Introduction to Nuclear Magnetic Resonance (NMR) 19
2.1.1. Deuterium is a Quadrupole Nuclei has spin 1 20
2.1.2. Energy Levels and Zeeman Effect 20
2.2. Solid State ^{2}H NMR Spectrometer 21
2.2.1. The magnet 21
2.2.2. The probe 22
2.2.3. The Variable Temperature Unit (VTU), Frequency Synthesizer and Ref. Phase 23
2.2.4. The data collecting station 24
2.3. The NMR experiments 24

2.3.1. The two pulses sequence 24
2.3.1.2 The Hahn Echo 25
2.3.1.2 The Quadrupolar Echo 25
2.3.2. Data Acquiring-Signal Averaging 25
2.3.3. Free Induction Decay (FID) and data processing 26
2.4. Spectral Analysis and application in lipid membranes 26
2.4.1. Chemical shift anisotropy (CSA) in ^{31P} NMR spectroscopy 26
2.4.2. Typical ^{2}H NMR spectral patterns for L_{β}, L_{α}, H_{II} phase 27
2.4.3. Anisotropic motion in the lipid membranes 29
2.4.4. Repetition time 31

Chapter 3. Material and Methods 32
3.1. Materials 32
3.2. DSPS model membrane 33
3.2.1. DSPS model membrane for ^{31}P NMR experiment 33
3.2.2. DSPS-d70 model membrane for ^{2}H NMR experiment 34
DSPS testing solid phase 34
3.3. XTC2/DSPS model membrane 35
3.3.1. XTC2/DSPS model membrane for ^{31}P NMR experiment at pH 7.4 and 4.75 (For results shown in 5.1 and 5.6) 35
3.3.2. Preparation of XTC2/DSPS-d70 model membrane at pH 8.4 and 4.75 for ^{2}H NMR experiment 35
Preparation of XTC2/DSPS model membrane pH 4.75 containing different [Na^{+}] 36

Chapter 4. Results: DSPS in a Model Membrane 38
4.1. DSPS model membrane studied by ^{31}P NMR 38
4.2. DSPS-70 model membrane studied by ^{2}H NMR Spectroscopy 40
4.3. DSPS-d70 depaked Spectrum and Order Parameter Profile 44
4.4. Melting Behaviour of DSPS and DSPS-d70 membranes 47

Chapter 5. Results: XTC2/DSPS Model Membrane 49
5.1. At pH 8.4: Observe Gel to Liquid Crystalline Phase Transition 49
5.2. At pH 4.75: XTC2/DSPS model membrane undergoes a gel to H_{II} phase transition 58
5.2.1. ^{31}P NMR spectroscopy of XTC2/DSPS in pH 4.75 sodium acetate buffer undergo bilayer to H_{II} phase transition around 293K 58
5.2.2. Temperature dependence of ^{2}H NMR spectra of XTC2/DSPS-d70 at pH 4.75 in sodium acetate buffer 61
5.2.3. De-Paked spectrum for H_{II} phase 63
5.3. Discussion of the pH dependence of the XTC2/DSPS-d70 model system 67
5.4. The XTC2/DSPS-d70 model system has a T_{BH} which is sensitive to Salt Concentrations 69
5.4.1. The system at high salt, 1M Na^{+} 70

5.4.2. At medium salt concentration, 0.5M Na^+, the XTC2/DSPS-d70 has a lower T_{BH} than at 1M Na^+ 72
5.4.3. Comparison between XTC2/DSPS-d70 ^2H NMR spectra as a function of salt concentration reveals that salt stabilizes the gel phase 72
5.4.4. The existence of the H_{II} phase can be confirmed by examining the order parameter profile 74
5.4.5. M_1 allows us to compare the phase behaviour of XTC2/DSPS-d70 for three salt concentrations 76

Chapter 6. Summary and Future Work 79
6.1. Summary of the XTC2/DSPS model system's phase behaviour 79
6.1.1. The Gel/L_α, Gel/H_{II}, H_{II}/Isotropic phase transitions temperatures are pH and salt concentration sensitive 79
6.1.2. ^2H NMR reveals lipid chain packing information in L_a and H_{II} phase 81
6.1.3. Increasing salt concentration stabilized the gel phase of XTC2/DSPS-d70 84
6.2. Conclusion and Future Work 84

References 86

List of Figures

Figure 1.1. Structural illustrations of model membranes. 3

Figure 1.2. Illustration of extruded vesicle sizes using freeze-fracture EM. 4

Figure 1.3. Illustration of the pH gradient. 6

Figure 1.4. The microfluidics apparatus for making LNPs. 7

Figure 1.5. An illustration of LNP structure proposed 8

Figure 1.6. The current proposed LNP delivery mechanism. 10

Figure 1.7. The cross sectional images of four common lipid phases. 12

Figure 1.8. An ion pair model is formed by electrostatic interaction. 13

Figure 1.9. The effect of pH and salt concentration on DPPS T_m. 16

Figure 1.10. The chemical formula of the cationic lipid DLin-KC2-DMA. 17

Figure 1.11. The chemical formula of the cationic lipid DLin-MC3-DMA. 18

Figure 2.1. The energy levels of deuteron. 21

Figure 2.2. The OXFORD 300 magnet. 22

Figure 2.3. Parts of the probe 23

Figure 2.4. The Various Temperature Control Units (VTU). 24

Figure 2.5. Spin Echo sequence for ^{31}P NMR experiment 25

Figure 2.6. Quadrupolar echo pulse sequence for ^{2}H NMR experiments. 25

Figure 2.7. From NMR signal to NMR spectrum 26

Figure 2.8. DPPC-d31 in lamellar phase (L_α) and gel phase. 28

Figure 2.9. Literature ^{2}H NMR spectra for (a) bilayer (L_α) and (b) H_{II} phase. 29

Figure 2.10. An indication of molecular vector of a lipid chain. 30

Figure 2.11. The Pake doublet is a superposition of two spectra. 31

Figure 3.1. Structure of DSPS-d70. 32

Figure 3.2. Structure of DLin-KC2-DMA (neutral form). 33

Figure 3.3. Structure of DLin-KC2-DMA (cationic form). 33

Figure 4.1. ^{31}P NMR spectra of the DSPS as a function of temperature. 39
Figure 4.2. ^{2}H NMR spectra of DSPS-d70 as a function of temperature. 40
Figure 4.3. The gel to L_α phase transition of the DSPS-d70 membrane. 42
Figure 4.4. The average spectral width, M_1, for DSPS-d70. 43
Figure 4.5. The effect of thermal history. 44
Figure 4.6. ^{2}H NMR de-Paked spectrum for DSPS-d70 at 341.5K. 45
Figure 4.7. The order parameter S_{CD} for DSPS-d70 at 341.5K. 46
Figure 4.8. Deuteration effect on T_m of the PC and PS membrane. 48
Figure 5.1. ^{31}P NMR spectra of XTC2/DSPS membrane at pH 7.4. 52
Figure 5.2. ^{2}H NMR spectra of XTC2/DSPS-d70 pH 8.4 overview. 53
Figure 5.3. ^{2}H NMR spectra of XTC2/DSPS-d70 pH 8.4 every 10 degree. 54
Figure 5.4. M_1 plot for XTC2/DSPS-d70 in pH 8.4 HEPES buffer. 55
Figure 5.5. ^{2}H NMR spectra show XTC2/DSPS-d70 pH 8.4 gel to L_α transition. 57
Figure 5.6. ^{31}P NMR spectra of XTC2/DSPS pH 4.75 in 0.25 M NaOAc buffer. 60
Figure 5.7. ^{2}H NMR spectra of XTC2/DSPS-d70 pH 4.75 in 0.25M NaOAc. 62
Figure 5.8. ^{2}H NMR dePaked spectrum of DSPS-d70/XTC2 at 307K pH=4.75 63
Figure 5.9. S_{CD} for XTC2/DSPS-d70 at pH 4.75 at 307K. 64
Figure 5.10. M_1 plot for XTC2/DSPS-d70 at pH of 4.75. 65
Figure 5.11. The percentage gel calculated from equation 6 67
Figure 5.12. Comparison of XTC2/DSPS-d70 pH 8.4 and 4.75 spectra shape. 68
Figure 5.13. ^{2}H NMR spectra of XTC2/DSPS-d70 pH 4.75 with 1M NaCl. 70
Figure 5.14. ^{2}H spectra of XTC2/DSPS-d70 with 1M NaCl salt 310-320K. 71
Figure 5.15. ^{2}H NMR spectra of the XTC2/DSPS-d70 pH 4.75 with 0.5 M NaCl. 72
Figure 5.16. Comparison of XTC2/DSPS-d70 at 0.25M NaOAc and 1M NaCl. 73
Figure 5.17. De-Paked spectrum of XTC2/DSPS-d70 with 1M Na^+ at 312K. 74
Figure 5.18. S_{CD} obtained from XTC2/DSPS-d70 at 312K pH 4.75 with 1M Na^+. 75
Figure 5.19. M_1 comparison for XTC2/DSPS-d70 at different [Na^+]. 77
Figure 5.20. Proposed mechanism for higher T_{BH} at higher [Na^+]. 78

Figure 6.1. M_1 comparisons for DSPS, XTC2/DSPS-d70 without and with salt. 80
Figure 6.2. Spectral shape comparison for lamellar phase and H_{II} phase. 82
Figure 6.3 Comparison of experimental and simulated S_{CD} results. 83

List of Equations

1. Residual CSA 27
2. Area under the Curve 27
3. Average Spectral Width 27
4. Order Parameter Profile S_{CD} 29
5. Quadrupolar Splitting 30
6. Percentage Gel 66

List of Tables

Table 3.1. The M_0 and M_1 for DSPS-d70 at 298K with different reptimes. 35
Table 4.1. S_{CD} for DSPS-d70 at 341.5K. 46
Table 4.2. Effect of deuteration on PC and PS. 47
Table 5.1. S_{CD} for XTC2/DSPS-d70 pH 4.75 at 307K. 64
Table 5.2. Fraction of the gel phase in the XTC2/DSPS-d70 pH 4.75. 66
Table 5.3. S_{CD} for DSPS-d70/XTC2 pH 4.75 with 1M NaCl at 312K. 74
Table 6.1. Summary of T_m and T_{BH} obtained from ^{31}P and ^{2}H NMR results. 81

List of Acronyms

ddw	deuterium depleted water
DMPC	1,2-dimyristoyl-*sn*-glycero-3-phosphocholine
DMPS	1,2-dimyristoyl-*sn*-glycero-3-phospho-L-serine
DPPC	1,2-dipalmitoyl-*sn*-glycero-3-phosphocholine
DPPS	1,2-dipalmitoyl-*sn*-glycero-3-phospho-L-serine
DSPC	1,2-distearoyl-*sn*-glycero-3-phosphocholine
DSPS	1,2-distearoyl-*sn*-glycero-3-phospho-L-serine
DSPS-d70	1,2-distearoyl-(d70)-*sn*-glycero-3-phospho-L-serine
HEPES	4-(2-hydroxyethyl)-1-piperazineethanesulfonic acid
LNP	Lipid Nanoparticles
NMR	Nuclear Magnetic Resonance
XTC2	DLin-KC2-DMA

Chapter 1. Introduction

1.1. Lipid Nanoparticles and Drug Delivery Systems

The efficacy of treatment for diseases, such as cancer therapy, typically relies upon not only the effectiveness of the pharmaceutical drug administered but also its controlled release to the targeted cells. Once the drug has entered the bloodstream, it needs to be transported to its intracellular destination without degrading during its delivery process. This delivery process must also have a low toxicity to the organism. Although certain drugs have the capacity to circulate in the blood, most drugs require an alternate transport method. To circumvent this problem, therapeutic drugs can be encapsulated in a drug delivery vehicle to be sustained in circulation and later released at the disease site (Mahato, 2012)

Many approaches have been used to design these drug delivery vehicles using bio-compatible molecules such as lipids to envelop the drug in a vesicle-like system. These drug carriers include liposomes, micelles, microspheres, and nanoparticles (Mahato, 2012). A revolutionary development for drug delivery in medicine was the innovation of lipid nanoparticles (LNPs). In particular, LNPs have proven successful in delivering small interfering ribonucleic acid (siRNA) through the bloodstream to the disease site (Semple et al., 2010). LNPs can then enable a controlled release of the siRNA into the target cells, followed by participation of the siRNA in the RNA interference (RNAi) pathway to silence the desired gene. This resolves the problem that the siRNA have anionic charges and high molecular weight, therefore they cannot diffuse passively through the biological membrane (Jayaraman et al., 2012). Moreover, the short siRNA circulation time makes packing into a compatible carrier essential to enhance its efficacy. Nonetheless, gene therapy using LNPs has already proven its effectiveness in human clinical trials. For example, Alnylam is developing a product targeting the proprotein convertase subtilisin/kexin type 9 which results in lowering LDL-C in circulation for the treatment of familial hypercholesterolemia(Tam et al., 2013).

Due to the limited understanding of lipid nanoparticles, a considerable amount of research is needed to improve the rational design of the LNPs. This chapter will focus on the development of LNPs beginning with the history of liposomes, methods of liposome formations, mechanisms of action of modern LNPs, current understandings of their applications, and contributions of this research project.

1.2. Liposomes

Bangham et al (1965) first identified and characterized swollen phospholipid systems (Bangham et al., 1965). A visitor to the Bangham lab, Gerald Weissmann, proposed the term “liposomes”, defined as the microscopic vesicles composed of one or more lipid bilayers (Sessa & Weissmann, 1968). The lipid bilayer membrane is composed of amphipathic phospholipids which consist of a hydrophilic head group that contains a phosphate group and a hydrophobic region that typically contains two hydrocarbon fatty acid chains. In the presence of excess water, the hydrophilic head group orients towards the aqueous solution while the hydrophobic tails are oriented away from the aqueous solution, composing the interior of the lipid bilayer membrane. This amphiphilic nature of the phospholipids enables a liposome to envelop an aqueous compartment with its lipid bilayer. This led Gregory Gregoriadis to establish the notion of employing liposomes for drug delivery systems only a short time after the discovery of liposomes (Gregoriadis & Ryman, 1971). Poste and Papahadjopoulos (1976) showed that the unilamellar and multilamellar vesicles can enter cells by fusion and endocytosis. (Poste & Papahadjopoulos, 1976). These unilamellar and multilamellar vesicles are of various types and can composed thousands of bilayers. Different types of liposomes are illustrated in Figure 1.1.

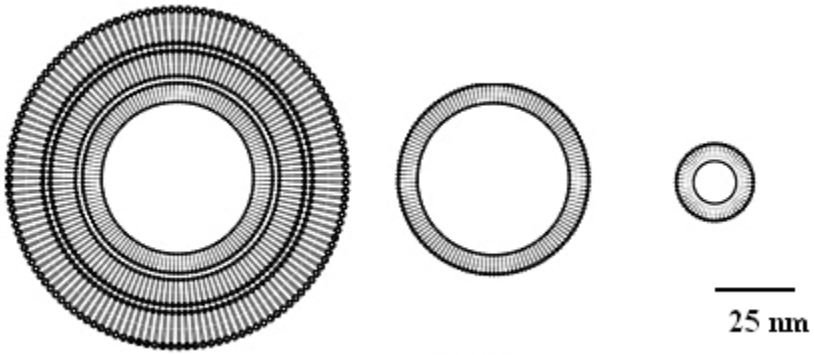

Figure 1.1. Structural illustrations of model membranes.
Far left, a model multilamellar vesicle (MLV) is hundreds of nm in diameter; center, large unilamellar vesicle (LUV) has a diameter of 50-500 nm, and small unilamellar vesicles (SUV) has a diameter of <50 nm (Lipid vesicles sizes were obtained from MacLachlan, I, Chapter 9. Antisense, Drug Technology, 2nd ed, pp. 238, 2006).

1.3. Liposome preparation techniques

Liposomes, also called lipid vesicles can be characterized as multilamellar vesicles (MLVs) for systems from 100-5000 nm, large unilamellar vesicles (LUVs) for systems from 50-500 nm in diameter or as small unilamellar vesicles (SUVs) for systems smaller than 50 nm (MacLachlan, 2006; Sharma & Sharma, 1997);. During pharmaceutical drug preparations, the choice of the liposomal system is dependent upon the liposome's encapsulation efficiency, drug/lipid ratio, drug retention, liposome and drug stability, and drug dispersion efficacy (Mayer et al., 1986). Drug encapsulation often employs passive entrapment, which relies upon the ability of the liposome to envelope an aqueous compartment during formation. The encapsulation efficiencies of passive entrapment vary greatly according to the preparation technique and are specific to the type of liposome formed. For instance, encapsulation efficiencies range from as low as 1% for SUVs to as high as 88% for MLVs (Mayer et al., 1986). Various techniques have been developed over the past few decades for producing vesicles, which include extrusion, sonication and microfluidics.

1.3.1. Sonication

Sonication is a technique commonly used for the production of SUVs. Specifically, sonication is the process of subjecting the lipid suspension to sound

(ultrasound) energy to agitate the particles in the sample and cause their rearrangement. Thus a dispersion of MLVs can be converted to a solution of SUVs ranging in size from 0.02 to 0.05μm via sonication. Although this technique is simple and quick, the SUVs produced have very low encapsulation efficiency for drugs ranging from 1% to 5% (Mayer et al., 1986).To optimize the efficacy of the drug delivery system improved drug encapsulation efficiency is desired, as observed in LUVs created by extrusion.

1.3.2. Extrusion

Liposomes were prepared with defined size distribution by extrusion through polycarbonate membranes (Olson et al., 1979). An early preparation method illustrates how liposomes are passed through sequentially smaller pore size membranes to achieve a mean diameter approaching the membrane pore diameter (Olson et al., 1979). The extrusion method passes liposomes through a polycarbonate filter membrane with a particular pore size (Figure 1.2), producing a population of vesicles that have sizes closely resembling the pore size of the polycarbonate membrane. For example, when extruded through a filter with 0.2 μm pore size the mean diameter will be 0.27 μm, slightly bigger than the pore size 0.2 μm. This results in a mixture of vesicles of homogenous size with a large enough interior aqueous volume (Olson et al., 1979).

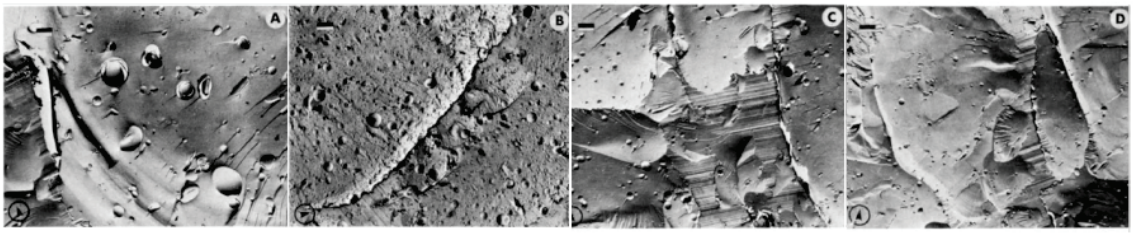

Figure 1.2. Illustration of extruded vesicle sizes using freeze-fracture EM.
a) Without extrusion, b) extruded through a 1 μm membrane, c) extruded through 0.4 μm membrane, d) extruded from 0.2 μm membrane. Bar in left top corner indicates 1.0 μm. (Reprinted from Biochemica et Biophysica Acta (BBA)-Biomembranes. Preparation of liposomes of defined size distribution by extrusion through polycarbonate membranes. 557.16., Copyright (1979), with permission from Elsevier.)

Extruding MLVs was then later shown to be a good method to generate LUVs for drug delivery. Hope et al. (1985) showed that LUVs can be produced by repeated extrusion of MLVs using a freeze-thaw protocol without organic solvent. Specifically, MLVs are injected into a chamber above the polycarbonate filters and then they are pushed through the filter under moderate pressure 100-500 lb/in^2 under a constant flow

rate. Then the LUVs are collected and re-injected and passed through the same filter another ten times under the same parameters. When the preparation process involves a freeze-thaw procedure, vesicles are first extruded to certain sizes and then freeze-thawed with liquid nitrogen and later sized again through new filters (Hope et al., 1985).

One device for generating LUVs is called a Lipex extruder and was developed by Northern Lipids Inc. The MLVs are input on the top of the device, are pressured by the nitrogen, and undergo extrusion through a polycarbonate filter of certain pore size. The LUVs are then collected at the bottom. Another device created by Avanti Polar Lipids, Inc allows the extrusion of the unilamellar vesicles at higher than room temperatures using a Hamilton syringes with a holder or heating block.

1.3.3. Active Drug Trapping Techniques: pH gradient

A pH gradient across the membrane has been exploited to incorporate the drug into the liposome. For instance, hydrophilic drugs that are pH dependent can have their encapsulation efficiency increased by using an established pH gradient between the interior and exterior of the liposome. The importance of pH gradients has long been appreciated for its contribution to the trans-bilayer asymmetry of phospholipids and the various distributions of fatty acids within cellular membranes (Hope & Cullis, 1987). It has been noticed that many biological membranes possess transmembrane pH gradients of 2-3 units (Cullis et al., 1997). According to Cullis et al (1987), a pH gradient of 3 units leads to a 1000-fold higher concentration of weak base to accumulate inside the vesicle relative to the outside. This leads to the redistribution of weak acids and weak bases inside and outside the lipid bilayer respectively. A weak base, A, can exist in neutral form, A, and protonated form, AH^+. The neutral form, A, will tend to passively diffuse across the membrane until the inside and outside reach equilibrium. When the weak base, A, reaches the acidic environment inside the cell, it becomes protonated and effectively decreases the concentration of A in the interior. This mechanism drives the uptake of A from the exterior. Eventually, the unprotonated A will be transported completely to the interior of the vesicle by the pH gradient (external pH 7.4 and internal pH 4), as shown in Figure 1.3 below.

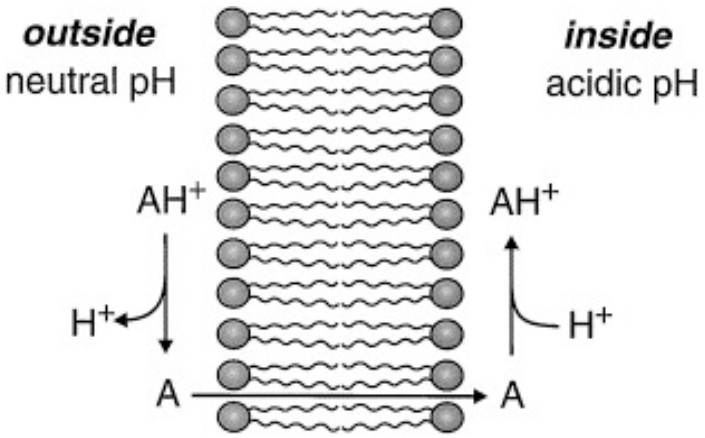

Figure 1.3. Illustration of the pH gradient.
The neutral form of the weak base, A, diffuses passively across the membrane and is protonated to AH^+ inside the acidic interior of the vesicle (Reprinted from Biochemica et Biophysica Acta (BBA)-Reviews on Biomembranes.*1331*. Cullis et al. Influence of pH gradients on the transbilayer transport of drugs, lipids, peptides and metal ions into large unilamellar vesicles, 19., Copyright (1997), with permission from Elsevier.)

1.4. Microfluidics and LNP development

The conventional (extrusion) method of preparing LUVs solves the problem of selecting the size of the vesicles; however, it is time consuming and the equipment is highly specialized. Microfluidics is an emerging technology that has been reported to produce micro and nano sized liposomes with a much more homogenous set of particle sizes. Continuous-flow microfluidics can also be used for generating lipid nanoparticles (Yu et al., 2009).

Belliveau et al. (2012) developed a lipid nanoparticle (LNP) synthesis method using microfluidics with a staggered herringbone micromixture that allows millisecond mixing at the nanoscale (Fig 1.4). This formulation is accomplished by pumping lipid in ethanol and siRNA in aqueous solution into the two inlets of the microfluidic mixing apparatus with a syringe pump. As the ethanol and aqueous phases are passed through the staggered herringbone structures, they undergo rapid mixing and rotational flow due to advection of the laminar streams. The generated LNP showed nearly full 100% encapsulating rate at siRNA/lipid ratio of 0.01 and 0.2 (wt/wt). Furthermore, cryo-transmission electron microscopy showed that the siRNA-LNP complex has an electron dense lipid core.

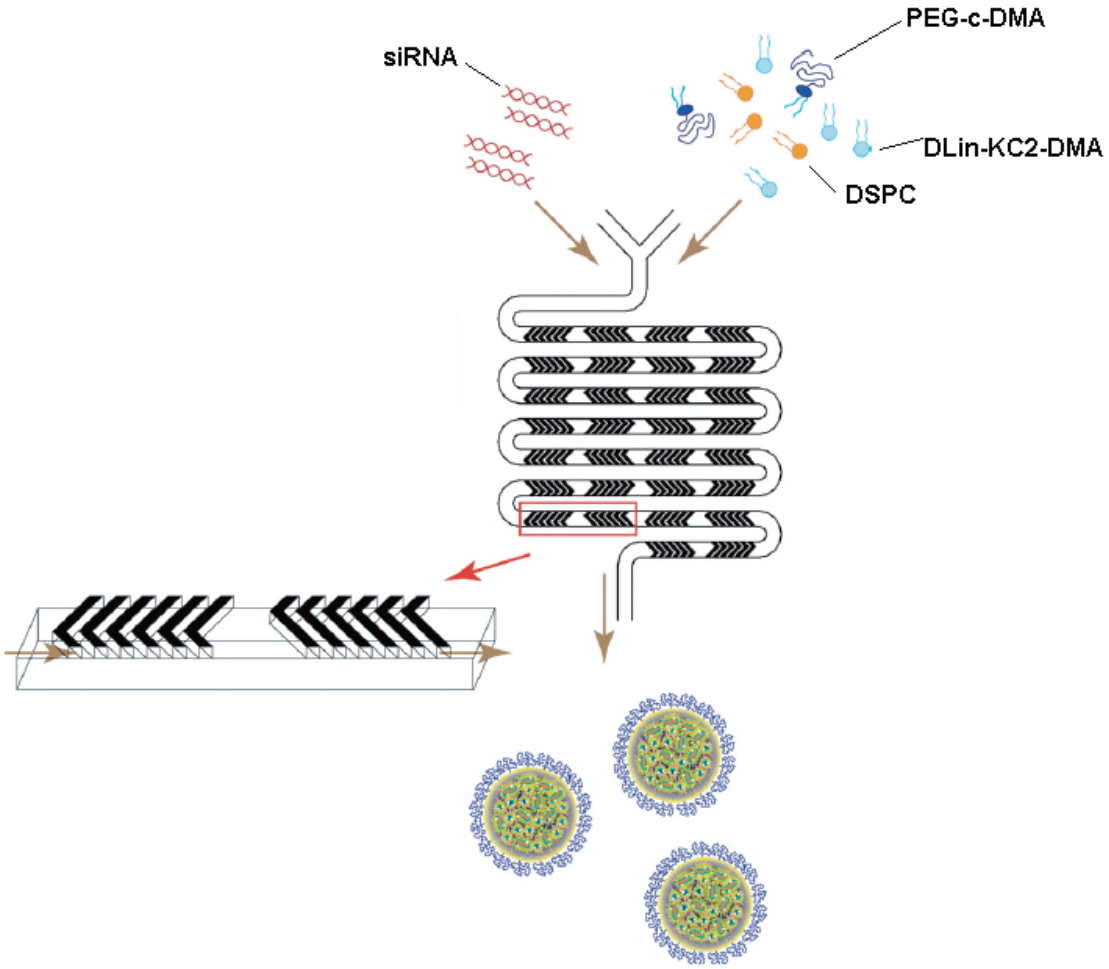

Figure 1.4. The microfluidics apparatus for making LNPs.
LNPs are formed by mixing the siRNA and lipid in an aqueous ethanol stream (Figure modified from Belliveau, et al, 2012).

1.5. Current Model of the LNP and the Proposed Drug Delivery Mechanism

Lipid nanoparticles used for siRNA delivery are prepared with a cationic lipid, DSPC, cholesterol, and polyethylene glycol lipid (PEG-lipid) in a 40:10:40:10 molar ratio and a siRNA to lipid weight ratio of ~ 0.05 (Figure 1.5). The phosphatidylcholine DSPC is responsible for stabilizing the LNP. The size of the LNPs can be controlled by changing the PEG-lipid content. The LNPs circulation time is increased by PEG-lipid which lowers the surface charge (Allen & Cullis, 2013; Semple et al., 2010).

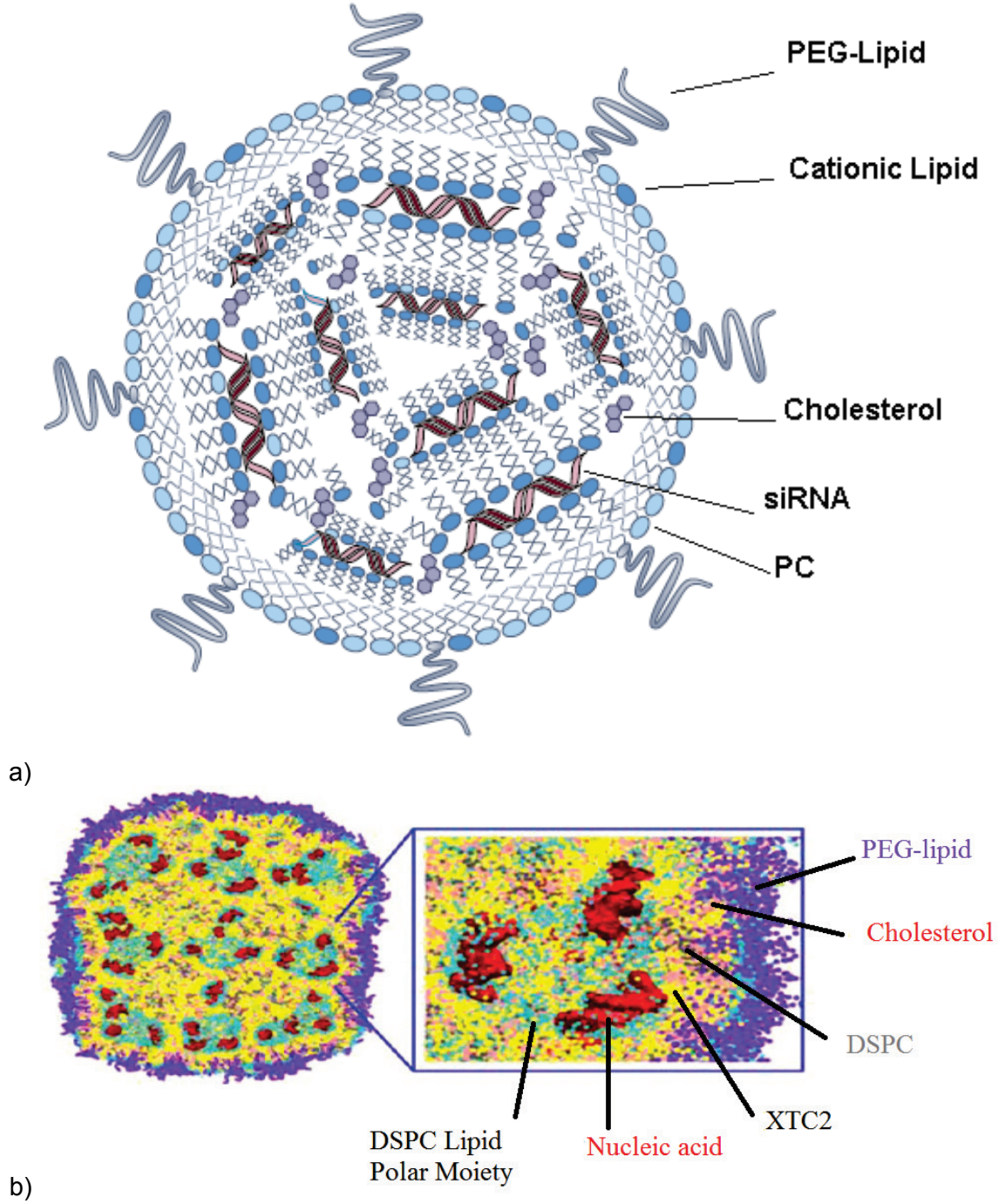

Figure 1.5. An illustration of LNP structure proposed.

a) The cartoon LNP composed of a cationic lipid: phosphatidylcholine: cholesterol: PEG lipid in 40:10:40:10 molar ratio with a siRNA to lipid ratio of ~0.05 (wt/wt)(Figure from Alnylam, presentation by Martin Maier, 2012 http://www.alnylam.com/capella/wp-content/uploads/2012/11/ALNY-OTS-LNP-Oct2012.pdf). (b) Computationally simulated LNP features an electron dense core. The LNP composition was DLin-KC2-DMA/DSPC/cholesterol/PEG-lipid in a 40:10:40:10 molar ratio and DNA to lipid ratio is ~0.05 weight ratio.DLin-KC2-DMA is shown in yellow, DSPC in gray, DSPC Lipid polar moiety in cyan, cholesterol in pink, PEG-lipid in violet, and nucleic acids (duplex in DNA) in red. (Leung et al., 2012) Adapted with permission from Leung et al, (2012). "Lipid Nanoparticles Containing siRNA synthesized by Microfluidic Mixing Exhibit an Electron-Dense Nanostructured Core. The Journal of Physical Chemistry C, 116(34), 18440-18450. Copyright (2012) American Chemical Society)

The proposed mechanism of drug delivery is shown in Figure 1.6. The LNP enters the body via injection into the blood stream. Since the LNP has a size similar to the LDL (low density lipoprotein) it will thus be recognized by Apolipoprotein E (ApoE), which binds to the LNP. It is then transported through the blood stream to the hepatocyte plasma membrane. The LNP is recognized by the surface receptor for ApoE and subsequently undergoes receptor mediated endocytosis to form the early endosomal membrane. As the endosome develops it acidifies and the cationic lipid becomes protonated. The protonated cationic lipid then interacts with naturally occurring anionic lipids in the cell, such that the electrostatic interactions of the lipid headgroups induces the formation of the inverse hexagonal phase. This disrupts the endosomal membrane and releases the siRNA into the cytoplasm where it can bind to the RISC complex and enter the RNA interference pathway (RNAi), where the RISC-siRNA complex recognizes and cleaves the complementary mRNA of the siRNA to effectively silence that gene. Even with these optimized LNPs, about 90% of the LNPs can be delivered from the blood to the hepatocyte, however only 1% of the LNP is successfully released.

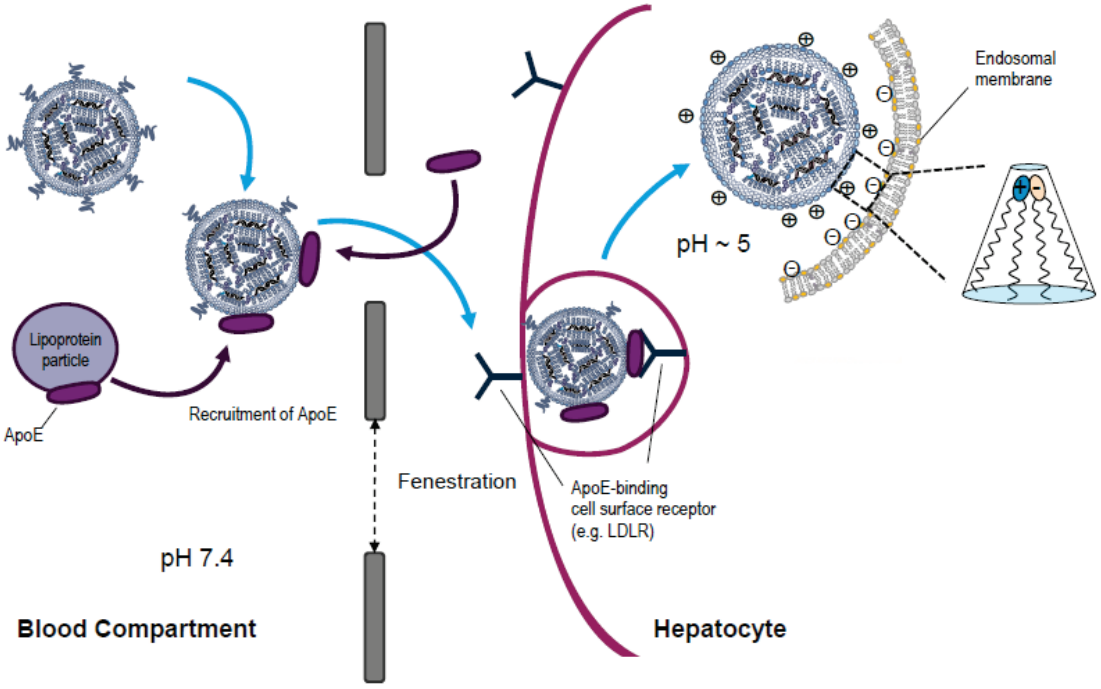

Figure 1.6. The current proposed LNP delivery mechanism.
The LNP circulates in the bloodstream, picked up by ApoE, delivered to the hepatocyte via endocytosis. In the acidic environment, the LNP cationic lipids form ion pairs with the endosomal anionic lipids, leading to disruption of the endosomal membrane and release of the siRNA to the cytosol. (Figure modified from Alnylam presentation by Martin Maier, 2012 http://www.alnylam.com/capella/wp-content/uploads/2012/11/ALNY-OTS-LNP-Oct2012.pdf).

To improve the design of the LNPs, Semple et al took a rational approach for selecting the best ionisable lipid. A series of lipid based on DLinDMA were evaluated by *in vivo* screening of lipid potency in mouse Factor VII model. The surface charge of the lipids was assessed by measuring fluorescence intensity of fluorescence probe 2-(p-toluidino)-6-napthanlene sulfonic acid (TNS). The apparent pK_a was measured by titration of the surface charge as a function of pH. The T_{BH} of the cationic lipid with equimolar DSPS were measured using ^{31}P NMR and differential scanning calorimetry. Semple et al (2010) found that the DLin-K series have similar optimal T_{BH}, between 18-20°C, and within the DLin-K series DLin-K-DMA and DLin-KC2-DMA have pK_a values that allow the LNPs to remain bilayer at neutral pH and become protonated in the endosome. The DLin-KC2-DMA was screened to have the lowest ED_{50} and then chosen to be incorporated into the design for LNPs (Semple, et al 2010).

1.6. Lipid Polymorphism

To study the bilayer to H_{II} phase transition happens in the endosome during drug release, we first need to understand lipid polymorphism. Lipid polymorphism describes the various structural phases lipids can aggregate and assemble into under specific conditions. The characteristics of the phospholipids determine which lipid phase is dominant under specific conditions.

1.6.1. Early shape theory

Lipid phases can be predicted based on the characteristics of the lipids that compose the lipid systems. It has been found that each lipid has a characteristic angle and surface headgroup area (Israelachvili et al., 1976). When the surface headgroup areas are greater than the fatty-acid tail end areas they are called tapered lipids (inverse cone shape), such as phosphatidylcholine (PC) and phosphatidylserine (PS). When the headgroup area is less than the area of the lipid chain, the molecule is cone shaped, such as cholesterol. Phosphatidylethanolamine (PE) can form either bilayer or H_{II} depends on composition and temperature. Non-bilayer lipids such as PE can form bilayer with present of bilayer preferring lipids such as phosphatidylcholine (PC), phosphatidylserine (PS) or sphingomyelin (SPM). It is found that when H_{II} preferring lipid PE mix with bilayer preferring lipid, it needs 1/5 or 1/2 molar ratio of the bilayer preferring lipid to maintain a net bilayer form (Cullis et al., 1986). Regarding the effect of temperature, in the gel phase, PE prefers the bilayer morphology since the headgroup and chain area match. It was shown that DOPE undergoes a bilayer to H_{II} phase transition when temperature is increased to 50-55°C whereas the DLPE (two 12:0 chains) remains in the bilayer phase even when the temperature is increased to 90°C (Cullis & de Kruijff, 1978). PS has a negative charge and can form a vesicle with a radius of 125 Å in 0.1 M NaCl solution but forms a vesicle with a much reduced diameter of 82 Å without salt. It is believed that the decrease in ion strength has an increase on the solid angle causing the lipid to become more tapered leading to a decreased vesicle size. There are numerous parameters which contribute to determining which lipid phase is most favoured at a given temperature.

1.6.2. Lipid Phases

Phospholipid systems can exist in more than one organized structural arrangement, known as a lipid phase, but only one lipid phase will predominate under specific parameters. The common lipid phases include the lamellar liquid crystalline phase (L_α), lamellar gel phase (L_β), hexagonal I phase (H_I), and the Inverse Hexagonal phase (H_{II}). These phases are illustrated in Figure 1.7.

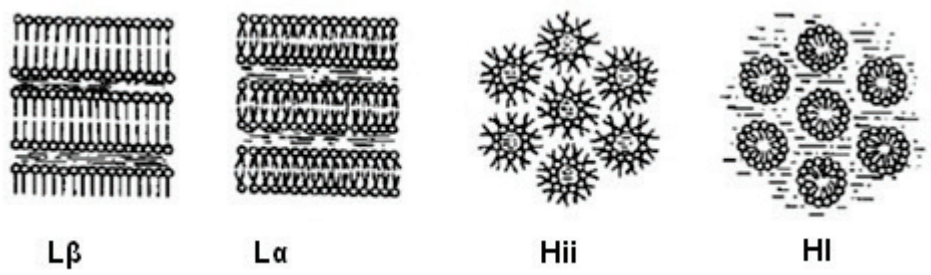

Figure 1.7. The cross sectional images of four common lipid phases.
Lamellar gel phase (L_β), lamellar liquid crystalline phase (L_α), and inverse hexagonal phase (H_{II}) and hexagonal I phase (H_I) (Figure modified from Gennis, RB)

In the lamellar liquid crystalline phase, the lipid and water system is considered a class of lyotropic liquid crystals. "Liquid crystalline" (L_α) describes molecules that have the crystalline property but are not necessarily packed in a lattice (Gruner, et al, 1985). That is, individual lipids can diffuse laterally in the L_α phase. L_α is composed of stacked lipid bilayers with water interspersed between the bilayer membranes. Liquid crystalline is used to describe the fatty acyl chains when the lipids undergo trans-gauche isomerization. The "gel phase" (L_β) also forms a bilayer similar to L_α but L_β lipids have stiffer chains and experience very slow lateral diffusion. The lipids in the gel phase are generally packed more tightly together in comparison to the L_α phase. Typically the L_β phase is favored at lower temperatures while the L_α phase usually predominates at higher temperatures. Lipids may also undergo isotropic motion, lateral diffusion, and motional averaging and this is most commonly associated with cubic, rhombic, micellar, inverted micellar and vesicle forms (Cullis & Dekruijff, 1979). The two common non-bilayer structures are hexagonal I phase (H_I) and hexagonal II phase (H_{II}). Hexagonal I phase is characterized by the lipids organizing into cylinders with the polar head groups facing outward and the hydrophobic hydrocarbon tails facing inward, e.g lysolipid. The

cylinders are arranged into a hexagonal pattern. Similarly, lipids in the H_{II} phase are also assembled into cylinders that are arranged in a hexagonal pattern but contrast to H_I, the lipids have the hydrophobic tail regions facing outward and the hydrophilic headgroups facing inwards.

1.6.3. Lipid Phase Transitions of a Model Lipid System

In a model membrane composed of an anionic lipid, such as phosphatidylserine (PS), and a pH-dependent cationic lipid, it can be expected that different lipid phases will predominate at different pH. This is due to the different charge states of the pH dependent cationic lipid. For instance, at neutral pH it can be expected that the cationic lipid is in its neutral form while the anionic lipid will have it's a negative charge. This favors the bilayer phase. As the pH is lowered, the cationic lipid is protonated and adopts a positive charge, forming an ion pair with the negatively charged PS. This results in a decrease in the area ratio of the headgroup to the chain (A_H/A_C) and form a cone shape, illustrated in Figure 1.8.

This cone shape then disrupts the bilayer and forces the lipids to adopt the inverse hexagonal phase. Thus, a lipid system featuring an anionic phospholipid and a pH-dependent cationic lipid can form a stable bilayer state at higher pH and an H_{II} phase at lower pH due to the geometrical shapes caused by the electrostatic interactions of the headgroups, as illustrated in Figure 1.8.

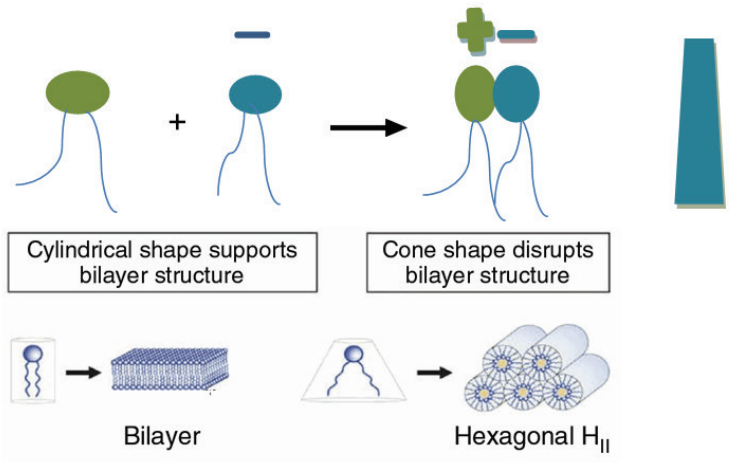

Figure 1.8. An ion pair model is formed by electrostatic interaction.
The reduction of the head group to chain area leads to a cone shape which favors the formation of the inverse hexagonal phase (Figure modified from Semple et al, 2010).

1.6.4. Factors that Influence Lipid Phase Transitions

In a model membrane of a specific composition, phase transitions are affected by pH and divalent cations. In a study by Hope and Cullis (1980) showed that the bilayer to H_{II} phase transition is affected by pH for the hydrated sodium salt of egg phosphatidylserine as shown by ^{31}P NMR. At pH 7.4, egg phosphatidylserine exhibits a stable bilayer phase and adopts the inverse hexagonal (H_{II}) at pH 3.5 phase at 50ºC. Protonation and neutralization of PS promotes tighter headgroup interaction reducing $A_{H.}$ The effect of divalent cations, especially the divalent cations Ca^{2+} was shown to induce headgroup immobilization in egg phosphatidylserine membranes (Hope and Cullis, 1980).

1.7. The Model Membrane Chosen for This Study

Two ionizable lipids were selected for this study: DLin-KC2-DMA (XTC2) and anionic lipid DSPS (1, 2-distearoyl (d70)-Sn-glycero-3-[phospho-L-serine]). When incorporated into the LNP system as the cationic lipid, XTC2 (structure is shown in section 1.7.2) has shown to have a potent *in vivo* activity in its drug delivery capacity. On the other hand, PS is reflective of the intracellular conditions the cationic lipid may encounter. DSPS was chosen because it has two fully saturated acyl chains and does not by itself adopt the H_{II} phase. Thus DSPS bilayer destabilization presents a real challenge for XTC2.

To determine the effectiveness of the XTC2 in the LNP system in the proposed drug delivery mechanism further information is required about the lipid phase behavior of the model membrane consisting of the XTC2 and DSPS. The different lipid phases, such as the bilayer phase and the reverse hexagonal phase can be studied using ^{31}P NMR and ^{2}H NMR (Semple et al., 2010). Specifically, ^{31}P NMR can be used to investigate the behavior of the phosphate containing headgroups of the lipids while ^{2}H NMR can be used to investigate the behavior of the tail region of a deuterated lipid. Solid state deuterium nuclear magnetic resonance (SS ^{2}H NMR) is a powerful experimental tool for the study of phospholipid structure in lipid membranes. The labelling of the acyl chain allows us to observe the spectral width and line shape between different physiological environments. The lamellar to inverted hexagonal phase

transition temperature, which is affected by various physical parameters of the membrane, can be measured using ^2H NMR. In order to fully understand and predict the behaviour of the XTC2, a full understanding of the properties and characteristics of DSPS is required.

1.7.1. Anionic Lipid: PS

PS has an ionisable headgroup consisting of a carboxyl with a negative charge, an amine group with a positive charge and a phosphate headgroup with a negative charge. The pK_a of the carboxyl and amine headgroup decides the overall charge of the headgroup at different pH.

The intrinsic pK_a is defined as the pH at which 50% of the PS molecules are charged. It is known that the intrinsic pK_a is a fixed value and it is significantly lower than the apparent pK_a. As summarized by (Moncelli et al., 1994), the intrinsic pK_a of the PS has been investigated in several studies and there are variations in literature values that have been reported. For the carboxyl group of the PS alone in dispersion was determined as 2.7 (Macdonald et al., 1976). For PS in mixtures with PC vesicles the pK_a was 3.6 measured by titrations (Tsui et al., 1986). The intrinsic pK_a of PS carboxyl group was obtained as 3.3 in pure PS and ~2.3 in PS/PC mixtures by deposited the lipid on Mercury electrodes method (Moncelli et al., 1994). The apparent pK_a varies with salt concentration.

The transition temperature of PS from gel to liquid crystalline at low pH 4.0 is around 72ºC, where PS is neutral. At higher pH (around pH 7), the DPPS melting temperature, T_m, is around 57ºC, where DPPS is negatively charged. Increasing NaCl concentration was shown to reduce the surface potential and lower the apparent pK_a of DPPS as shown in Fig. 1.9 (Macdonald et al., 1976). It has been shown that the T_m of the DPPS decreases as the salt concentration increases e.g 0.01M Na^+, 0.1M Na^+ and 1M Na^+ (Macdonald et al, 1976) at both neutral pH.

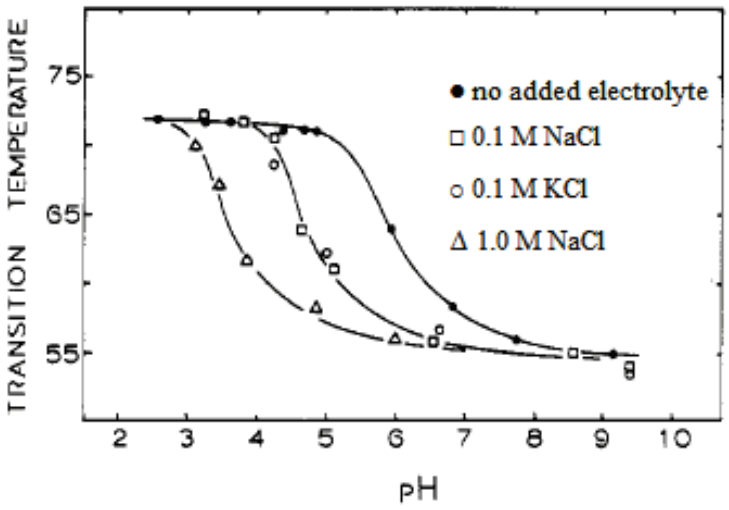

Figure 1.9. The effect of pH and salt concentration on DPPS T_m.
Aqueous phases were ● no added electrolyte, □ 0.1 M NaCl,○ 0.1 M KCl, Δ 1.0 M NaCl+0.05 M phosphate buffer (Figure modified from Macdonald, et al 1976).

The intrinsic pK_a of the PS headgroup is around 3.6, the apparent pK_a of the PS at high pH various with salt concentration. "The salt effect is due to the decrease in the local proton concentration at the membrane surface at low ionic strength." (Tsui et al., 1986)

The PS membrane is negatively charged and protons are attracted to the membrane surface. With addition of high salt, it reduces the difference between bulk PKa and intrinsic pK_a because the higher $[Na^+]$ competes with H^+. Normally, the surface pH is less than the bulk pH. With the presence of high $[Na^+]$, pK_a is close to the intrinsic pK_a because there is less $[H^+]$ at the membrane surface than in the bulk. At low ionic strength, more $[H^+]$ is attracted to the negatively charged membrane surface, more COO^- become COOH, and the PS headgroup overall is neutral. The lower bulk pK_a then gives higher T_m. At high ionic strength, (i.e. 1M $[Na^+]$), the greater difference between bulk pK_a and intrinsic pK_a, more PS is charged, results of a low T_m.

1.7.2. Cationic Lipid: XTC2

XTC2 is the one of the most potent cationic lipid in delivering of the silencing siRNA gene. This was tested through a series of the cationic lipids that have a similar headgroup and acyl chains but different linker groups. The cationic lipids were screened by in vivo experiments using a murine factor VII (FVII) model. Their abilities to inhibit

FVII production by hepatocytes were compared. It was shown that the optimized cationic lipids used in the LNP siRNA systems gene silencing function in hypatocyte endosomal membrane disruption at doses as low as 0.005 mg siRNA/kg body weight in mouse models(Jayaraman et al., 2012; Semple et al., 2010; Wan et al., 2013).

The best performing cationic lipid was selected to be DLin-KC2-DMA(an ionizable lipid with a pK_a of ~ 6.7) from all of the cationic lipids tested which have a pK_a range from 5.3 to 7 (Figure 1.10). This linoleyl lipid features two double bonds in each fatty acyl chain and the linker group controls its enzymatic stability and hydrophobicity (Semple et al., 2010). It was also shown that the ketal ring possesses a high gene silencing activity by *in vivo* experiments. The head-group is crucial in terms of deciding the pK_a of the cationic lipid. In particular, it was concluded that the distance between the dimethylamino group and the dioxolane linker affects the flexibility of the charged head group (Semple et al., 2010). When two methylene groups are present in the headgroup, the potency of the lipid increases four times as compared to the single methylene group. The optimum number of methylene groups is 2 as this results in the highest potency as compared with 1, 3 or 4 methylenes tethered to the headgroup (Semple et al., 2010).

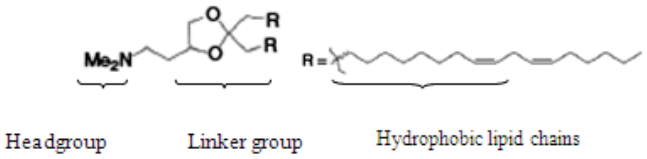

Figure 1.10. The chemical formula of the cationic lipid DLin-KC2-DMA.
The headgroup, linker group, and the hydrophobic chains are labeled.

The potency of gene silencing is directly related to the endosomal membrane destabilizing ability where DLin-DMA has a T_{BH} of 27ºC and DLin-KC2-DMA has a T_{BH} of 20ºC. This illustrates that DLin-KC2-DMA (XTC2) has a greater ability to destabilize the endosomal membrane at lower temperatures. This can be explained structurally as the extra methylene group gives rise to more flexibility of the charged headgroup. Overall, the pK_a, the value of T_{BH}, and the distance of the headgroup all account for the gene silencing ability and DLin-KC2-DMA was shown to have the minimum effective dose (ED50). The characteristics of the cationic lipid are of vital importance to enhancing the drug delivery efficacy, based on the current proposed drug delivery mechanism. The

most up to date study shows that the pK_a of the amine group has strong correlation with the optimal in vivo activity and the optimal pK_a is between 6.2 and 6.5 (Jayaraman, et al, 2012). The lipid DLin-MC3-DMA was designed by modifying the hydrophilic head-group region of XTC2 (Figure 1.11). It has a pK_a of 6.44 so it is not protonated until it arrives in the low pH endosomal compartment and been characterized as the most active cationic lipid so far (Jayaraman et al., 2012).

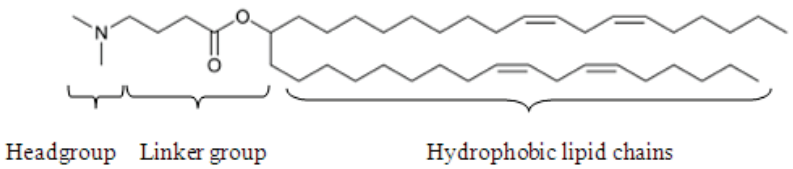

Figure 1.11. The chemical formula of the cationic lipid DLin-MC3-DMA.
The headgroup, linker group, and the hydrophobic chains are labeled.

1.7.3. PS and XTC2 model membrane

Mixing of cationic lipids and anionic phospholipid induces the inverse hexagonal phase (H_{II}). A studied by Hafez et al, (2001) on the mixing DODAC with different species of phospholipids such as DOPA, Lysobisphosphatidic acid (LBPA, enriched in the late endosomal membrane), tetraoleoyl-cardiolipin (CL), phosphatidylinositol derived from liver (PI) and 1-palmitoyl-2-oleoyl phosphatidylglycerol(POPG) all induce H_{II} phase (Hafez, et al, 2001). The ability of the cationic lipid in the LNP to bind the anionic lipid in the endosomal membrane depends on the charge state of both the pK_a of the ionizable cationic lipid and the charge state of the anionic lipid. This is also called the bilayer destabilizing ability. The T_{BH} of the DLin-KC2-DMA and DSPS at pH 4.8 was determined to be around ~20ºC (Semple et al., 2010).

1.7.4. Project Objective

The objective of this project is to improve the current understanding of the structure and function of LNPs especially to improve the controlled release. This is understood by studying the interaction of the anionic and cationic lipids and determine the phase behavior of phosphatidylserine cationic lipid XTC2. The influence of physical parameters, such as pH (8.4 and 4.75) and salt concentration (0.25, 1 and 0.5M Na^+) on the phase transition will be investigated.

Chapter 2. Nuclear Magnetic Resonance Theory and Its Application to Study Lipid Biomembranes

This chapter will give an introduction to Nuclear Magnetic Resonance (NMR) spectroscopy and its application in lipid membrane and includes three main parts. The first part introduces the basics of NMR, followed by an overview of the components of the NMR spectrometer and how ^{2}H NMR experiments are operated. The second part explains the data processing from NMR signal to NMR spectra. The last section draws attention to spectral analysis, explaining how the experimental parameters determine the lipid phases and dynamics properties.

2.1. Introduction to Nuclear Magnetic Resonance (NMR)

One technique for studying lipid membranes is Nuclear Magnetic Resonance (NMR) spectroscopy. In this project, NMR spectroscopy was employed to investigate the the physical properties of XTC2 and DSPS and their phase behavior in a model membrane under various parameters. The biophysics of the membrane can be studied by both ^{31}P and ^{2}H NMR spectroscopy. Specifically, the phosphate headgroup will be reflected by ^{31}P NMR. The application of ^{2}H NMR in studying liquid crystals and membranes have been used since the 1970s (Seelig, 1977). Deuterium labeled molecules combined deuterium NMR studies on liquid crystals emerged in 1965 (Rowell et al., 1965). The biomembrane has been studied with D_2O in 1973 (Finer, 1973). The deuterated lipid was studied by Seelig between 1974 and 1977. With the lineshapes of the ^{2}H NMR spectra yield extra information on the hydrocarbon acyl tails such that the motion of the lipid and fluidity state of the membrane can be obtained. It is known that lipid undergoes lateral diffusion and rotation about its long axis and the NMR time scales are in the range of 10^{6} and 10^{10} sec^{-1} correlation time, respectively (Gennis, 1989). Progressively, lipid phases have been and are still widely being studied by exploiting the

natural spin dynamics of nuclei with the development of solid state NMR techniques, which investigate the anisotropic (direction dependent) interactions of the nuclei. NMR spectroscopy is a powerful technique that will be the principal method of investigation in this study.

2.1.1. Deuterium is a Quadrupole Nuclei has spin 1

^{2}H have a spin of 1 together with ^{14}N and ^{6}Li. Substituting ^{1}H with ^{2}H is allows us to study specific biomolecules by nuclear magnetic resonance.

Nuclei with spin-1/2 are spherical in shape and have convenient magnetic properties (Levitt, 2008). Most chemical element such as alkali and alkaline metals don't possess spin-1/2 but in organic materials spin-1/2 is well represented, such as ^{1}H and ^{31}P.

On the other hand, the quadrupolar nuclei with an integer spin is rich in nature but often used in difficult field such as solid state NMR. For instance, ^{2}H has low natural abundance as well as easy to be prepared by substituting ^{1}H to ^{2}H making deuterium labelled samples. It becomes gradually popular in solid state NMR.

Proteins, lipids, and other biomolecules are usually studied by solution state NMR, increasing popularity has been addressed in solid state NMR.

2.1.2. Energy Levels and Zeeman Effect

Deuterium is a quadrupolar nucleus that has natural spin I= 1. Spin-1 nuclei have three eigenstates $\langle M \rangle$=2I+1 of angular momentum along the z-axis (Fig 2.1). The quantum number M equals to +1, 0, or -1.

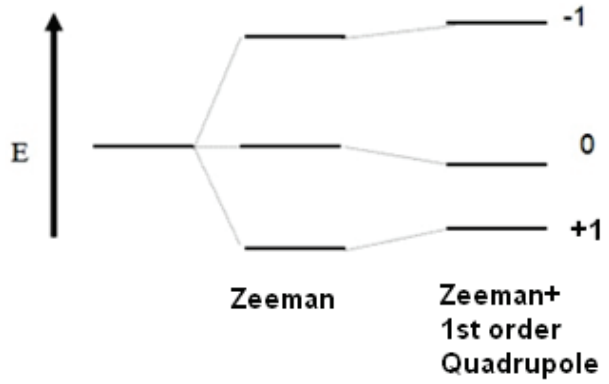

Figure 2.1. The energy levels of deuteron.
Three states are generated after Zeeman Effect and 1st order Quadrupole effect. These effects lead to different spectra shapes.

2.2. Solid State ^{2}H NMR Spectrometer

In this study, we will introduce the OXFORD NMR 300 solid state NMR spectrometer. This spectrometer is specially built for studying lipid sample in solid state. Four main components will be introduced: The magnet, the probe, and variable temperature units and the data processing station.

2.2.1. The magnet

This spectrometer contains a 300 Hz Oxford Superconducting magnet. It produces a 7T magnetic field. The magnet is submerged in liquid helium surrounded by liquid nitrogen (Fig 2.2). The central component of an NMR magnet is a Nb-Sn coil immersed in liquid He. The liquid He is insulated by a large reservoir of liquid N_2. The N_2 reservoir is what we visualize from the outside.

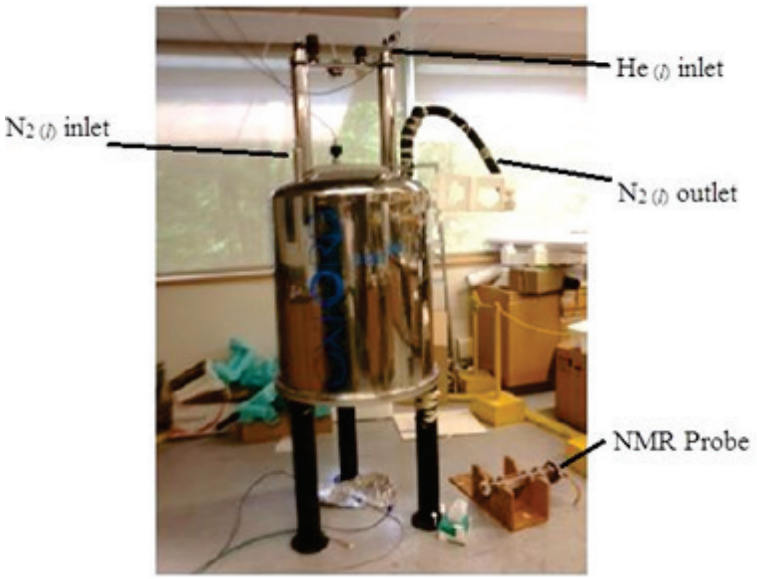

Figure 2.2. The OXFORD 300 magnet.
It is located in Thewalt's biomembrane biophysics lab in Simon Fraser University.

2.2.2. The probe

The centre of the superconducting coil is a large hole called the bore. The cylindrical device that is inserted into the bore is called a probe. The probe consists of the coil, the thermal couple, capacitor rods for tuning and matching (Fig. 2.3). The probe plays a complex function. It includes the r.f electronic circuits. It is also responsible for stabilization of the temperature. At room temperature, air is circulated from the air tube to the sample holder. For temperatures greater than room temperature, a heater is used to insert to the probe to warm up the air circulating around the sample. The thermal coupler is used to give an indication of the sample temperature.

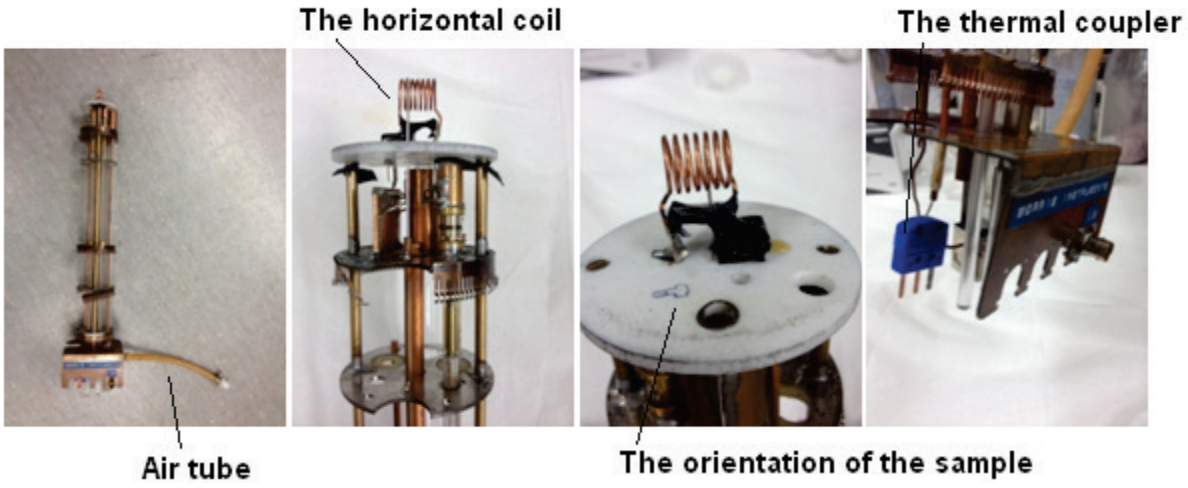

Figure 2.3. Parts of the probe
The probe is consists of an air tube, a horizontal coil, and the thermalcouple.

2.2.3. The Variable Temperature Unit (VTU), Frequency Synthesizer and Ref. Phase

The variable temperature unit (VTU) is the central part for adjusting the sample temperature during an experiment (Fig 2.4). It has a target temperature setting unit composed of four up and down arrows. The target temperature will be shown in the red numerical letters. The real temperature and the set temperature need to be equilibrated to the same before doing experiment. This is done by setting up the heater power limit to the correspondent temperature for the high temperature, as well as the nitrogen evaporator power to high when temperature needs to be cooled down.

For this spectrometer, the frequency synthesizer is set specifically to the deuterium frequency ν_0 =46.794821 MHz for the lipid (CD_2) resonance frequency. Also, each time the reference phase is adjusted before experiment to achieve a proper line shape of both the real and imaginary channel signals and this is done by adjusting the reference phase four digits numerals.

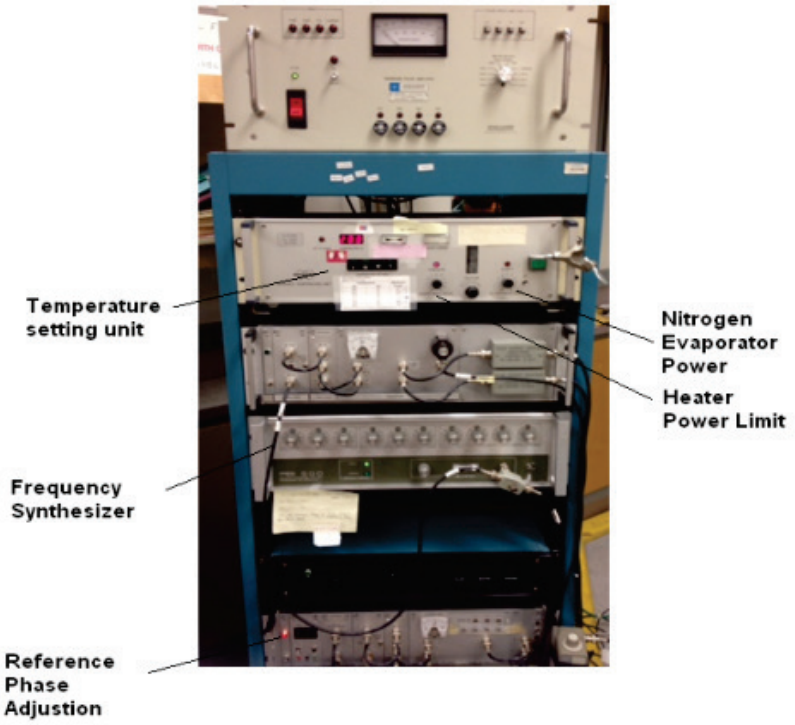

Figure 2.4. The Various Temperature Control Units (VTU).
The VTU controls the temperatures, nitrogen evaporator power, and heater power limit. It is located above the frequency synthesizer and reference phase adjusting unit.

2.2.4. The data collecting station

The work station is used to both set up the specific parameters for the experiment and collect the NMR signals. Before the experiment, the number of scans, dwell time, phase cycles and spectral width are input to the computer. During the experiment, reference phases are adjusted to get a good line shape. After the experiment, the NMR signals are acquired in the following work station and saved as digit text file, and then they are processed in Igor to obtain an NMR spectrum.

2.3. The NMR experiments

2.3.1. The two pulses sequence

In this study, two different NMR experiments were studied, the ^{31}P solution NMR and the ^{2}H solid state NMR.

2.3.1.2 The Hahn Echo

For ^{31}P experiment, Hahn Echo pulse sequence was used as shown in Fig 2.5.

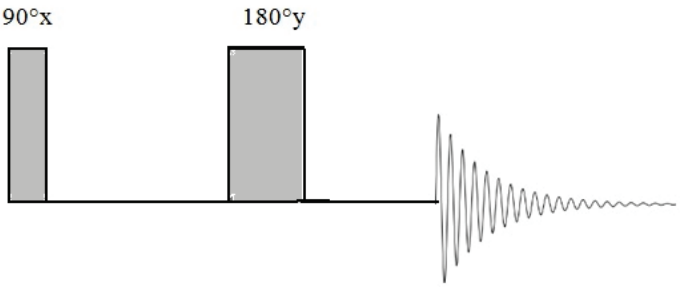

Figure 2.5. Spin Echo sequence for ^{31}P NMR experiment

2.3.1.2 The Quadrupolar Echo

A powder ^{2}H spectrum has a 200 kHz width, which corresponds to Free Induction Decay (FID) that needs 5 μs from the beginning of the pulse to the end. This is too rapid decay to be detected due to the electrical interference, thus by generating a spin echo we can displace the NMR signal to a time frame (Levitt, 2008). For a ^{2}H experiment, Quadrupolar Echo pulse sequence was used (Fig 2.6).

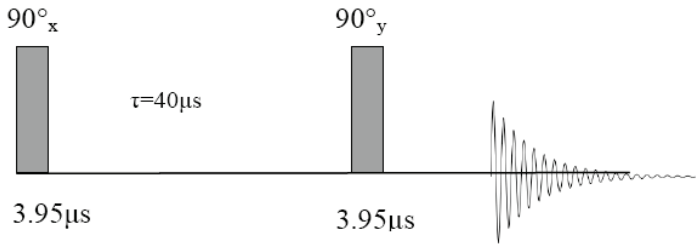

Figure 2.6. Quadrupolar echo pulse sequence for ^{2}H NMR experiments.
It is composed of 90°x-τ-90°y-τ with the pulse time 3.95 μs and τ (interpulse delay) of 40 μs and repetition time of 300 ms.

2.3.2. Data Acquiring-Signal Averaging

Multiple scans were used to increase the signal to noise ratio. When adding the signal together, this is called signal averaging. The signal averaging results in a superposition of the overall signals. The more transients or scans, the less noisy the spectra look.

2.3.3. Free Induction Decay (FID) and data processing

Lipids that are labelled with ^{2}H in the acyl chain components are subject to magnetic field. The R.F pulse will give rise to free induction decay (FID)

An NMR experiment is composed of these four steps: initialization, excitation, Detection, and processing and display. The signal of transverse magnetization is detected and it decays over time. It is called a Free Induction Decay (FID). The FID is then transformed to the frequency domain via Fourier transformation (FT) shown in Fig 2.7. It is observed as an oscillating magnetic field. Fourier transform convert a NMR signal to an NMR spectrum.

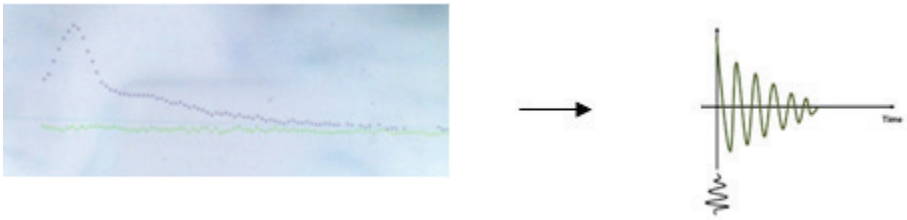

Figure 2.7. From NMR signal to NMR spectrum
. On the left, the real and Imaginary channel are illustrated by purple and green, it is fourier transformed and the free induction decay after 90° pulse is shown on the right

2.4. Spectral Analysis and application in lipid membranes

In this section, first, the lipid headgroup motion and orientational behavior can be measured by the ^{31}P NMR chemical shift anisotropy. Secondly, the dynamical properties of the lipid chains can be explained by the ^{2}H NMR experiment design and spectral analysis. The acyl chains motions of the membrane in different phases were studied by the M_1, M_0, order parameter S_{CD} and T_1 relaxation times.

2.4.1. Chemical shift anisotropy (CSA) in ^{31P} NMR spectroscopy

In the ^{31}P NMR, the chemical shift anisotropy is extensively employed in terms of analysing the lineshape of the spectra. The chemical shift anisotropy reflects changes in the symmetry of the motion between bilayer and inverted hexagonal phases. When the induced field $B_j^{induced}$ along three directions X, Y, Z axis are equal, the chemical shift

tensor is called isotropic. If one is different from the other two, the chemical shift tensor is called anisotropic.

The residual CSA measured in this study,

1. Residual CSA

$$\Delta\sigma = \sigma_{//} - \sigma_{\perp}$$

where $\sigma_{//}$ represents the chemical shift in ppm of the 0° shoulder and $\sigma_{\perp}$ represents the chemical shift in ppm of the 90° peak (Seelig, 1978). The $\Delta\sigma$ was measured from the 90º peak to 0 º shoulder in consistency with Cullis & de Kruijff, 1978 (Cullis & de Kruijff, 1978). Lipid polymorphism results in different spectral shapes observed by solid state NMR. Therefore we observe different residual CSA values.

Area under the curve M_0 and Average Spectral Width M_1

M_0 measures the area under the curve. It is proportional to the echo height. M_1 measure the average spectral width.

2. Area under the Curve

$$M_0 = \sum I(w) \cdot \Delta\omega$$

3. Average Spectral Width

$$M_1 = \frac{\sum|\omega|I(\omega)}{\sum I(\omega)} \quad (s^{-1})$$

In which $I\omega$ is the spectral intensity at frequency ω. M_1 has an important physical meaning that it reflects the T_m of the lipid. The midpoint of the steepest slope of the M_1 plot is gives the melting temperature of the lipid membrane.

2.4.2. Typical ^{2}H NMR spectral patterns for L_β, L_α, H_{II} phase

Solid state NMR techniques are useful for identifying and characterizing the lipid phase present in the sample. In deuterium (^{2}H) NMR analysis, a change of the line shape and order parameter aids in the identification of the phase of the lipid mixture.

Typical deuterium NMR line shapes are observed for lipid-water mixtures in the following phases:

1. Lamellar liquid crystalline phase (L_α). (Pake doublet, no preferred orientation of lipid long axes. All angles present.) It is shown in Fig. 2.8 (a).

2. Lamellar gel phase (L_β) (also powder spectrum but much broader) shown in Fig. 2.8 (b)

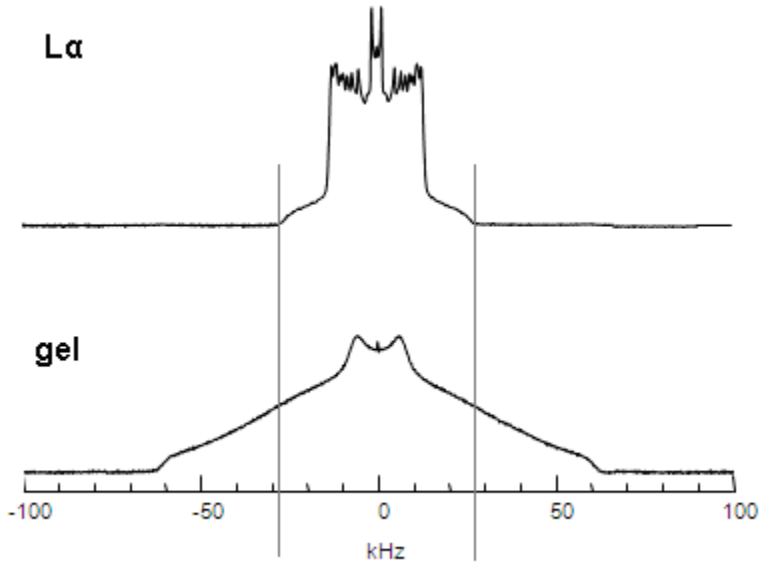

Figure 2.8. DPPC-d31 in lamellar phase (L_α) and gel phase.
Figures modified and used with permission from Dr. Jenifer Thewalt. Part (a) shows the DPPC-d_{31} in L_α phase, part (b) in gel phase. Vertical lines indicate the region where M_1 is measured for L_a phase.

3. Inverse hexagonal phase (H_{II}): Spectral width is half of the L_α phase and more defined edge, almost triangle shape) shown in Figure 2.9 (b).

4. Isotropic phase: The lipids assemble into small vesicles or droplets (sharp peak at 0 kHz)

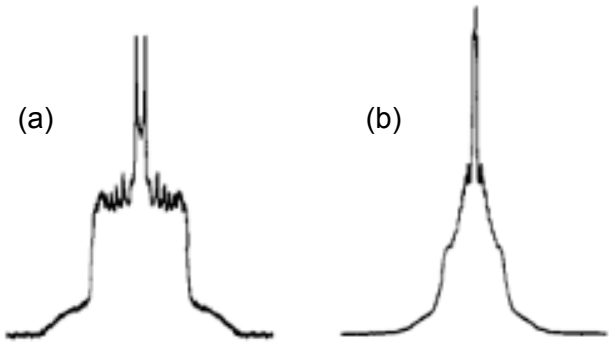

Figure 2.9. Literature ^{2}H NMR spectra for (a) bilayer (L_α) and (b) H_{II} phase.
The lipid studied was PLPE-d31 by Thurmond et al (1993). Figure modified from (Thurmond et al., 1993).(a)shows Lα phase at 323K and (b) shows the H_{II} phase at 343K.

2.4.3. Anisotropic motion in the lipid membranes

In this study, the membranes organize in these two symmetries: lamellar and inverse hexagonal phase. Solid state ^{2}H NMR analyzes the anisotropic interactions (directionally dependent motions) in the sample (Seelig, 1977). The lipids in the bilayer phase (L_α) rotate around its axis of symmetry which is the lipid long axis (i.e. perpendicular to surface of the membrane). Lipids in the H_{II} phase not only have axial symmetric motion about the lipid long axis but in addition lipids can diffuse all around the cylinder axis. The two motions are perpendicular and relatively fast on NMR time scale and the cylinder gives an extra narrowing by a factor of ½.

4. Order Parameter Profile S_{CD}

The average fluctuation of the CD bond with respect to lipid long axes are measured using the order parameter S_{CD} (Seelig, 1977)

$$S_{CD} = \frac{1}{2}(3cos^2\theta_i - 1)$$

in which θ is the time average of the angular fluctuation around the lipid long axis shown in Fig. 2.10.

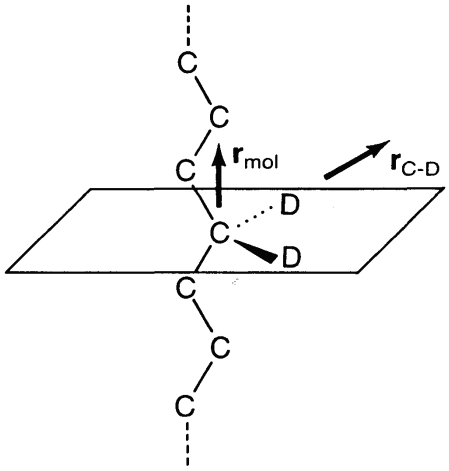

Figure 2.10. An indication of molecular vector of a lipid chain.
The r_{mol} and $r_{C\text{-}D}$ are used in computing S_{CD} in ^{2}H NMR (Figure from Gennis R.B pp 53).

$$\text{If } \theta = 90°,\ S_{CD} = \frac{-1}{2} \text{ and if } \theta = 0°,\ S_{CD} = 1.$$

Due to hexagonal phase has $\frac{3<cos^2\theta°-1>}{2} = \frac{-1}{2}$ therefore the quadrupolar splittings $\Delta\nu_Q$ should be reduced by a factor of $\frac{1}{2}$ relative to theL_α.

Experimentally, the order parameter S_{CD} can be calculated from the quadrupole splitting $\Delta\nu$ measured in the ^{2}H NMR spectra,

5. Quadrupolar Splitting

$$\Delta\nu = (3/4)\ (e^2\mathrm{qQ/h})S_{CD}$$

where the e^2qQ/h is the quadrupolar coupling constant in the absence of motion, with a determined value 168 kHz. Different orientation θ would result in different power patterns (Fig 2.11).

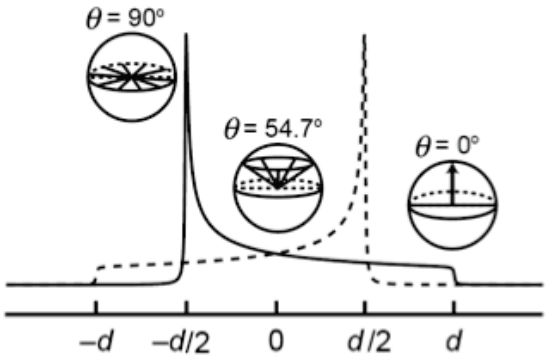

Figure 2.11. The Pake doublet is a superposition of two spectra.
The highest intensity represents the 90° orientation and the lowest peak represents the 0° orientation. Zero frequency represents the magic angle 54.7°.d is the maximum extent of the spectrum which equals the $\Delta\nu$ 90°.

2.4.4. Repetition time

In membrane lipid study, the main relaxation is quadrupole interaction (Seelig, 1977). The spin-lattice relaxation T_1 refers to the time a spin returns to its equilibrium state. It is used to determine the repetition time between experiments.

T_1 measures longitudinal relaxation time back to the Z-magnetization. In lipid NMR research, the methyl group on the lipid chain CD_3 has a long T_1 relaxation time and is too slow to be measured properly within 300 ms. Therefore two different repetition time scales were used: 1s and 2s. This is very useful in terms of determine the existence of a solid phase.

Chapter 3. Material and Methods

3.1. Materials

The lipids 1,2-distearoyl-*sn*-glycero-3-[phosphor-L-serine] (sodium salt) (18:0 PS #840029P powder M.W.814.06 g/mol) (Fig. 3.1) and1,2-distearoyl(d70)-*sn*-glycero-3-[phosphor-L-serine] (DSPS-d70) (sodium salt) (#860402P Lot# 180D70PS-13 powder M.W. 884.5 g/mol) (Fig 3.2) were purchased in powder form from Avanti polar lipid (Albaster, Alabama) and stored at -20ºC. The cationic lipid 2, 2-dilinoleyl-4-(2-dimethylaminoethyl)-[1, 3]-dioxolane (DLin-KC2-DMA abbreviated as XTC2) was obtained in oil form from AlCana Technologies Inc. (Vancouver, BC) (Fig 3.3). N2-hydroxyethylpiperazine-N'-2-Ethanesulfonic Acid (HEPES) powder was purchased from Bioshop, Biotechnology, (Lot # 8C7226, Bioshop Canada Inc, Burlington, Ontario). Sodium hydroxide in pellet form was purchased from EM science, Affiliates of Merck KGaA (Darmstadt, Germany). The glacial acetic acid was purchased from Anachemia Science Canada Inc (Vancouver, BC) Chloroform ($CHCl_3$) was purchased from Sigmal Aldrich 366927-4L. Deuterium-depleted water was obtained from Sigma Aldrich (Sigmal Chemical Co. St. Louise, MO 63178, USA) Lot # SZ1519V (≤1ppm deuterium oxide). Sodium chloride was purchased from BDH Inc. (350 Evans Ave. Toronto Canada M8Z 1K5). Parafilm was purchased from Bemis flexible packing. (Neenah, WI 54956).

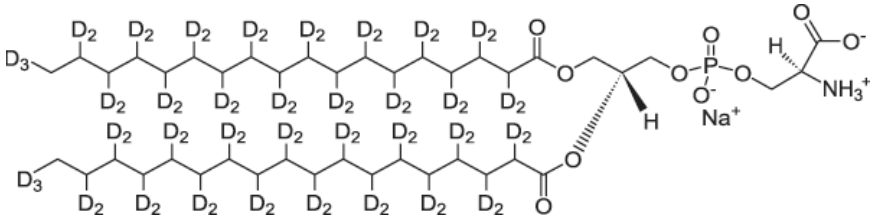

Figure 3.1. Structure of DSPS-d70.
The structure of 1, 2-distearoyl(d70)-sn-glycero-3-[phosphor-L-serine] (DSPS) (sodium salt). Its molecular formula is $C_{42}H_{11}NO_{10}PNaD_{70}$. It has a molecular weight of 884.488 g/mol (Figure from Avantilipids.com).

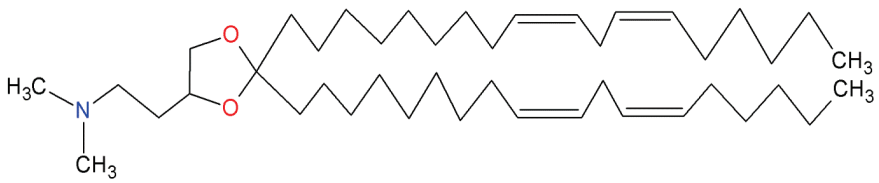

Figure 3.2. Structure of DLin-KC2-DMA (neutral form).
The DLin-KC2-DMA (XTC2) that has a tertiary amine is neutral when pH>pK_a 6.7.

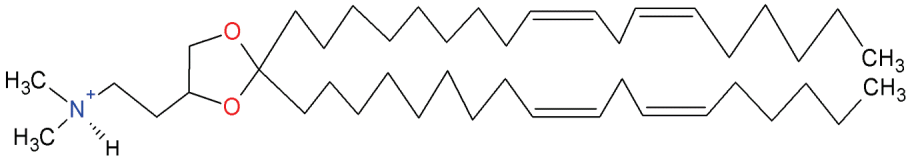

Figure 3.3. Structure of DLin-KC2-DMA (cationic form).
DLin-KC2-DMA (XTC2) consists of a pH-dependent cationic headgroup, a linker group, and two unsaturated hydrocarbon chains. When pH < pK_a 6.7 the XTC2 is protonated, the headgroup becomes positive.

Equipment

The sample was prepared using a mini vortexer (mv1, VWR scientific product), analytical balance (SARTORIUS, bp210s), Sand bath (hi-temp bath, Fisher Scientific), borosilicate glass culture tube 16×100mm, thermometer, and microwave, vacuum pump, and Saran wrap (SC Johnson). A lyophilizer (The VirTis Company, Gardiner. N.Y. 12525) was used to dry the sample from water. Two pH meters (SB20, VWR and Beckman 350 pH/Temp/mV Meter) and pH paper (ColorpHast, pH 4.0 - 7.0, EM-Reagents, Cat #: 9582) were used for determining the pH values of the solutions.

3.2. DSPS model membrane

3.2.1. DSPS model membrane for ^{31}P NMR experiment

For result shown in Fig. 4.1, 20 mg of the DSPS powder was dissolved in 400 µL of H_2O and vortexed to obtain multilamellar vesicles (MLVs). The milky suspension was then transferred to the standard borosilicate NMR tube for ^{31}P NMR experiments performed in the 600 MHz NMR facility in SFU.

The phosphorus NMR experiments for measuring the DSPS were performed on the 400 MHz Bruker Spectrometer in the SFU NMR facility center under the guidance of

Dr. Andrew Lewis. The samples were loaded into a 4mm magic angle spinning tube but sample remain still. The proton decoupled Hahn Echo sequence was used with a 2.6 μs 90° pulse and the runs were set with a 28 µs delay time. The ^{31}P NMR spectra collected 600 scans for each spectrum using a 3 μs recycle delay between 298 and 345K.

3.2.2. DSPS-d70 model membrane for ^{2}H NMR experiment

The DSPS-d70 model membrane was prepared by dissolving 50 mg of DSPS-d70 in 700 uL of deuterium-depleted water (ddw) in a scintillation vial. The DSPS-d70 in ddw was then heated at temperatures around 60^{o}C for one minute followed by one minute of vortexing. This process was repeated three times to form MLVs. The solution was subsequently processed with four cycles of freeze-thaw-vortex which consisted of freezing at -20^{o}C for 20 minutes, followed by thawing at room temperature for 20 minutes, and vortexing for 1 minute. The completion of these four cycles yielded a milky white suspension. The dissolved DSPS-d70 was then transferred to a deuterium NMR tube and sealed with Teflon tape and Parafilm. Its mass was recorded with an analytical balance.

The ^{2}H NMR experiments were performed on the OXFORD 300 NMR spectrometer. 8 cycles were used to cancel the imperfections of the phase of the pulses and the receiver phase. The settings of 300ms repetition time, 2μs and 5μs dwell time were used. Each spectrum was collected with 20,000 scans. For the de-Paked spectrum, 100,000 scans were averaged to obtain a less noisy spectrum.

DSPS testing solid phase

Three different repetition times were compared to determine if a solid phase is present in DSPS-d70 multilamellar vesicles at low temperatures. Temperature runs were done at 283, 288, 289 and 298K with a reptime 300ms, 1s, and 2s. The invariance of the parameters in Table 3.1 means that there is no solid phase in DSPS.

Table 3.1. The M_0 and M_1 for DSPS-d70 at 298K with different reptimes.

reptime	M_0	M_1	M_1/1000
0.3	0.604	128222.8	128.2228
1	0.6079	130246.4	130.2464
2	0.6115	129436.4	129.4364

3.3. XTC2/DSPS model membrane

3.3.1. XTC2/DSPS model membrane for ^{31}P NMR experiment at pH 7.4 and 4.75 (For results shown in 5.1 and 5.6)

This experiment for XTC2/DSPS was performed with Dr. Ismail Hafez at Cullis lab at UBC and NMR facility at CDRD. The protocol is described in section 3.3.2 (with modifications for deuterated sample). The proton decoupled ^{31}P NMR experiments for XTC2/DSPS were performed with a Bruker AVII 400 MHz spectrometer at CDRD at UBC. Standard single pulse zgpg was used for obtaining ^{1}H-decoupled ^{31}P spectra. The free induction decays (FID) were obtained using a 15 μs, 55º flip angle with a 1s interpulse delay and a spectral width of 64 kHz. The sample temperature was regulated by a Bruker BVT 3200 temperature unit.

3.3.2. Preparation of XTC2/DSPS-d70 model membrane at pH 8.4 and 4.75 for ^{2}H NMR experiment

The experiment was performed based on Dr. Ismail Hafez's preparation method with modification designed for ^{2}H NMR experiment.

The XTC2/DSPS-d70 lipid system was prepared by first measuring out approximately equal molar amounts of lipids. The actual experimental weights measured were 38.6mg (60.12 μmol) of XTC2 in oil form and 53.3mg (60.29 μmol) of DSPS-d70 in powder. XTC2 was dissolved in chloroform at room temperature in a separate, sealed glass vessel. DSPS-d70 was dissolved in chloroform heated to 80^{o}C. The two lipid solutions were then mixed in a glass culture tube. Chloroform was used to rinse out any residue lipid from the original vessels. The tube containing the lipid mixture was then vortexed and placed in a warm water bath where the temperature was slightly higher than 25°C. The chloroform was removed by blowing nitrogen gas into the

tube while gently swirling the tube. A lipid film formed and the removal of chloroform with nitrogen gas was ceased once the amount of chloroform was less than 1 mL. The residual amount of chloroform was removed using a high vacuum pump overnight.

The lipid film was hydrated with HEPES buffer. The HEPES buffer was prepared by measuring 0.0119g of HEPES powder and dissolving it in 465.84 µL of deuterium-depleted water. The lipid mixture was then rehydrated in 600µL of the 10 mM HEPES buffer to obtain a 250 mM total lipid concentration. The hydration step was done in a cell culture tube with 10 cycles of heating at 70^{o}C in a sand bath for 1 minute, and vortex for 1 minute (3 cycles in the protocol). The lipid mixture in the HEPES buffer was then transferred to the NMR tube and the pH was determined to be approximately 8.4.

The sample was acidified to pH 4.75. The acidification was prepared by adding sodium acetate buffer to the lipid mixture. The amount of sodium acetate buffer was determined by the Henderson Hasselbalch Equation. An amount of 93.1 µL of the sodium acetate in deuterium depleted water was added to make the final concentration of the sodium acetate to be 250 mM pH 4.75. The glacial acetic acid (pH~0) was titrated to the sodium hydroxide (pH ~8) to obtain a pH of 3.86 sodium acetate buffer. The final buffer concentration was 250 mM sodium acetate and 8.3 mM HEPES with pH ~4.7 (pK_a of acetic acid is 4.7). This solution causes the lipids to cling to the wall of the NMR tube.

^{2}H NMR experiments were performed at various temperatures to determine the phase behaviour at low pH. Afterwards, approximately 54 mg of sample was loaded into a 4mm NMR tube for ^{31}P NMR experiments (experimental results were not shown for clarity). The sample from the 4 mm NMR tube was returned to the original ^{2}H NMR tube.

Preparation of XTC2/DSPS model membrane pH 4.75 containing different [Na^+]

The effect of salt concentration was investigated by examining the effects of different Na^+ ion concentrations. A 6M stock NaCl was prepared by dissolving 0.7030g of sodium chloride (MW=58.44g/mol, 100%) in 2 mL of ddw .

The low salt concentration (0.25M Na^+) was prepared by the acidification step discussed earlier in Section 3.3.2. The 0.25M Na^+ salt concentration derives from the 0.25M NaOAc buffer created in the acidification step.

To obtain a higher Na^+ salt concentration of 1 M Na^+, the initial salt concentration derived from the 0.25 M NaOAc buffer dissolving the DSPS-d70/XTC2 sample needs to be considered. Thus, only 22.5 µL of concentrated NaCl stock (6M) was required in the ~150 µL sample in the original NMR tube to reach a final concentration of 1M Na^+ in the solution.

A moderate salt concentration was chosen to be 0.625M Na^+. To obtain this salt concentration from the 1M Na^+ solution, the sample was diluted by adding a 5:1 ratio of HEPES and NaOAc buffers such that the salt concentration was diluted but the pH of the sample was maintained fairly constant around pH 4.7. This was obtained by adding 17.25 µL of NaOAc buffer and 86.25 µL HEPES buffer to the 172.5 µL of the sample remaining in the NMR tube.

Five cycles of heating at ~70^oC in a sand bath for 1 minute and vortexing the sample for 1 minute were done after each salt concentration adjustment. For the final salt adjustment, the sample was also subjected to four cycles of freezing the sample at -20^oC for 20 minutes, thawing at room temperature for 20 minutes, and vortexing for 1 minute.

Chapter 4. Results: DSPS in a Model Membrane

This chapter will summarize the biophysical properties of DSPS and DSPS-d70 in model membranes. Specifically, the phase behaviour of multilamellar vesicles composed of DSPS and DSPS-d70 was investigated. The T_m for DSPS obtained by ^{31}P NMR spectroscopy was compared with literature value. The T_m for DSPS-d70 was determined by ^{2}H NMR spectroscopy. The order parameter profile S_{CD} vs. carbon number was obtained through de-Paked spectrum of DSPS-d70. The effects of different head groups and chain lengths on the main transition temperature of membranes composed of saturated PS or PC will be summarized.

4.1. DSPS model membrane studied by ^{31}P NMR

Phosphorus-31 NMR Spectroscopy of DSPS in H_2O shows a gel to liquid crystalline (L_α) phase transition T_m at 339K. Figure 4.1 shows the phosphorus NMR spectra of DSPS as a function of temperature. The observed ^{31}P NMR spectra arose from the phosphoserine head group of DSPS. Fig. 4.1 (a-b) show that the DSPS is in gel phase at 298K as characterized by the broad peak centered at -22 ppm. As temperature was increased to 333K, the spectrum gets sharper but maintains one peak as shown in Fig 4.1 (c). In part (d), two peaks can be observed: one high intensity lower field peak at -18 ppm (representing the 90° orientation) predominated and another low intensity peak at higher field, 36 ppm (representing the 0° orientation) began to emerge. Fig. 4.1 (e to g) shows that as temperature was increased from 339 to 345K, the 90° peak became sharper and the 0° shoulder becomes more obvious. No gel phase component is observed at -22 ppm indicating that the DSPS model system was purely L_α phase at 345K. In summary, the DSPS model system is in gel phase below 333K, underwent a complete transition by 339K and is in L_α phase above 339K. It has been reported that

the transition temperature for DSPS is 341K (Avanti polar lipid). Our results show 2 degrees lower than the literature value.

As seen in Fig 4.1 (a through g) the sharp small peak located at 0 ppm present from the beginning to the end of the temperature series experiment. This is possibly due to microstructures of DSPS such as micelle, small vesicles.

It is worth noting that these spectra were obtained using a 600 mHz solution state NMR spectrometer. Distortions of the multilamellar vesicles may be the reason that the typical phosphorus powder pattern is not obvious at high magnetic field.

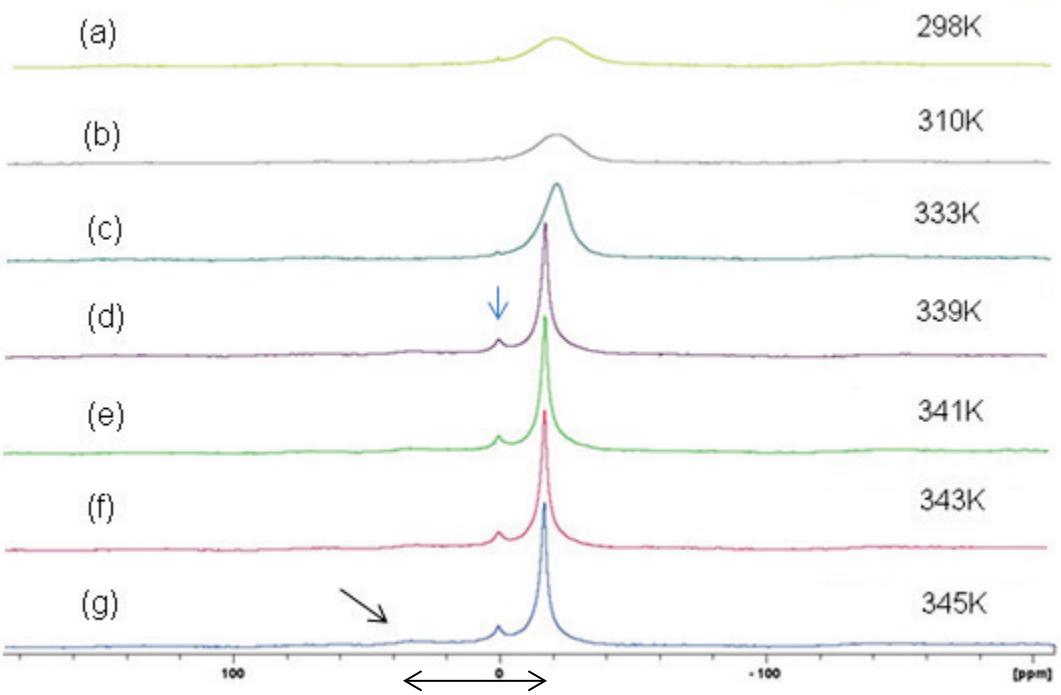

Figure 4.1. ^{31}P NMR spectra of the DSPS as a function of temperature.
The arrow in (d) indicates the isotropic peak at 0 ppm. The arrow in (g) indicates the 0° shoulder of the powder pattern. Buffer is H_2O.The double arrow indicates the range of the residual chemical shift anisotropy.

Although the T_m of the DSPS has been reported in the literature, the transition temperature T_m obtained by the ^{31}P NMR still has significant meaning as it is 2 degree lower than the reported value and it is also a comparison with the T_m study for the DSPS-d70.

4.2. DSPS-70 model membrane studied by ^{2}H NMR Spectroscopy

Deuterium NMR spectroscopy of the DSPS-d70 model membrane is in the gel phase for temperatures up to at least 328K. Figure 4.2 shows ^{2}H NMR spectra of DSPS-d70 in ddw over a temperature range of 283 to 328K. The gel phase spectrum is characterized by the end of the shoulder at +/-63 kHz as observed in the 283K spectrum. It was observed that the gel phase spectrum was also temperature dependent. The shoulder at +/-35 kHz becomes more pronounced as temperature increases.

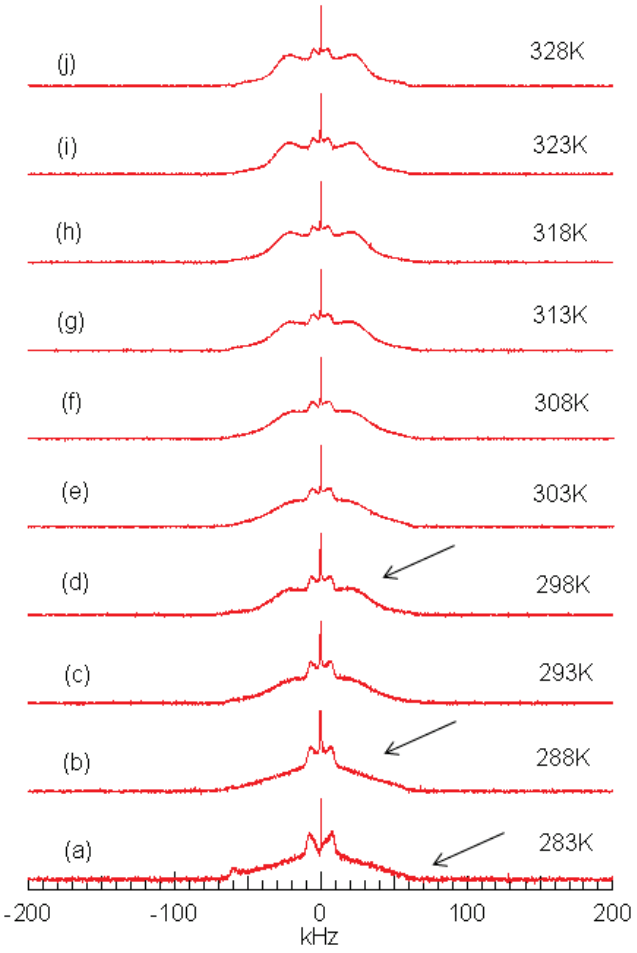

Figure 4.2. ^{2}H NMR spectra of DSPS-d70 as a function of temperature.
DSPS-d70 was dissolved in pH 8.4 HEPES buffer. The arrow in (a) indicates the end of the 0° shoulder. The arrow in (b) and (d) show the increasing intensity of the 90° peak.

Above 328K, the DSPS-d70 membrane undergoes a gel to L_α phase transition. A detailed examination of the ^2H NMR spectral shape (Fig 4.3) indicates that the DSPS-d70 model membrane gel to liquid crystalline phase transition temperature, T_m is near 338K. As shown in Fig 4.3 (a-b), the DSPS-70 model system is still mainly in the gel phase. As the temperature is increased to 338K, the central components with a spectral width of +/-15 kHz, characteristic of the L_α phase, emerge from the gel phase. This indicates that the system has coexisting gel and L_α phases at 338K. The system completes its phase transition by 343K as seen in Fig 4.3 (d) where the spectral intensity is zero outside the +/- 30 kHz shoulders.

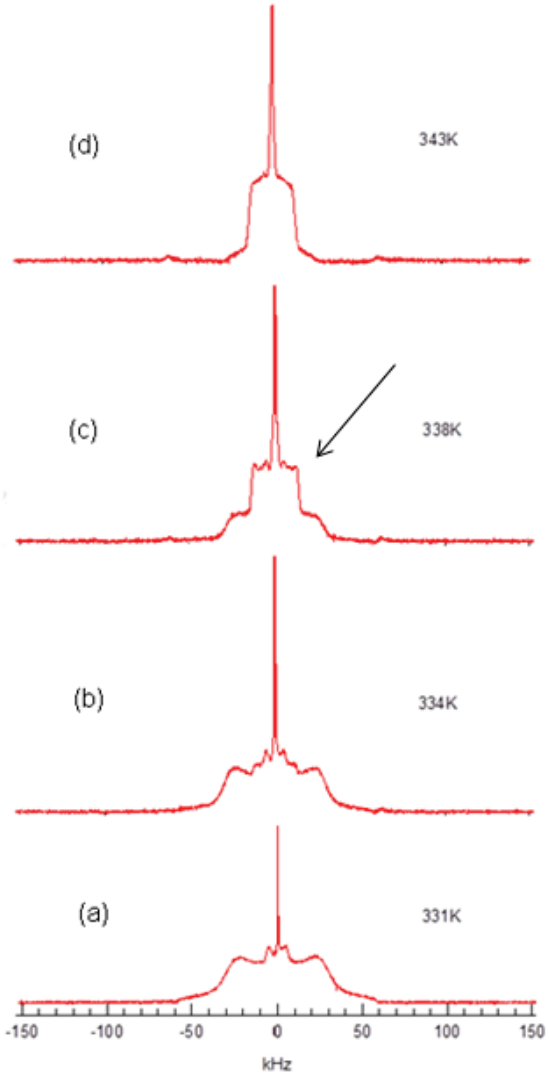

Figure 4.3. The gel to L_α phase transition of the DSPS-d70 membrane.
At temperature (a) 331K DSPS-d70 is in the gel phase (b) 334K gel and trace amount of L_α, (c) 338K more L_α, and (d) 343K pure L_α. The arrow indicates the growing L_α spectral component.

When M_1 is plotted as a function of temperature (Fig 4.4) it is found that the transition temperature of DSPS-d70 is between 331 and 341 K. From 283-328K, M_1 is rather constant. From 331 to 341K, M_1 decrease steeply, and above 341K the slope of M_1 vs. T diminishes. The T_m DSPS-d70 is estimated to be in the middle of the steepest slope, around 336K. More precisely, lines were fitted as a function of T. The intersections define the beginning and end of the transition at 331K and 341K. The transition midpoint is half-way along the steepest slope marked with a star, between 336 and 337K.

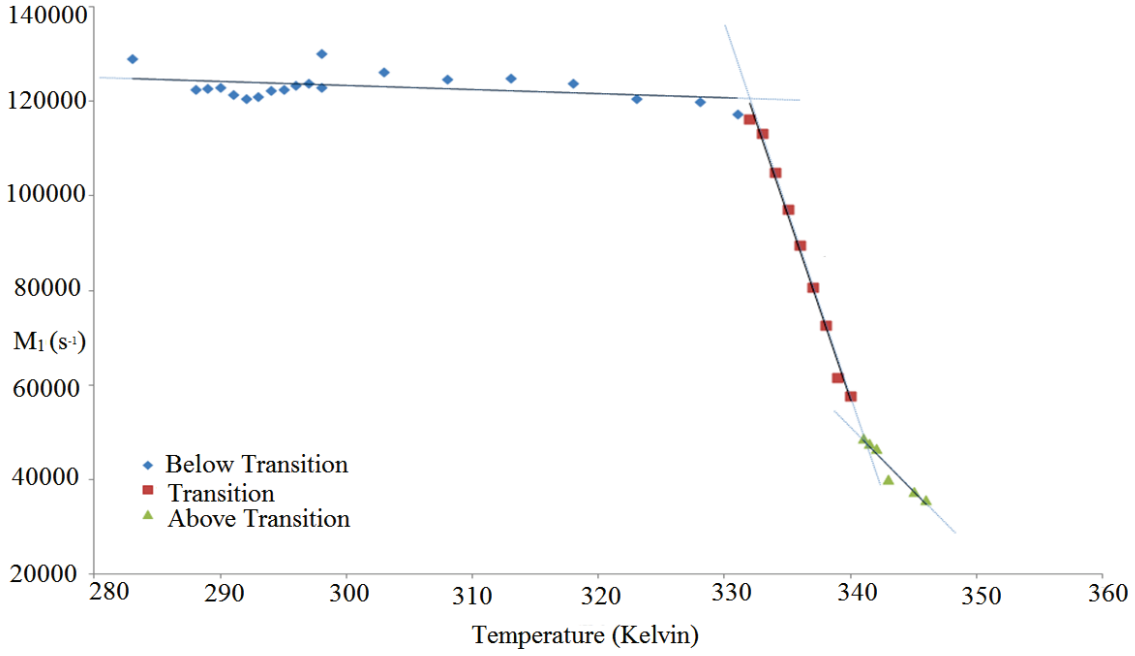

Figure 4.4. The average spectral width, M_1, for DSPS-d70.
M_1 was analyzed for 283 to 346 K. The lines of best fit are shown. The best fit lines are elongated to obtain intersections, representing the beginning and the end of the transition.

As shown in Figure 4.5 (a) and (b), at 298K, the DSPS-d70 membrane gives different spectral shape based on its thermal history. The right one was obtained after cooling down to 283K then increased temperature back to 298K. By comparing the M_0 at 300ms and 1s repetition times, area under the curve of the spectra didn't increase by increase amount of time between experiments. The area under M_0 tells the sample volume is the same and the long reptime shows no solid phase even after being cooled and reheated.

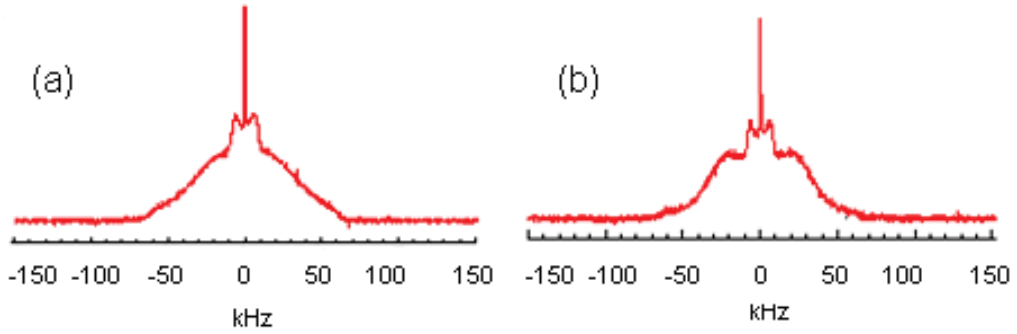

Figure 4.5. The effect of thermal history.
Two spectra obtained at 298K were compared. The DSPS-d70 was dissolved in ddw at room temperature (a), and the same sample after a temperature run from 298 to 346K and a low temperature run from 283K to 298K.

4.3. DSPS-d70 depaked Spectrum and Order Parameter Profile

The order parameter profile was obtained by de-Paking the pure L_α spectrum observed at 341.5K (Fig 4.6). The quadrupolar slitting of the chain C-D segment $\Delta\nu$ was measured and listed in Table 4.2. The quadrupolar splittings $\Delta\nu$ was measured and the order parameter profile was obtained via the equation $\Delta\nu = \frac{3}{4}\left(\frac{e^2qQ}{h}\right)|S_{CD}|$ where $\left(\frac{e^2qQ}{h}\right)$ equals 168 kHz (Fig 4.7). The order parameter profile obtained showed a maximum S_{CD} of 0.22 which agrees with literature value of previous values from experimental and simulations on DPPS (Browning and Seelig, 1980; Berkowitz and Pandit, 2002).

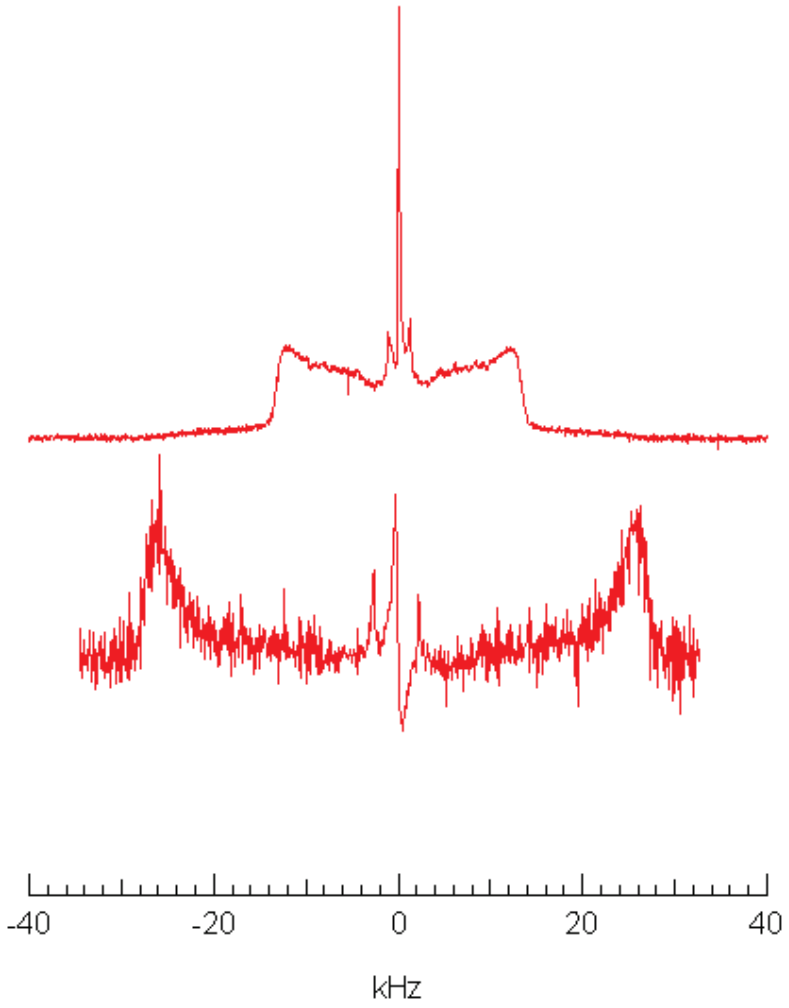

Figure 4.6. **^{2}H NMR de-Paked spectrum for DSPS-d70 at 341.5K.**
Spectra (above) and the corresponding depaked DSPS-d70 spectrum (below) are shown.

Table 4.1. S_{CD} for DSPS-d70 at 341.5K.

Carbon	X-right	x-left	$\Delta\nu_0$(Hz)	Δv (Hz)	Δv(kHz)	S_{CD}
18	2636.719	2246.094	4882.813	2441.406	2.441406	0.019376
17	10796.1	11020.2	21816.3	10908.15	10.90815	0.086573
16	16206.1	15020.2	31226.3	15613.15	15.61315	0.123914
15	18546.1	17920.2	36466.3	18233.15	18.23315	0.144708
14	20736.1	20450.2	41186.3	20593.15	20.59315	0.163438
13	22006.1	21930.2	43936.3	21968.15	21.96815	0.17435
12	22936.1	22980.2	45916.3	22958.15	22.95815	0.182208
11	23566.1	23730.2	47296.3	23648.15	23.64815	0.187684
10	24136.1	24360.2	48496.3	24248.15	24.24815	0.192446
9	24576.1	24840.2	49416.3	24708.15	24.70815	0.196096
8	24936.1	25270.2	50206.3	25103.15	25.10315	0.199231
7	25266.1	25640.2	50906.3	25453.15	25.45315	0.202009
6	25556.1	25950.2	51506.3	25753.15	25.75315	0.20439
5	25846.1	26280.2	52126.3	26063.15	26.06315	0.20685
4	26176.1	26670.2	52846.3	26423.15	26.42315	0.209708
3	26486.1	27040.2	53526.3	26763.15	26.76315	0.212406
2	26906.1	27600.2	54506.3	27253.15	27.25315	0.216295

For DSPS-d70, there are 18 carbons in each chain with no deuterons attached to carbon #1. The tabulated values of Δv therefore extend from C#2 to C#18 with 17 carbons in all. For C#2 to C#17 the splitting was obtained according to the "smoothed order parameter" (Lafleur et al, 1989). The splitting for methyl group C#18 was directly measured from the dePaked spectrum.

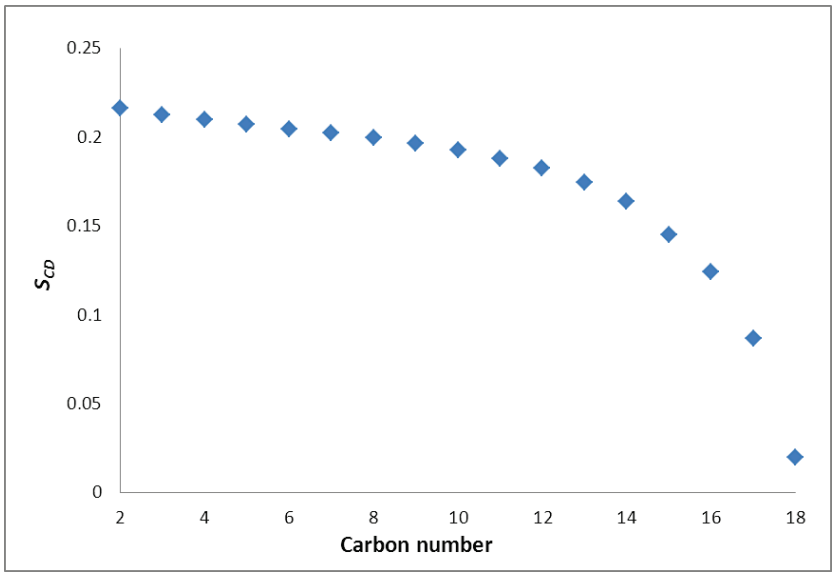

Figure 4.7. The order parameter S_{CD} for DSPS-d70 at 341.5K.
The S_{CD} is plotted as a function of carbon position from 2 to 18.

4.4. Melting Behaviour of DSPS and DSPS-d70 membranes

By studying the gel to liquid crystalline phase of DSPS and DSPS-d70 we obtained information for the chain melting for both chain saturated lipid. This can be compared with lipid which has same chain length different headgroup and/or same headgroup different chain lengths (Fig 4.8). It is shown in Table 4.2 that T_m is chain lengths dependent for saturated phosphatidylserine.

Table 4.2. Effect of deuteration on PC and PS.

lipid	No. of C	T_m , K	T_m range, K	lipid	No. of C	T_m ,K
DPPS[1]	14	309√	308-309	DMPC	14	297.46*
DPPS[1]	16	326√	326-327	DPPC	16	315.02*
DSPS	18	341†	339-341	DSPC	18	328.09*
DSPS[2]	18		333-339▪			
DMPS-d54	14			DMPC-d54	14	293.15*
DPPS-d70	16			DPPC-d62	16	310.12*
DSPS-d70	18	337•	332-341	DSPC-d70	18	323.52*

1. DPPS MLVs in 0.1M NaCl. 2. DSPS MLVs dissolved in H_2O. Values marked with √ were obtained from Browning and Seelig, 1980 (Browning & Seelig, 1980). Values marked with † were obtained from Avanti lipid.com. Values marked with * were obtained from Engle, A.S et al, 1985(Guard-Friar et al., 1985). Temperature range marked with ▪ was obtained by the ^{31}P NMR spectroscopy shown in Chapter 4.1. Value marked with• were obtained from the M_1 analysis of the ^{2}H NMR spectroscopy in Fig 4.4 in Chapter 4.2.

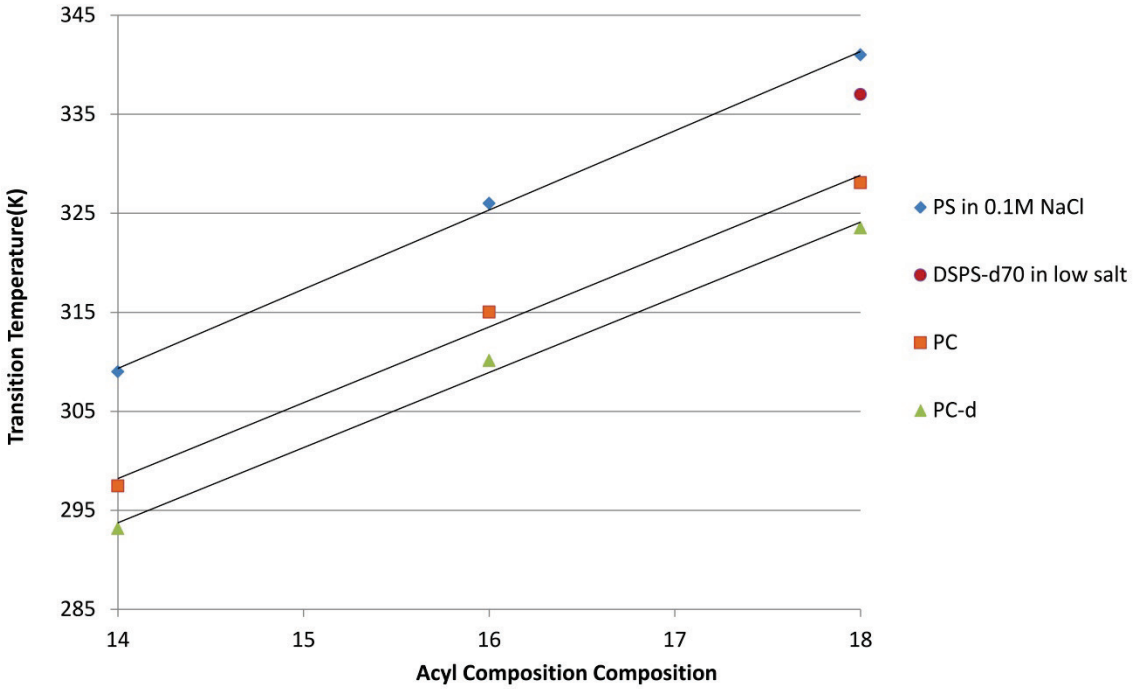

Figure 4.8. Deuteration effect on T_m of the PC and PS membrane.
T_m is chain length dependent for saturated phosphatidylserine (PS) and phosphatidylcholine (PC). Data marked with the red dot labelled "DSPS-d70 in low salt" was obtained in this study. Deuteration effect of the PC data was obtained from Guard-Friar et al 1985. (Guard-Friar et al., 1985).

In summary, (a) Phase transition temperature is sensitive to the headgroup and the chain composition of the lipid. An increase in chain length generally results in higher T_m values. (b) DSPS-d70 undergoes a broad phase transition from 332-341K and T_m is at 337-338K. This is ~4 degrees lower than the 341K T_m reported in the literature for non deuterated DSPS. The same trend was observed in PC such that when chains are perdeuterated, T_m is lowered by 4 degrees.

In conclusion, studying the thermal properties of on DSPS and DSPS-d70 model membranes allow us to lay a foundation for studying the XTC2/DSPS-d70 model membrane introduced in Chapter 5.

Chapter 5. Results: XTC2/DSPS Model Membrane

This chapter presents the results of the study of the interaction between DSPS-d70 and the cationic lipid XTC2 in an equimolar ratio. Three different parameters were varied: pH; temperature; and salt concentration. This chapter will show the results for XTC2/DSPS in pH 8.4 in HEPES and pH 4.75 NaOAc buffers. The pH 8.4 data will be compared with the DSPS model membrane results from Chapter 4. At pH 4.75, the system was studied at three different salt concentrations. The pH 4.75 data will be compared with the pH 8.4 result for the low salt concentration. Then the effect of salt on the membrane at pH 4.75 will be explored. ^{31}P NMR and ^{2}H NMR spectra will be analyzed as a function of temperature under each set of conditions.

5.1. At pH 8.4: Observe Gel to Liquid Crystalline Phase Transition

We first compare ^{31}P and ^{2}H NMR spectra at three temperatures chosen to represent the overall behaviour of the XTC2/DSPS membrane. Phosphorus NMR spectra show the XTC2/DSPS model membrane at pH 8.4 is primarily in the bilayer (L_α) phase coexisting with a certain amount of an isotropic phase. Figure 5.1 shows the ^{31}P NMR spectra of the equimolar of XTC2/DSPS model system in HEPES buffer at pH 8.4 at temperatures of 298, 310 and 333K. The observed ^{31}P NMR spectra arise from the phosphoserine headgroups of DSPS. Part (a-c) of Figure 5.1 shows that at pH 8.4, the XTC2/DSPS system produces ^{31}P NMR spectra mainly characterized by a lamellar phase signal with a low frequency, high intensity peak on the right and a smaller shoulder at higher frequency. There is little change upon heating the membrane from 298 to 310K. As the temperature is increased to 333K, Fig 5.1 (c) demonstrates a reduction in the width of the ^{31}P NMR spectrum and a flattening of the smaller higher frequency shoulder. This is because the increasing temperature leads to faster tumbling

of the lipid headgroup which in turn leads to smaller chemical shift anisotropy $\Delta\sigma$ from -45 to -30 ppm on the lower field and 70 to 55 ppm on the higher field. From the information obtained from the phosphorus headgroup, it can be seen that there is little change when when increasing temperature and keeping the pH constant.

The isotropic peak at zero frequency may be due to the formation of microstructures such as micelles, small oily droplets, cubic phases, small vesicles or the solvent. The ^{31}P NMR spectra indicate it may be due to small vesicles.

The ^{2}H NMR spectra of the XTC2/DSPS-d70 model system demonstrate the existence of gel phase at temperatures of 298 and 310K. In Figure 5.2 part (a-c) are shown ^{2}H NMR spectra of XTC2/DSPS-d70 are seen to be in bilayer phases (gel and L_{α}) and include an isotropic peak whose area increases with temperature. The ^{2}H NMR spectra observed are due to two saturated acyl chains of DSPS-d70. As the sample is heated to 310K, the shoulder visible at +/-25 kHz at 298K becomes less prominent. As well, the intensity of the gel phase component decreases. As the temperature is increased to 333K, the spectrum (c) contains no gel phase as characterized by the flat baseline at +/- 60 kHz. Instead, a liquid crystalline phase (L_{α}) signal is present as characterized by broadened 90° peaks shoulders in the range of +/-19 kHz to +/-40 kHz. The gel phase component can be seen in the part a and b at 298 and 310K respectively.

We compared the ^{31}P and ^{2}H NMR spectra of the XTC2/DSPS system and found that 1) the ^{2}H NMR gel phase spectrum reflects the lack of axially symmetric (rotation) motion in the membrane. This is a very clear indication of the gel phase. 2) The ^{31}P NMR gel phase spectrum is broader but not qualitatively different from the liquid crystalline spectrum. The headgroup motion is less affected by the transition than the chains are. For example, the observed 310K gel phase in the ^{2}H NMR spectrum was not obvious in the ^{31}P NMR spectrum suggesting that the acyl chains are in a stiff mode below 310K. At 333K, the growing isotropic peak seen in the ^{2}H NMR spectra is more obvious and this matches the isotropic peak seen in the ^{31}P NMR spectra Fig (5.1 a-c).

(a) 298K

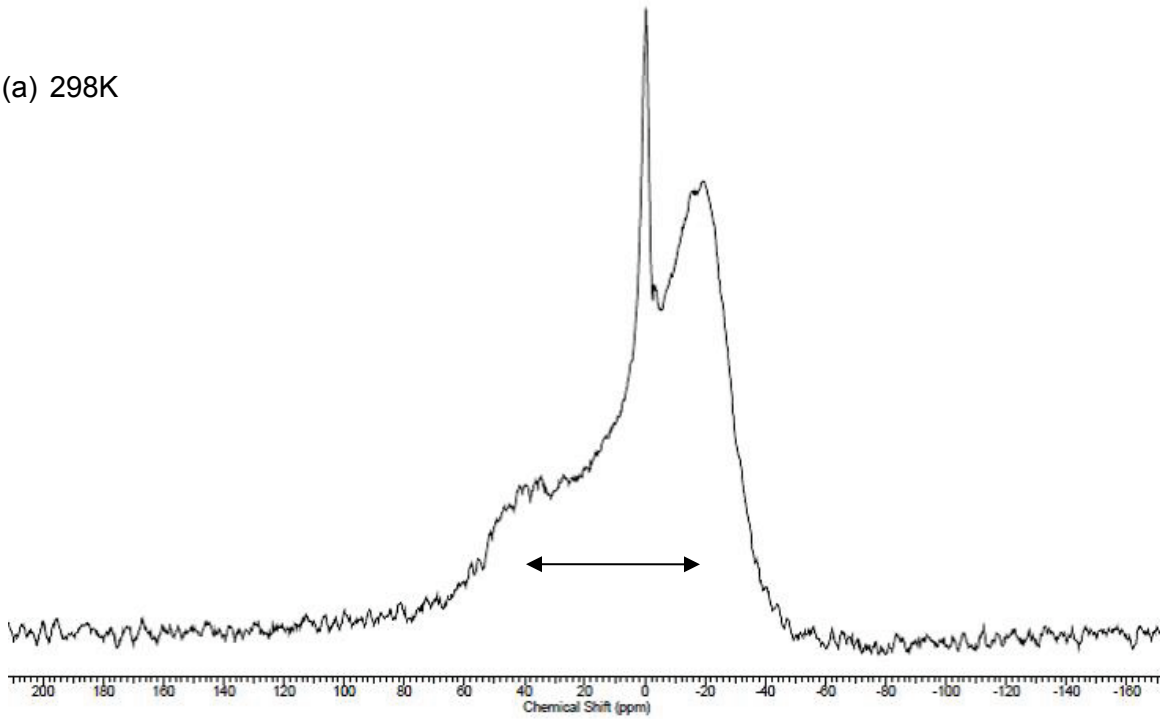
200 180 160 140 120 100 80 60 40 20 0 -20 -40 -60 -80 -100 -120 -140 -160
Chemical Shift (ppm)

(b) 310K

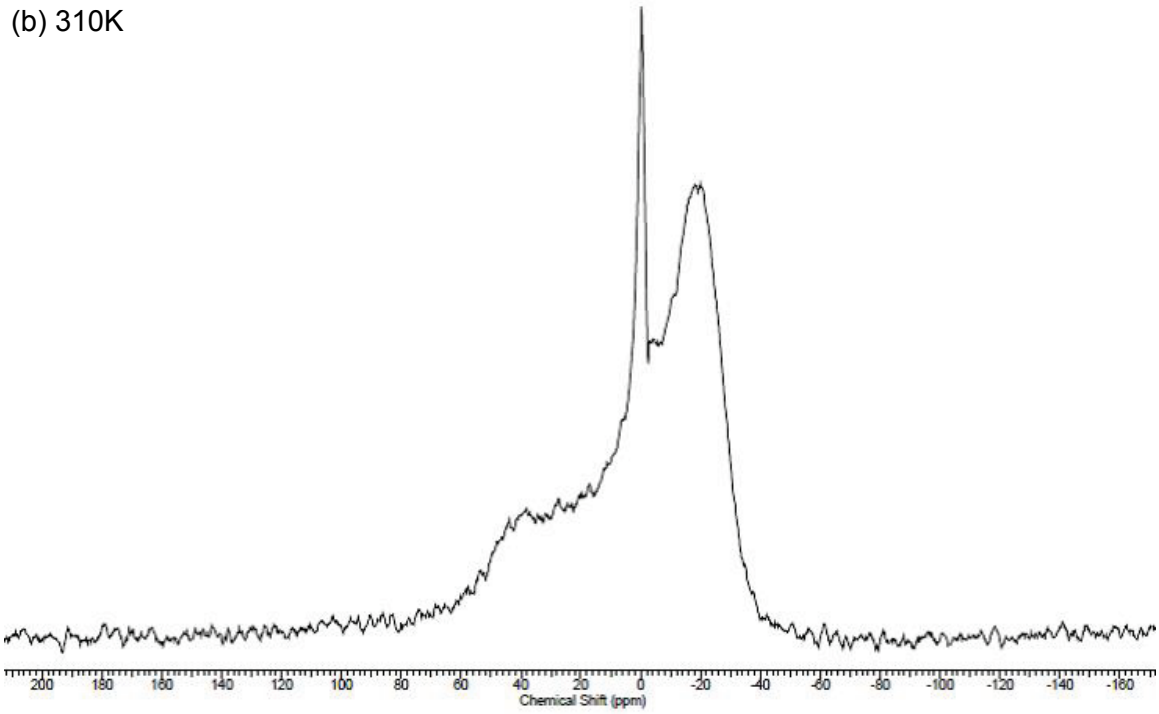
200 180 160 140 120 100 80 60 40 20 0 -20 -40 -60 -80 -100 -120 -140 -160
Chemical Shift (ppm)

(c) 333K

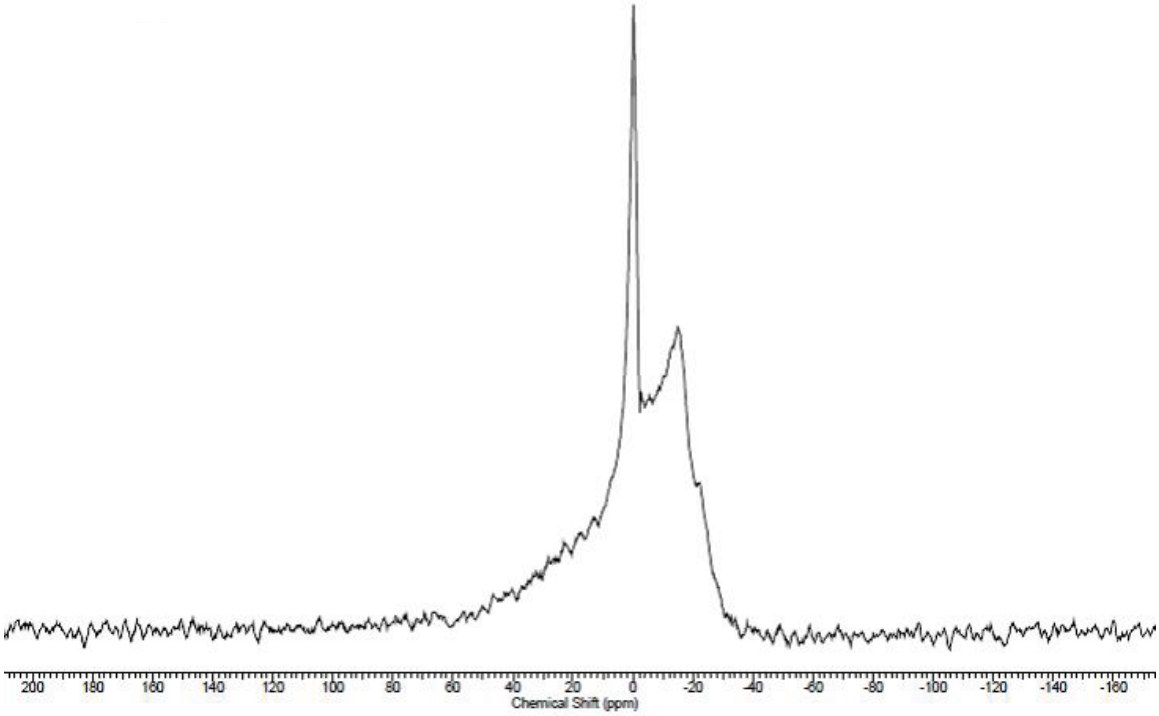

Figure 5.1. ^{31}P NMR spectra of XTC2/DSPS membrane at pH 7.4.
(a-c) shows ^{31}P NMR spectra of XTC2/DSPS membrane as a function of temperature. Arrow in (a) demonstrates the measurement of $\Delta\sigma$ from 0° shoulder in the high field to the 90° peak in the low field.

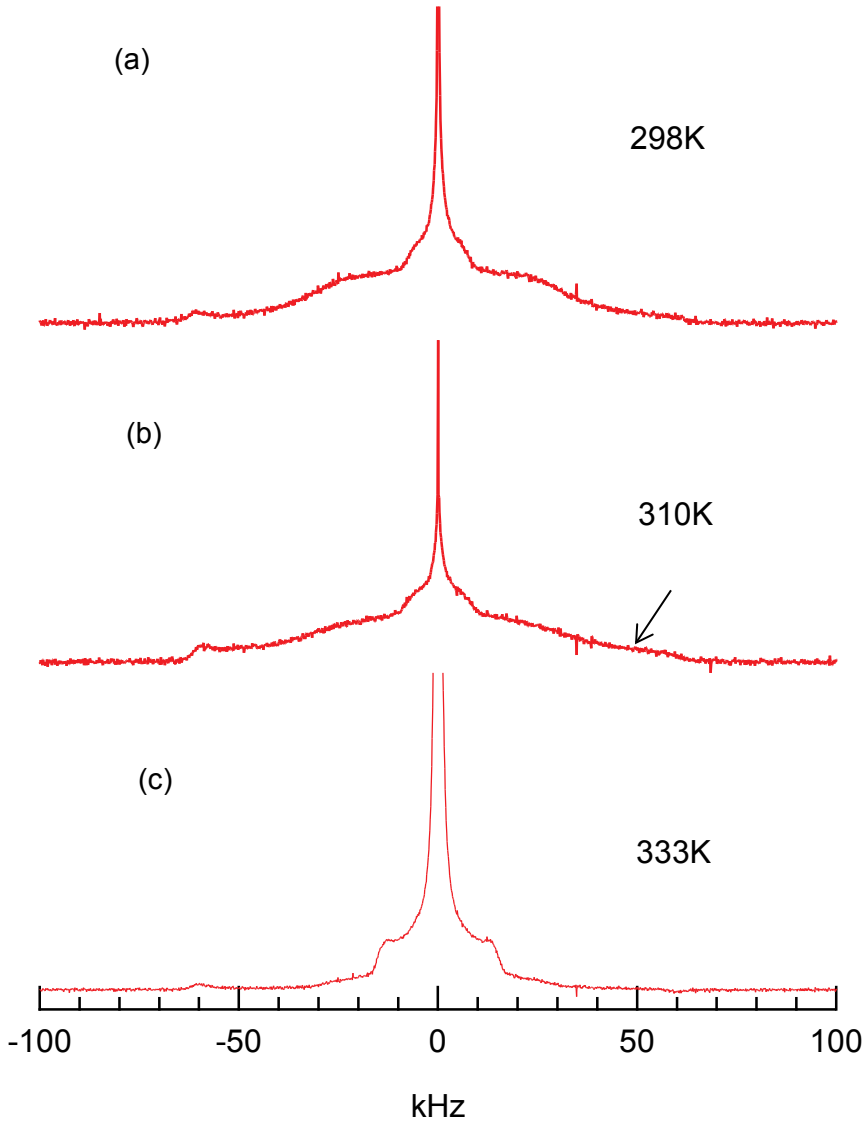

Figure 5.2. **^{2}H NMR spectra of XTC2/DSPS-d70 pH 8.4 overview.**
(a) At 298K sample is predominantly in a gel phase. (b) At 310K the sample is in gel phase with a growing isotropic peak. (c) At 333K the sample is in a liquid crystalline phase with isotropic, showing no gel phase component. The arrow points out the end of the 0° shoulder.

We now discuss the effect of temperature on the phase transition of XTC2/DSPS in some detail. Deuterium NMR spectra show XTC2/DSPS in HEPES buffer at pH=8.4 undergo gel to L_α phase transition in the presence of an isotropic phase in the range of 313-333K. In Figure 5.3 shows ^{2}H NMR spectra of XTC2/DSPS-d70 in gel phase at temperatures from 283-333K. Over this temperature range the sample is mainly in the gel phase, with subtle changes in the spectral shape as the membrane is heated from

283 to 323K. At 333K, as already discussed, a L_α phase spectrum is observed. The isotropic component is small at 293K and gradually increases with temperature. The observed spectra reveal the rigid lipid chains become more mobile and melt as indicated by the reduction of width from +/-63 kHz to +/-40 kHz at 283K and 333K respectively. As the gel phase is melting, more components are melted into liquid crystalline phase. Thus, the gel to L_α phase transition is in the range of 323-333K.

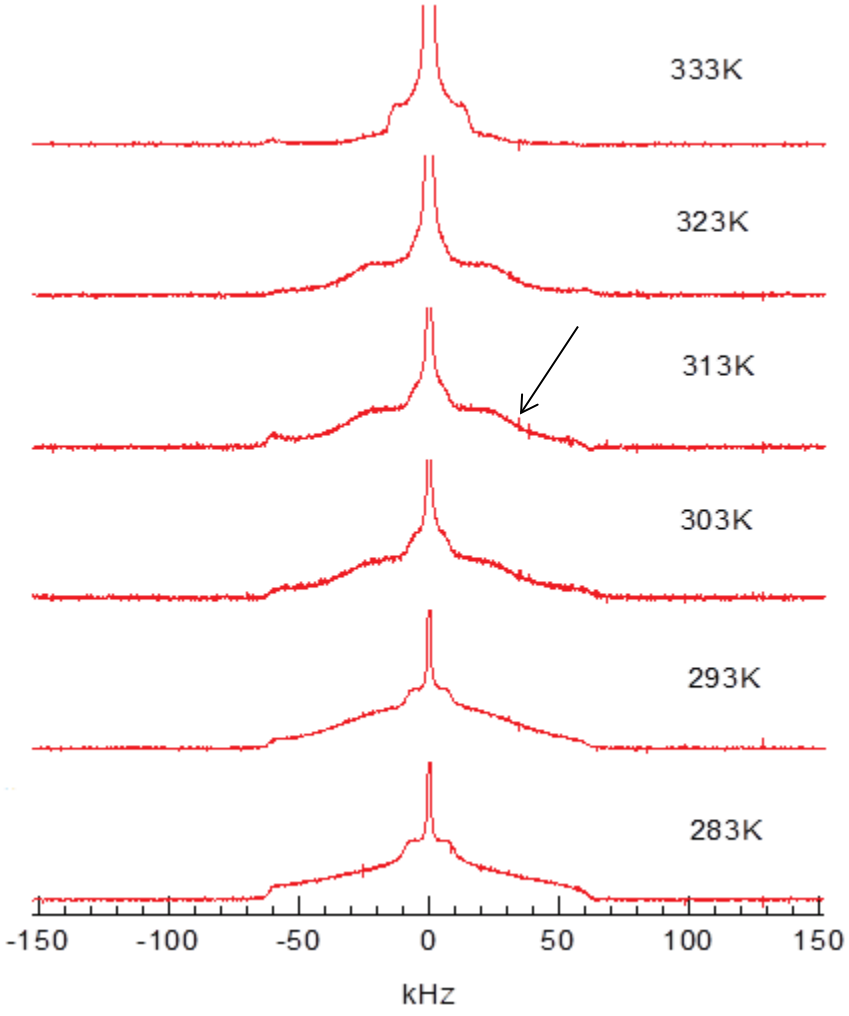

Figure 5.3. **^{2}H NMR spectra of XTC2/DSPS-d70 pH 8.4 every 10 degree.**
The arrow indicates the shoulder decreases as temperature increases.

The first moment M_1 value usually enables a calculation of T_m. The first moment M_1 measures the average width and for the XTC2/DSPS sample, it is very much influenced by the isotropic component. So in contrast to DSPS M_1 vs. T, M_1 vs. T for

XTC2/DSPS shown in Figure 5.4 does not allow us to quantitatively measure T_m. As shown in Figure 5.4, the M_1 value for the XTC2/DSPS model done in an increasing temperature manner (shown in diamonds) and the decreasing temperature rerun (shown in squares) were plotted against temperature. The steepest slope occurred between 323K and 333K as indicated with an arrow. This is the region where T_m is likely to be located. T_m obtained from M_1 values agree with the T_m obtained by the ^2H NMR spectra shape analysis. Also, it is worth noting that the XTC2/DSPS phase transition is reversible and experimentally reproducible. As shown in Figure 5.4, the two sets of M_1 data obtained by different hysteric heating and cooling processes have significant overlap, especially within the range of 300-310 K.

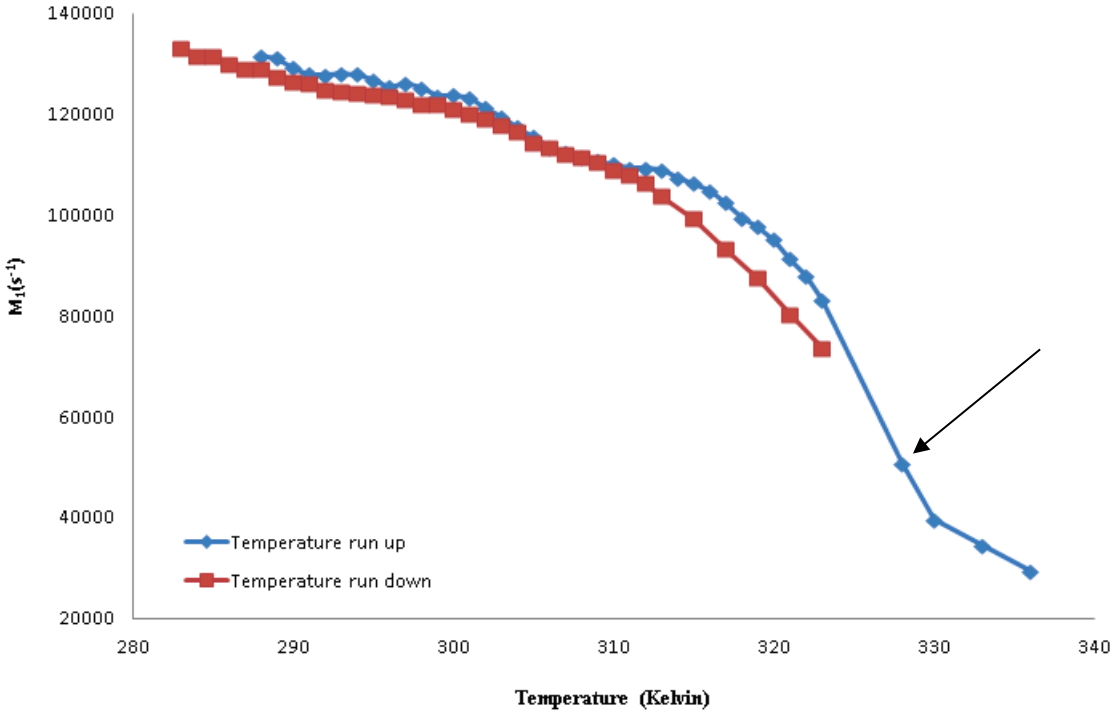

Figure 5.4. M_1 plot for XTC2/DSPS-d70 in pH 8.4 HEPES buffer.
Temperature ranges from 283K to 338K.

The ^2H NMR spectral shape changes suggest the melting temperature T_m for XTC2/DSPS in HEPES buffer at pH=8.4 around 328K. Figure 5.5 shows the ^2H NMR spectra of XTC2/DSPS-d70 from the beginning to the end of the gel to liquid crystalline phase (L_α) phase transition. It can be seen from part b, as temperature is increased to 328K, the L_α shoulder begins to emerge characterized by the +/-20 kHz shoulder on top

of the gel phase shoulder span between +/-50 kHz. As shown in part c, at temperature 330 K the shoulder at +/-40 kHz become more prominent, and the gel phase and L_α phase are at almost equal proportions. In part d, at 336K, the spectrum is almost completely flat at +/-60 kHz indicating an absence of gel component. The shoulder at +/-40 kHz arises from the pure L_α phase and indicates that the end of the transition for the model system is at 336K. Melting occurs between 328 and 336 K (55-63°C). It is worth noting that the transition temperature was significantly lowered than the DSPS model membrane (~66°C).

In summary, the XTC2/DSPS-d70 model membrane at pH 8.4 undergoes gel/isotropic to L_α/isotropic phase transition around 328-333K. At neutral pH, the lipid mixture only undergoes a gel to liquid crystalline phase transition, with a minimal isotropic phase. No H_{II} phase was observed.

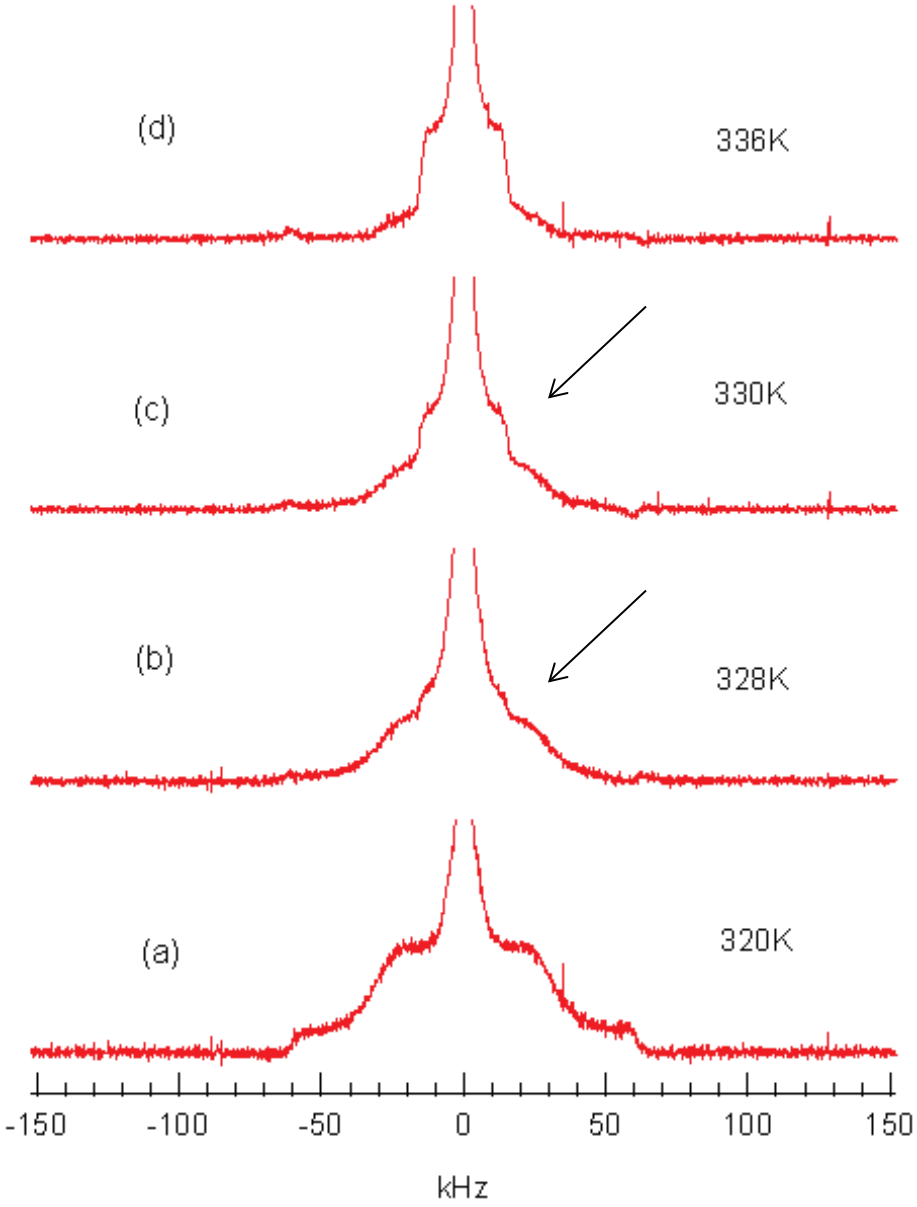

Figure 5.5. ^{2}H NMR spectra show XTC2/DSPS-d70 pH 8.4 gel to L_α transition.
Majority of the lipid mixture is in gel phase, starting to going to liquid crystalline phase at 328K and more L_α phase is observed at 330K and pure L_α phase is observed at 336K.

5.2. At pH 4.75: XTC2/DSPS model membrane undergoes a gel to H_{II} phase transition

5.2.1. ^{31}P NMR spectroscopy of XTC2/DSPS in pH 4.75 sodium acetate buffer undergo bilayer to H_{II} phase transition around 293K.

Figure 5.6 shows the phosphorus NMR spectra of XTC2/DSPS in a model membrane at pH 4.75 at temperature 310, 298, 293, 288K. The observed ^{31}P NMR spectra are due to the phosphoserine headgroup. The spectra were acquired by sequential cooling of sample. Part (a) of Figure 5.6 shows that at 310K the XTC2/DSPS model system is in an H_{II} with a predominant high frequency (left) maximum (+8 ppm) and a smaller low frequency (right) shoulder (-17 ±1ppm). As temperature decreased to 298K, we observed the same pattern (+9 ppm to -18 ppm) except for the baseline of the spectra which became pronounced as seen in part b.

At 293K, two peaks at +9 and -20 ppm representing the H_{II} and bilayer phases are superimposed. At 288K, a typical lamellar phase spectrum, characterized by a low field maximum (-20 ±1ppm) and high field small shoulder (39±3 ppm) is observed, indicating that the system is in bilayer form (Fig 5.6 (d)). The bilayer spectrum span from -20 ppm to +40 ppm, this is twice the magnitude of the residual chemical shift anisotropy (CSA) of the H_{II} phase spectrum which spans from +10 to -20 ppm. The ^{31}P NMR chemical shift anisotropy of the H_{II} phase is almost exactly -0.5× that of the bilayer phase. The reverse in sign and a doubling in width of the ^{31}P NMR spectra are due to the formation of bilayer phase.

(a) 310K

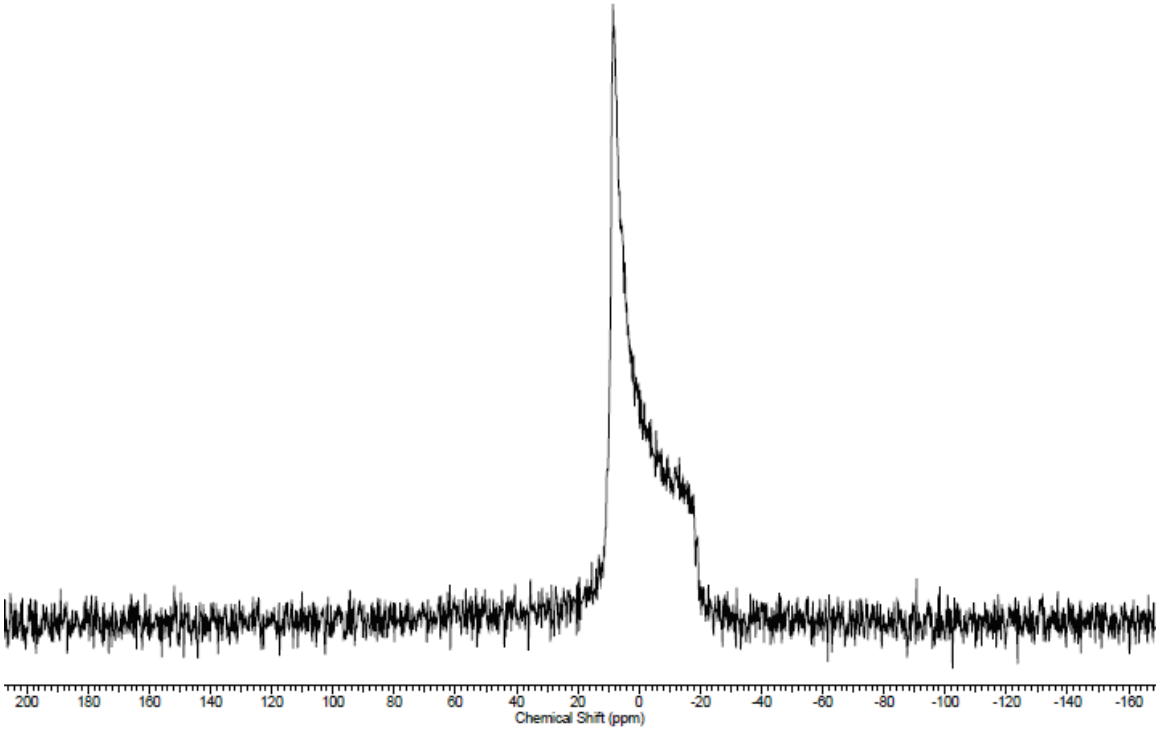
200 180 160 140 120 100 80 60 40 20 0 -20 -40 -60 -80 -100 -120 -140 -160
Chemical Shift (ppm)

(b) 298K

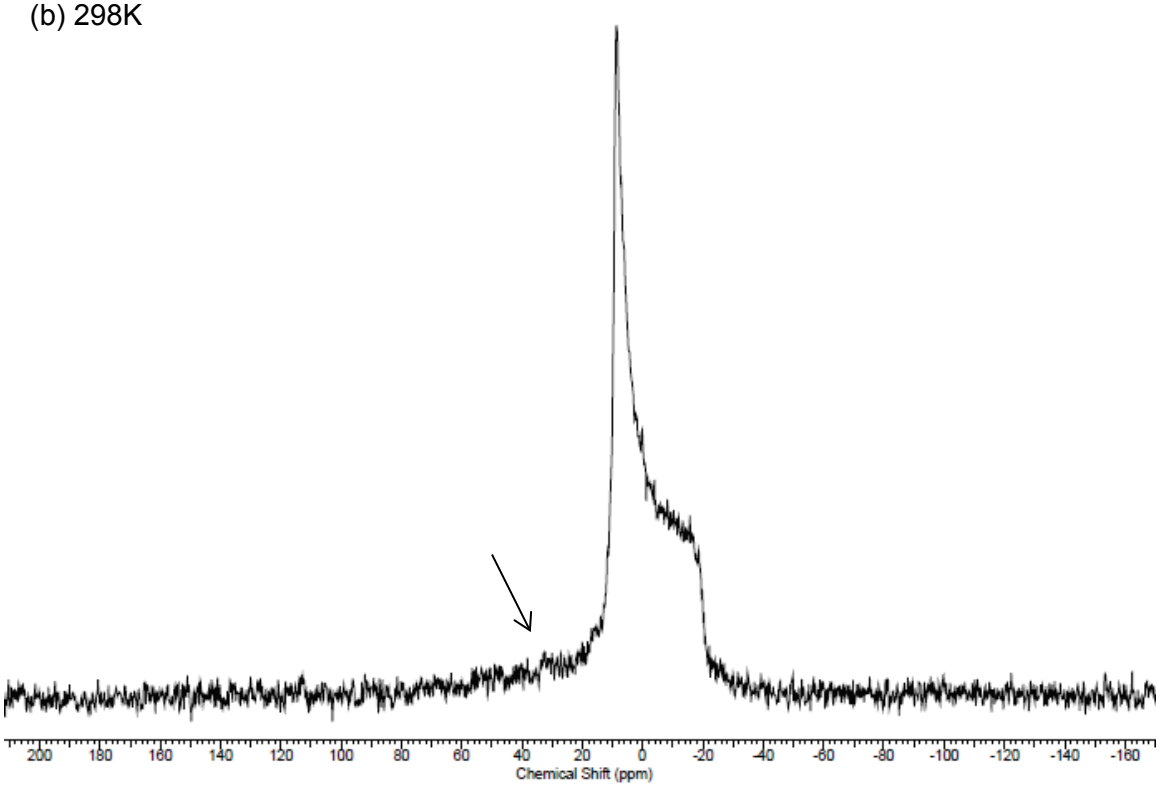
200 180 160 140 120 100 80 60 40 20 0 -20 -40 -60 -80 -100 -120 -140 -160
Chemical Shift (ppm)

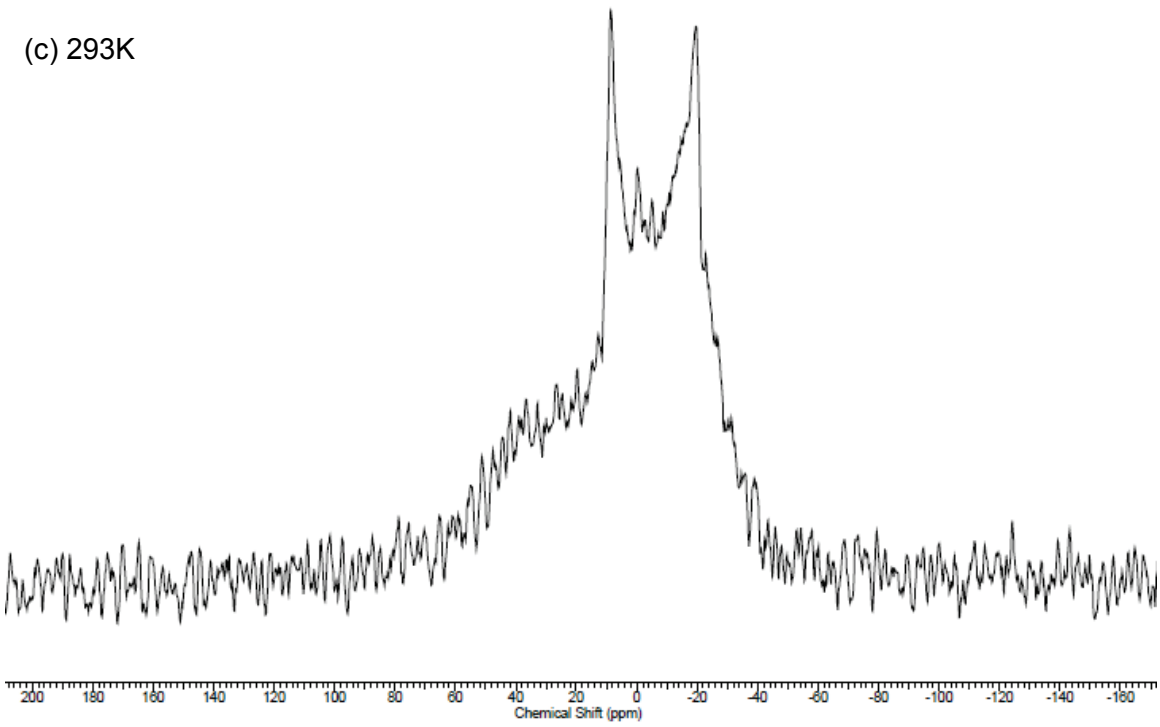

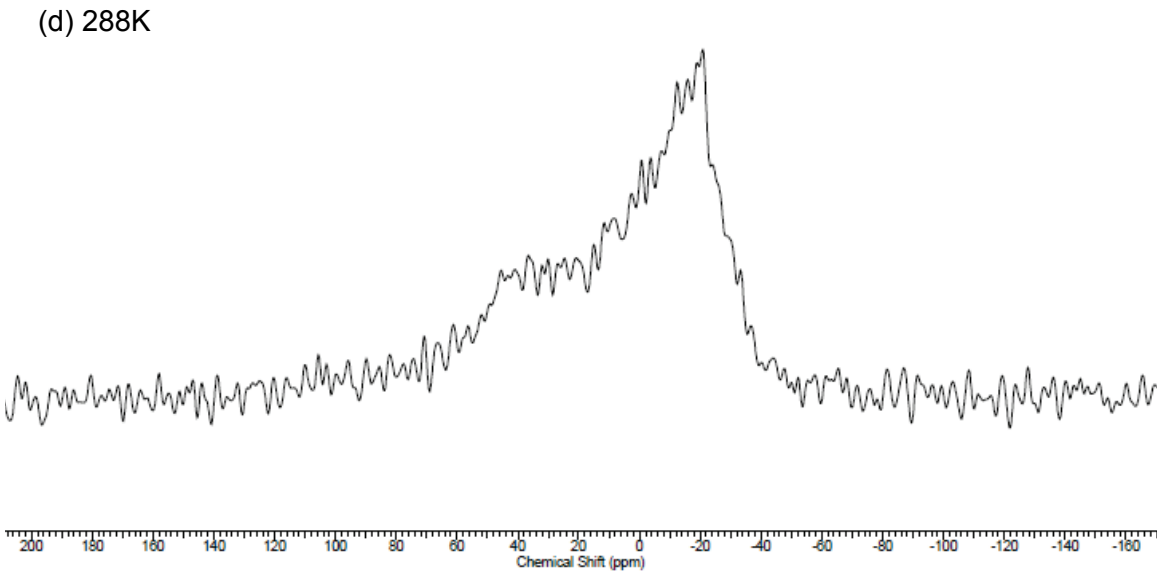

Figure 5.6. ^{31}P NMR spectra of XTC2/DSPS pH 4.75 in 0.25 M NaOAc buffer.
(a) At temperature 310K membrane is in H_{II} phase. (b) At 298K membrane is in a H_{II} form. (c) At temperature 293K membrane is in a bilayer and H_{II} coexisting phase. (d) At temperature 288K membrane is in a bilayer phase. Arrow in (b) indicates the formation of the gel phase.

5.2.2. Temperature dependence of ^{2}H NMR spectra of XTC2/DSPS-d70 at pH 4.75 in sodium acetate buffer

Deuterium NMR spectra of the XTC2/DSPS-d70 model membrane reveal acyl chain packing information. In this experiment the temperature was first increased from 298K to 307K then decreased from 293K to 288K. In agreement with the ^{31}P NMR data, at 298K, we observed mainly an H_{II} spectrum with a trace amount of gel phase not visible in Fig 5.7 (b). It becomes pure H_{II} at 307K shown in Fig 5.7 (a). As temperature is lowered to 293K, the amount of gel phase increased compared to the 298K spectrum (Fig 5.7 c). At 288K, we didn't observe the sharp edge of the H_{II} peak, instead, a more rounded line shape at +/-5 kHz indicating the increasing gel component (Figure 5.7 d). We observed the gel phase coexists with H_{II} phase at 288K shown in Fig 5.7 (d). In contrast to the ^{31}P NMR experiment which increases the temperature to 310K, this experiment ended at 307K.

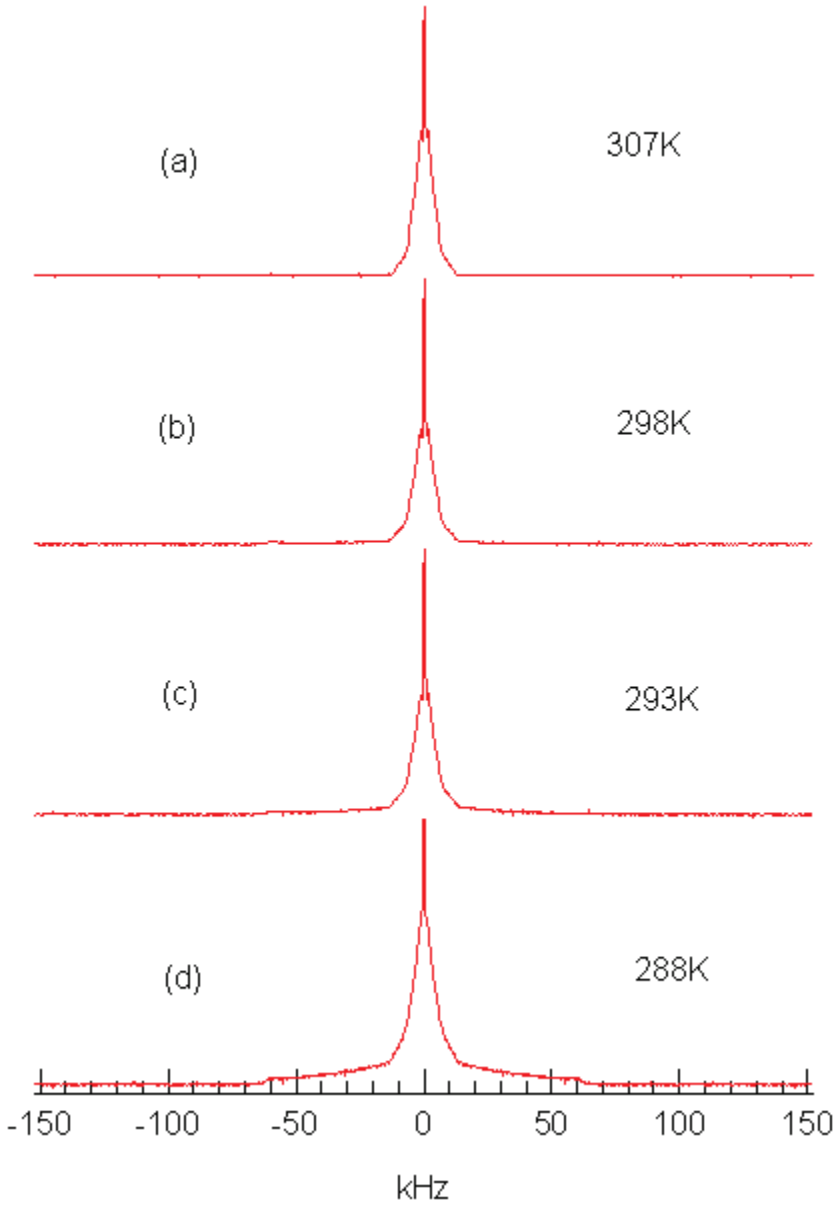

Figure 5.7. ^{2}H NMR spectra of XTC2/DSPS-d70 pH 4.75 in 0.25M NaOAc.
(A-c) At 307, 298 and 293K membrane is in a H_{II} phase. (d) At 288K membrane is in most of the H_{II} phase and little gel phase.

^{31}P and ^{2}H NMR spectra compared at 310/307K, 298/298K and 293/293K agree with each other. One difference is that H_{II} phase is present at 288K seen in Fig 5.7 (d) was not seen in Fig 5.6 (d). This may be because the H_{II} phase was formed in the 298K on the ^{2}H NMR but not on ^{31}P NMR and when T was lowered to 288K the H_{II} phase was too stable to revert to the bilayer phase.

5.2.3. De-Paked spectrum for H_{II} phase

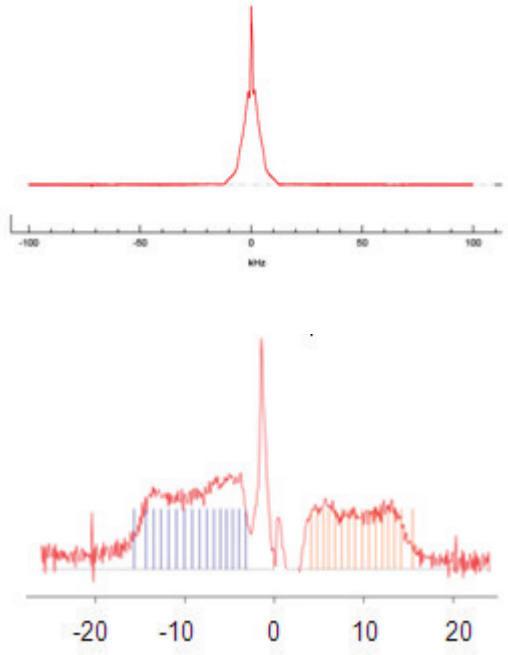

Figure 5.8. ^{2}H NMR dePaked spectrum of DSPS-d70/XTC2 at 307K pH=4.75
The dePaked spectrum was obtained by 100,000 scans and 5 µs dwell time. The innermost boundary was picked for the terminal methyl group at +/- 5 kHz and outer boundary was picked at around +/- 18 kHz. Blue and red vertical lines show the bins.

As shown in Figure 5.8, some line distortions are seen in the middle of the spectrum. T_1 of the methyl groups is longer than the T_1 of the methylene deuterons and have caused distortions because the T_1 was more than 5× the repetition time. Blue color shows 16 bins of carbons that attached with deuterons. In the de-Paked spectrum of DSPS-d70 each carbon splitting gradually increases.

The Order Parameter Profiles S_{CD} of XTC2/DSPS-d70 at pH 4.75 were obtained from the de-Paked spectrum and listed in Table 5.1. The S_{CD} were plotted in Fig. 5.9.

Table 5.1. S_{CD} for XTC2/DSPS-d70 pH 4.75 at 307K.

Carbon#	X-left	X-right	distance	Δv	Δv (kHz)	S_{CD}
18	2246.09	1562.5	3808.59	1904.3	1.9043	0.01511
17	2734.09	3394.5	6128.59	3064.3	3.0643	0.02432
16	3358.09	3950.5	7308.59	3654.3	3.6543	0.029
15	3946.09	4514.52	8460.61	4230.31	4.23031	0.03357
14	4510.08	5030.52	9540.60	4770.3	4.7703	0.03786
13	5114.08	5586.52	10700.60	5350.3	5.3503	0.04246
12	5710.08	6242.52	11952.60	5976.3	5.9763	0.04743
11	6350.08	6866.52	13216.60	6608.3	6.6083	0.05245
10	7050.08	7478.52	14528.60	7264.3	7.2643	0.05765
9	7726.08	8134.52	15860.60	7930.3	7.9303	0.06294
8	8454.08	8798.52	17252.60	8626.3	8.6263	0.06846
7	9198.08	9414.52	18612.60	9306.3	9.3063	0.07386
6	9938.08	10026.5	19964.60	9982.3	9.9823	0.07922
5	10654.08	10582.5	21236.60	10618.3	10.6183	0.08427
4	11330.08	11134.5	22464.60	11232.3	11.2323	0.08915
3	12054.08	11782.5	23836.56	11918.3	11.9183	0.09459
2	13162.08	12894.5	26056.60	13028.3	13.0283	0.1034

There are total 18 carbons in each chain with no deuteron attached to carbon #1, starts from C#2 to C#18 with 17 carbons in all. The splitting for methyl group C#18 was directly measured from the two major peaks.

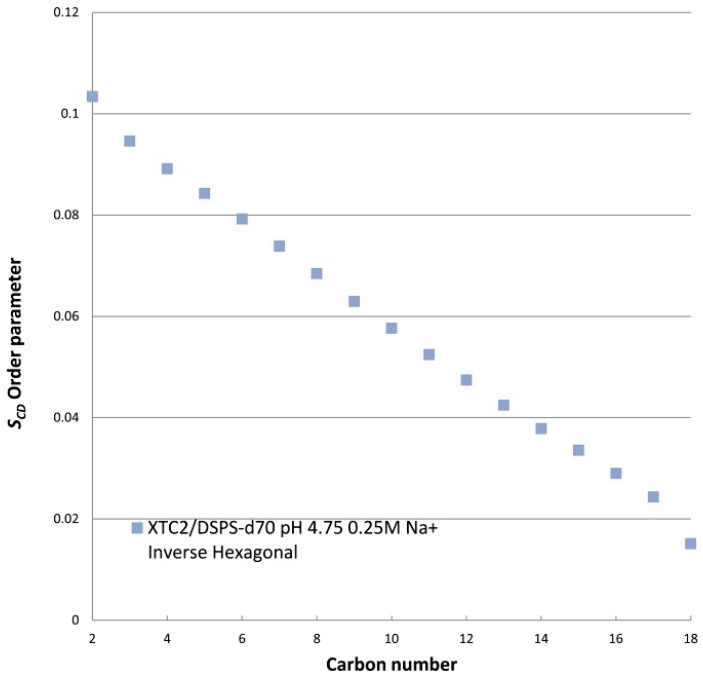

Figure 5.9. S_{CD} for XTC2/DSPS-d70 at pH 4.75 at 307K.
The S_{CD} is plotted as a function of carbon position from 2 to 18.

At low pH, XTC2/DSPS-d70 shows a steadily increasing proportion of inverse hexagonal phase as the temperature increases from 283K to 307K. No significant amount of isotropic phase was observed at any temperature. By plotting M_1 vs. T we can monitor changes to the spectral shape throughout the phase transition.

M_1 value shows a broad gel to H_{II} phase transition at below 283 to 304K (Fig. 5.10). For temperature from 293K to 303K, the spectra show only a small gel phase signal.

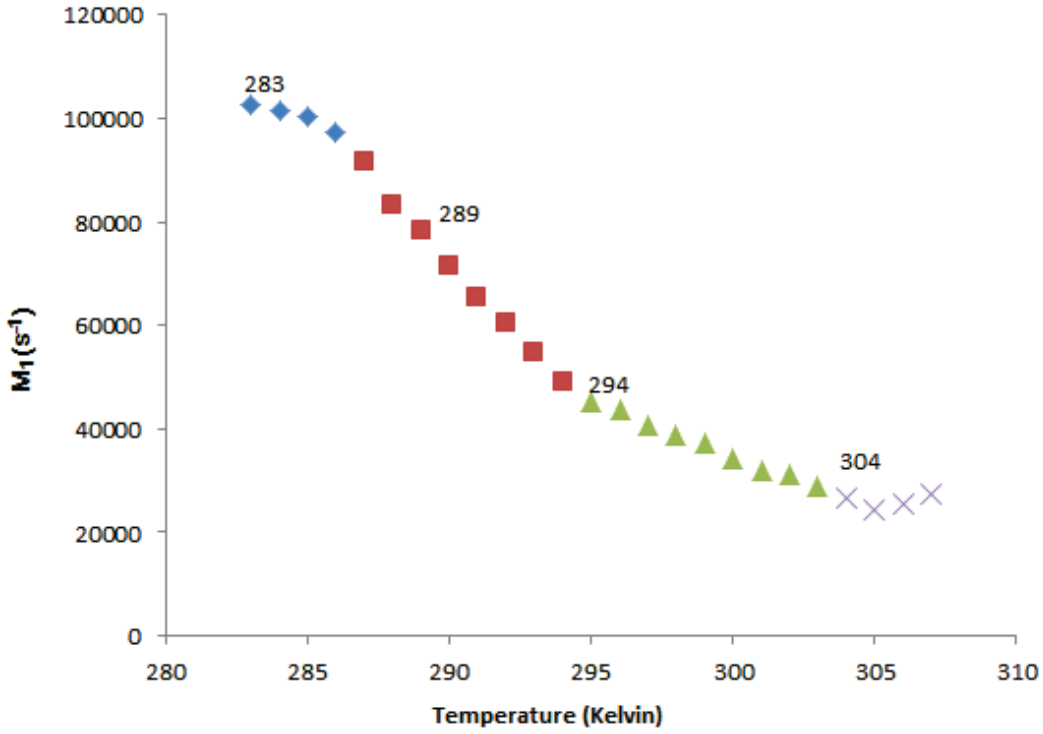

Figure 5.10. M_1 plot for XTC2/DSPS-d70 at pH of 4.75.
The model membrane was in 0.25 M sodium acetate buffer. The show a broad phase transition from 287 to 304K.

Assuming that a maximum of only two phases are present at each temperature, we can estimate the fraction of H_{II} signal as the sample is heated (Fig. 5.11). The M_1 of the gel phase at neutral pH is 131620.7s^{-1} and M_1 of the H_{II} measured from this sample 26732.8 s^{-1} that we estimated the fraction of H_{II}. The % of each component can be calculated by

6. Percentage Gel

$$M_1 = (x)(\text{Gel } M_1) + (1-x)(H_{II}\ M_1).$$

As shown in Table 5.2, the 49% gel is at T=289K. This assumes that DSPS-d70 and XTC2 are participating equally in both phases

Table 5.2. Fraction of the gel phase in the XTC2/DSPS-d70 pH 4.75..

T(K)	M_1	Gel M_1	$H_{II}\ M_1$	% Gel
283	102539.8	131620.7	26732.8	72.3
284	101539.2	131620.7	26732.8	71.3
285	100308.3	131620.7	26732.8	70.1
286	97179.1	131620.7	26732.8	67.2
287	91626.9	131620.7	26732.8	61.9
288	83075.9	131620.7	26732.8	53.7
289	**78425.2**	**131620.7**	**26732.8**	**49.3**
290	71629.4	131620.7	26732.8	42.8
291	65507.3	131620.7	26732.8	37.0
292	60456.9	131620.7	26732.8	32.2
293	54591.1	131620.7	26732.8	26.6
294	48975.3	131620.7	26732.8	21.2
295	45352.6	131620.7	26732.8	17.8
296	43844	131620.7	26732.8	16.3
297	40662.5	131620.7	26732.8	13.3
298	38782.9	131620.7	26732.8	11.5
299	37185.7	131620.7	26732.8	10.0
300	34183.9	131620.7	26732.8	7.1
301	32062.7	131620.7	26732.8	5.1
302	31284.4	131620.7	26732.8	4.3
303	29008.6	131620.7	26732.8	2.2
304	**26732.8**	**131620.7**	**26732.8**	**0.0**
305	24397.2	131620.7	26732.8	-2.2
306	25545.7	131620.7	26732.8	-1.1
307	27325	131620.7	26732.8	0.6

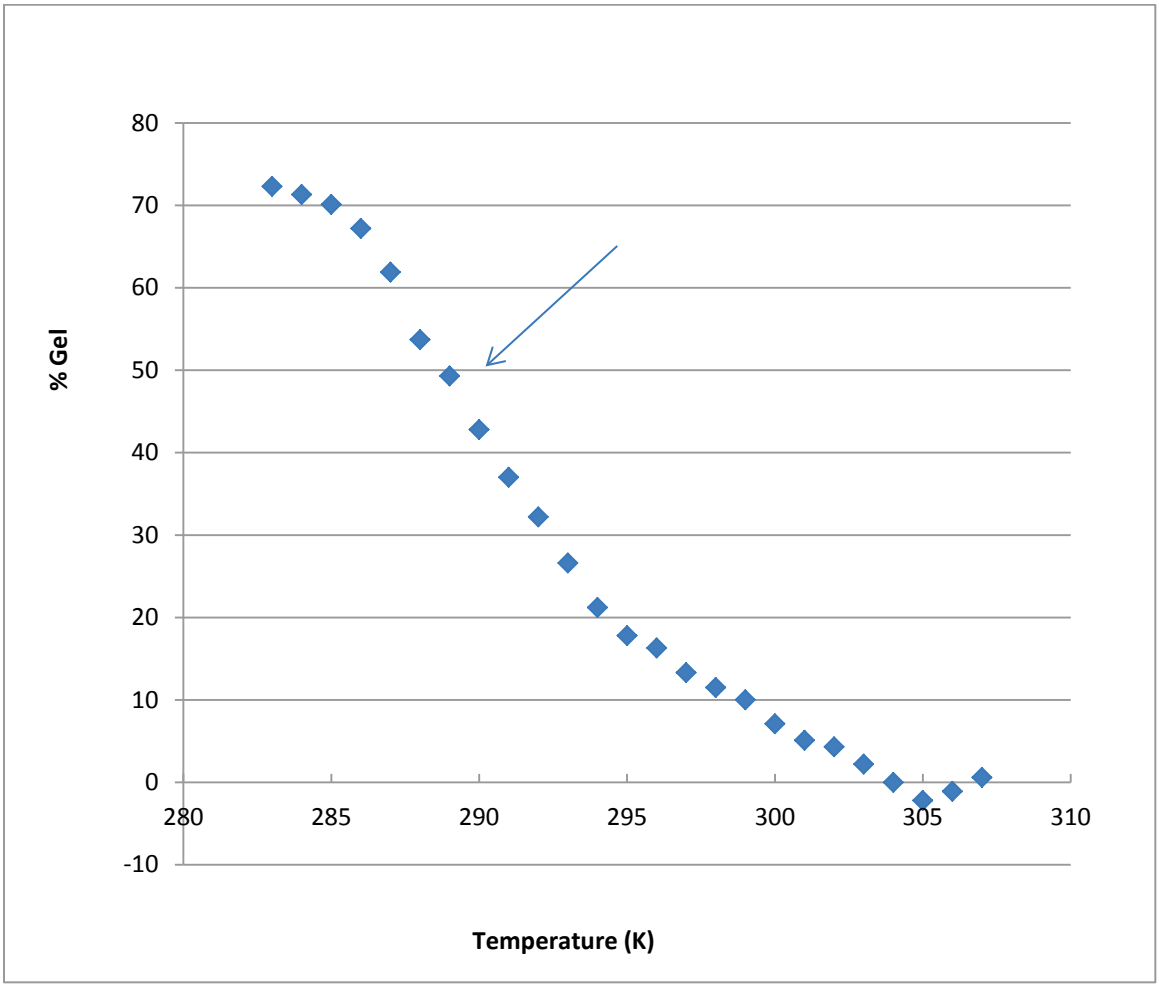

Figure 5.11. The percentage gel calculated from equation 6

. The percentage gel is calculated from equation $M_1 = (x)(\text{Gel } M_1) + (1-x)(H_{II}\ M_1)$. The 50% gel is located at 289K and 100% H_{II} is located at 304K.

5.3. Discussion of the pH dependence of the XTC2/DSPS-d70 model system

We compared DSPS-d70 and XTC2 in both pH 8.4 in HEPES buffer and pH 4.75 in sodium acetate buffer with temperature. The ^{2}H NMR spectra for 283K, 298K and 307K are shown in figure 5.12.

At pH 8, ^{2}H NMR spectra show mainly gel phase with a growing isotropic phase from 298K to 307K (Figure. 5.12 a-c). In comparison, at low pH there is a narrow peak within +/-15 kHz and a broad component within +/- 63 kHz (Figure. 5.12 d-f). This

indicates a coexisting gel and H_{II} phase. When the temperature is increased to 307K, the gel phase turns into the H_{II} phase completely with no broad component observed at +/- 63 kHz.

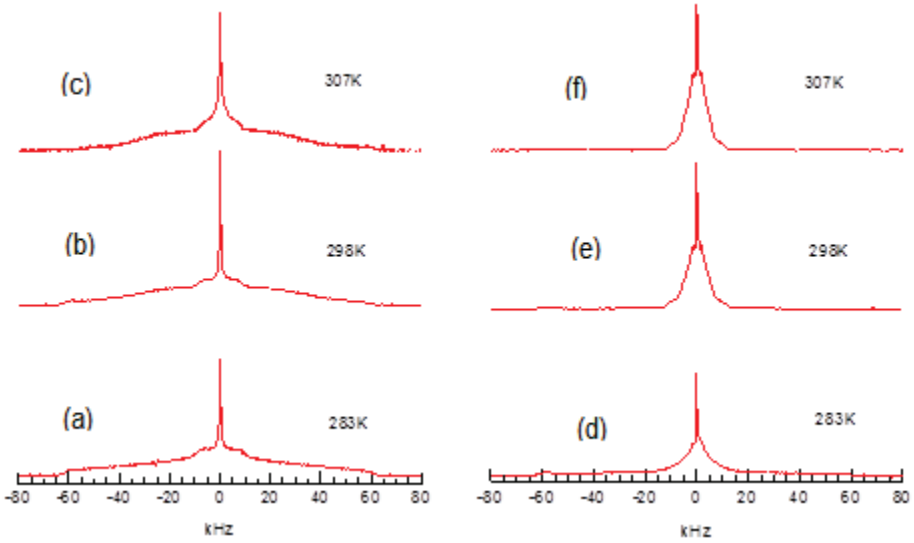

Figure 5.12. Comparison of XTC2/DSPS-d70 pH 8.4 and 4.75 spectra shape.
^{2}H NMR spectra of DSPS-d70/XTC2 in pH 8.4 HEPES buffer at (a) 283K, (b) 298K, and (c) 307K. On the right, (d) 283K, (e) 298K and (f) 307K in sodium acetate buffer pH 4.75.

As shown in the Figure 5.12, pH has effect on the phase transition of XTC2/DSPS model membrane. At pH 4.75, the XTC2 headgroup becomes protonated, adopts a positive charge. The anionic DSPS and cationic XTC2 experience electrostatic interaction. The headgroup are closed to each other form an ion pair, making the area of the headgroup region smaller than the area of the acyl chains, i.e. $A_{headgroup}/A_{chains} < 1$ (Israelachvili et al., 1976), the overall molecular shape changes from cylindrical to cone shape favoring the formation of the H_{II} phase. This is the foundation for the proposed biological mechanism for the LNPs. The cationic lipids of the LNPs bind to the anionic endosomal lipids forming an ion pairs. The bilayer to non-bilayer H_{II} phase change leads to the disruption of the endosomal phase and the release of the siRNA.

5.4. The XTC2/DSPS-d70 model system has a T_{BH} which is sensitive to Salt Concentrations

Salt influences membrane polymorphism especially for charged lipid. According to a study on the hexagonal phase of PE by Harolos and Eibl (1981), it is found that increasing chain length or the sodium salt concentration results in a decrease in the transition temperature T_{BH} done by differential scanning calorimetry and X-ray diffraction. The bilayer to H_{II} phase transition was found depend strongly on NaCl concentration with T_{BH} decreasing from 109.5 (with no salt) to 101.5 (with 1M NaCl), to 95.5 (with 2M NaCl) and to 88.5 (with 4M NaCl) (Harlos & Eibl, 1981). One could consider a pair of PE headgroups to be electrostatically similar to one XTC2/DSPS headgroup combination at low pH 4.75, as both will be approximately considered to be neutral. It has been shown in Chapter 4 that PS model membrane does not go to H_{II} phase with increasing temperature at neutral pH. However it has been shown that the XTC2/DSPS model membrane undergoes bilayer to H_{II} phase transition at low pH. We hypothesize that the two PE headgroups would resemble the XTC2/DSPS headgroup and observe a decrease in T_{BH}.

This trend is also seen by Scarzellow et al, (2005). They observed a H_{II} phase for a cationic amphiphile SAINT-2 and neutral DOPE mixture induced by an increase in ionic strength. They rationalized that the effect of the presence of NaCl is to screen the electrostatic repulsion between the headgroups of the charged amphiphiles (Scarzello et al., 2005). Thus we could hypothesize that our XTC2 resembles the cationic amphiphile SAINT-2 and DSPS resembles DOPE leading to a lower T_{BH} for the XTC2/DSPS model at increasing salt concentration.

In this section, three different salt concentrations were studied in the following sequence: the initial low salt concentration 0.25M was increased to 1.0 M and then reduced to 0.5 M. Spectral shapes, M_1 values, and transition temperatures T_{BH} were compared. Salt has been shown effect on the interaction of DSPS-d70 and XTC2 and XTC2 bilayer destabilizing ability.

5.4.1. The system at high salt, 1M Na^+

Deuterium NMR spectra were measured from 283 to 328K. At each temperature, the phase coexistence was observed.

Deuterium NMR spectra show that XTC2/DSPS-d70 is in gel/H_{II} phase coexisting at temperature below 313K. The spectra for both high (Fig. 5.13) and low salt concentrations (Fig. 5.12 0.25M and Fig. 5.15 0.5M) at 283K show H_{II} phase coexists with the presence of the gel phase. As discussed earlier, the gel phase component is characterized by the signal extending to +/- 63 kHz. The gel phase component became smaller as temperature increases as more lipids converted to H_{II} phase between 293K and 313K. As the temperature increases, the isotropic phase emerges. This can be observed at 323 K designated as the sharp peak at 0 kHz.

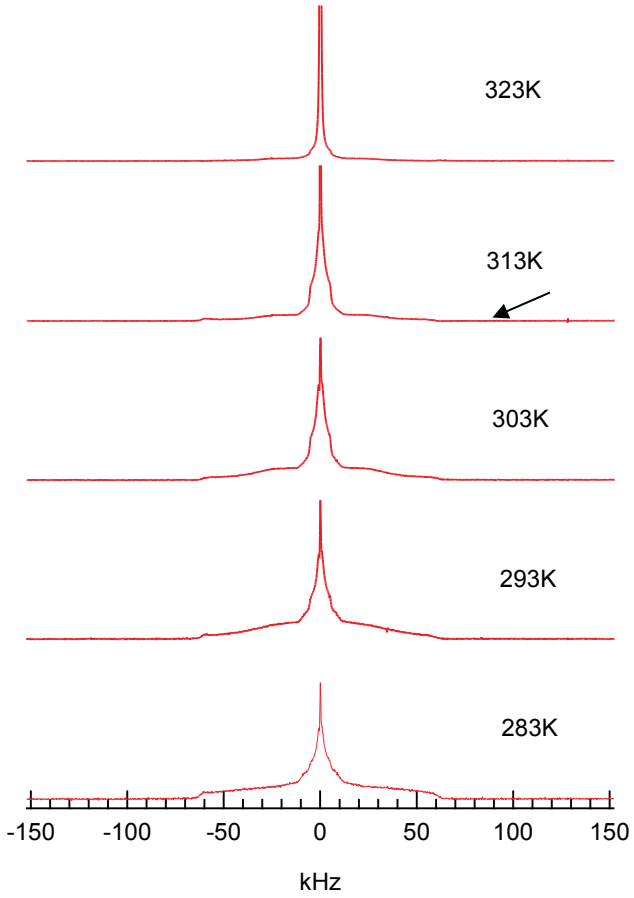

Figure 5.13. ^2H NMR spectra of XTC2/DSPS-d70 pH 4.75 with 1M NaCl.
The arrow indicates that the gel phase intensity decreases as the temperature increases.

Deuterium NMR spectra of XTC2/DSPS-d70 model system show the lipids are in the H_{II} phase with a growing isotropic phase component at temperatures above 313K.

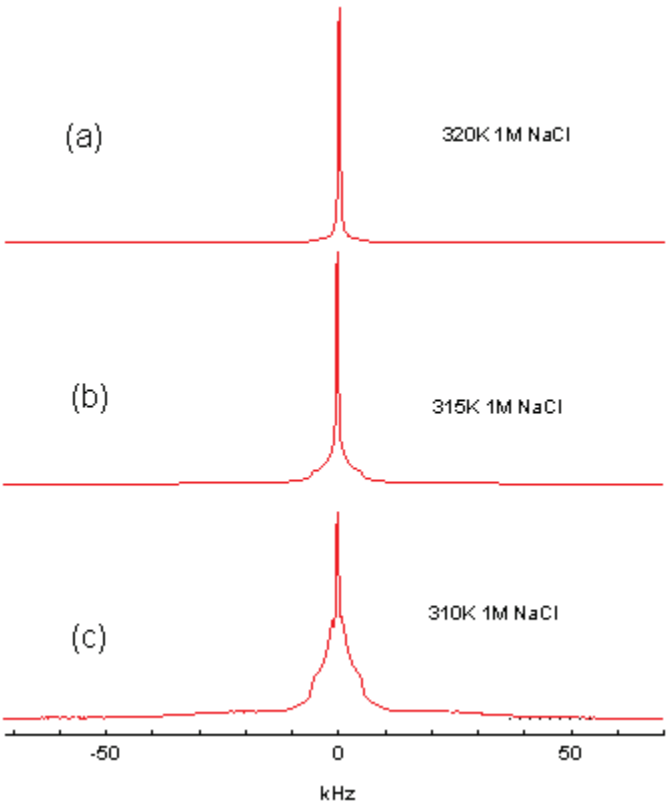

Figure 5.14. ^{2}H spectra of XTC2/DSPS-d70 with 1M NaCl salt 310-320K.
Spectra obtained at (a) 320K, (b) 315K and (c) 310K, showing the emergence of the isotropic peak.

At 310K, we observed a dominant H_{II} phase with a small amount of gel phase. We were aiming to get a pure H_{II} phase spectrum for our collaborators to simulate. Unfortunately, the gel phase indicated by non-zero spectral intensity extending to +/-63 kHz was visible even at 315K. We were unable to obtain a pure H_{II} phase spectra at higher temperatures because the spectra started to show isotropic at 313K. We stopped the experiment at 320K.

5.4.2. At medium salt concentration, 0.5M Na^+, the XTC2/DSPS-d70 has a lower T_{BH} than at 1M Na^+

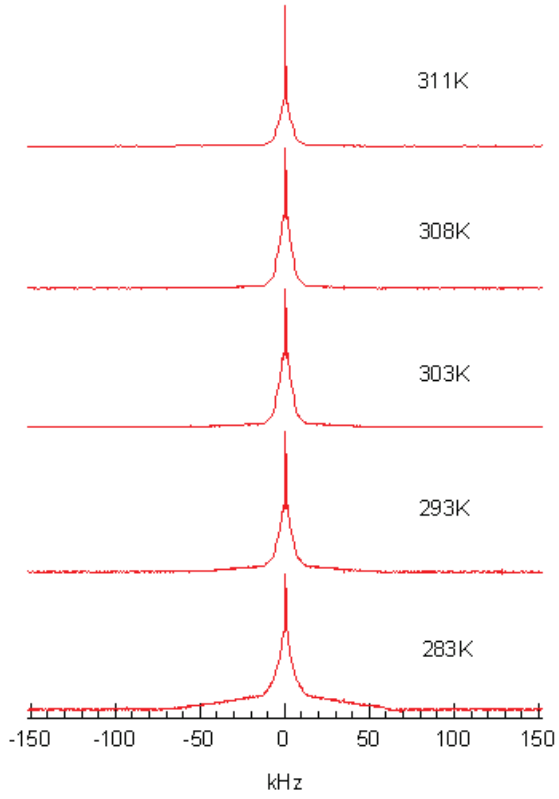

Figure 5.15. ^2H NMR spectra of the XTC2/DSPS-d70 pH 4.75 with 0.5 M NaCl.

At medium salt concentration (0.5M Na^+), we observed a lower T_{BH} for the system. The gel phase component was always present at low temperature e.g. 283K but it gradually converted to H_{II} phase at high temperatures. At 303K, we observed a nearly flat baseline indicating most of the gel phase component has converted to the H_{II} phase. The nearly flat baseline stage was not observed until 313K for the spectra at 1M Na^+, thus at high salt it took more energy for the gel component to be converted to H_{II} phase.

5.4.3. Comparison between XTC2/DSPS-d70 ^2H NMR spectra as a function of salt concentration reveals that salt stabilizes the gel phase

The low salt concentration experiments were stopped at 307K because we observed a pure H_{II} phase at this temperature. At 1M Na^+, the spectral shapes were markedly different from the spectral shapes at low salt. We compare the effect of salt concentration on membrane structure at several specific temperatures, 283, 298 and

307K (Fig. 5.16). ^{2}H NMR spectra show more gel phase component present at1M NaCl relative to 0.25M NaOAc at all three temperatures.

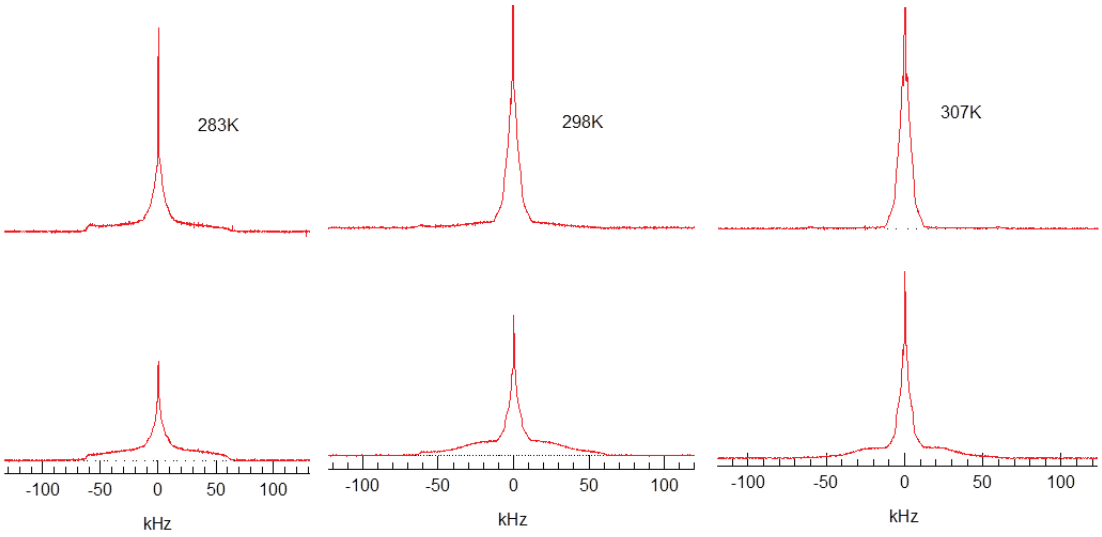

Figure 5.16. Comparison of XTC2/DSPS-d70 at 0.25M NaOAc and 1M NaCl.
The 0.25 M Na^{+} is shown above the 1M Na^{+} spectra. Temperatures are 283, 298, and 307K.

At 283K the gel phase component is present at both salt concentrations. At 298K, the gel phase is visible in both high and low salt concentrations but the gel phase is more prominent in the high salt solution. At 307K, we observed a pure H_{II} phase at low salt concentration. In contrast, we observed an H_{II} phase mixed with a gel phase at high salt concentration. The lipid system is more stable in the gel phase at high salt concentration as more intensity was observed in the gel phase spectral component.

5.4.4. The existence of the H_{II} phase can be confirmed by examining the order parameter profile

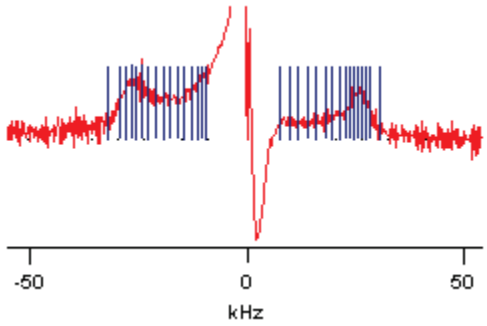

Figure 5.17. De-Paked spectrum of XTC2/DSPS-d70 with 1M Na^+ at 312K.
Even though the powder spectrum was not characterized as a pure H_{II} phase, it was possible to obtain a de-Paked spectrum.

The XTC2/DSPS-d70 with 1M Na^+ at 312K depaked spectrum is shown in Fig 5.17. The vertical lines represent bins for each carbon atom. The quadrupolar splitting $\Delta\nu$ can be obtained by measuring distance the central frequency of each bin (Table 5.3). The methyl group's $\Delta\nu$ was measured directly from the powder pattern. The central part for de-Paked spectrum was not shown as it is subject to distortion when an isotropic peak is present. The order parameter profile is plotted in Fig. 5.18. The final drop of the S_{CD} indicates the enhanced motional freedom of the methyl group (C18).

Table 5.3. S_{CD} for DSPS-d70/XTC2 pH 4.75 with 1M NaCl at 312K.

Carbon	left	right	2μs left	2μs right	distance	Δv	Δv (kHz)	S_{CD}
18	1220.7	2197.2	488.28	878.88	976.56	488.28	0.48828	0.003875
17	9313.2	7731.09	3725.28	3092.436	7450.56	3725.28	3.72528	0.029566
16	10373.2	9721.09	4149.28	3888.436	8298.56	4149.28	4.14928	0.032931
15	11563.2	11881.1	4625.28	4752.44	9250.56	4625.28	4.62528	0.036709
14	12913.2	14081.1	5165.28	5632.44	10330.56	5165.28	5.16528	0.040994
13	14403.2	16071.1	5761.28	6428.44	11522.56	5761.28	5.76128	0.045724
12	16013.2	18101.1	6405.28	7240.44	12810.56	6405.28	6.40528	0.050836
11	17733.2	19761.1	7093.28	7904.44	14186.56	7093.28	7.09328	0.056296
10	19393.2	21211.1	7757.28	8484.44	15514.56	7757.28	7.75728	0.061566
9	21103.2	22701.1	8441.28	9080.44	16882.56	8441.28	8.44128	0.066994
8	22703.2	23811.1	9081.28	9524.44	18162.56	9081.28	9.08128	0.072074

Carbon	left	right	2μs left	2μs right	distance	Δv	Δv (kHz)	S_{CD}
7	24243.2	24761.1	9697.28	9904.44	19394.56	9697.28	9.69728	0.076963
6	25453.2	25601.1	10181.28	10240.44	20362.56	10181.28	10.18128	0.080804
5	26603.2	26391.1	10641.28	10556.44	21282.56	10641.28	10.64128	0.084455
4	27843.2	27251.1	11137.28	10900.44	22274.56	11137.28	11.13728	0.088391
3	29423.2	28271.1	11769.28	11308.44	23538.56	11769.28	11.76928	0.093407
2	32293.2	30411.1	12917.28	12164.44	25834.56	12917.28	12.91728	0.102518

The spectrum was mainly in H_{II} phase with little gel phase present.

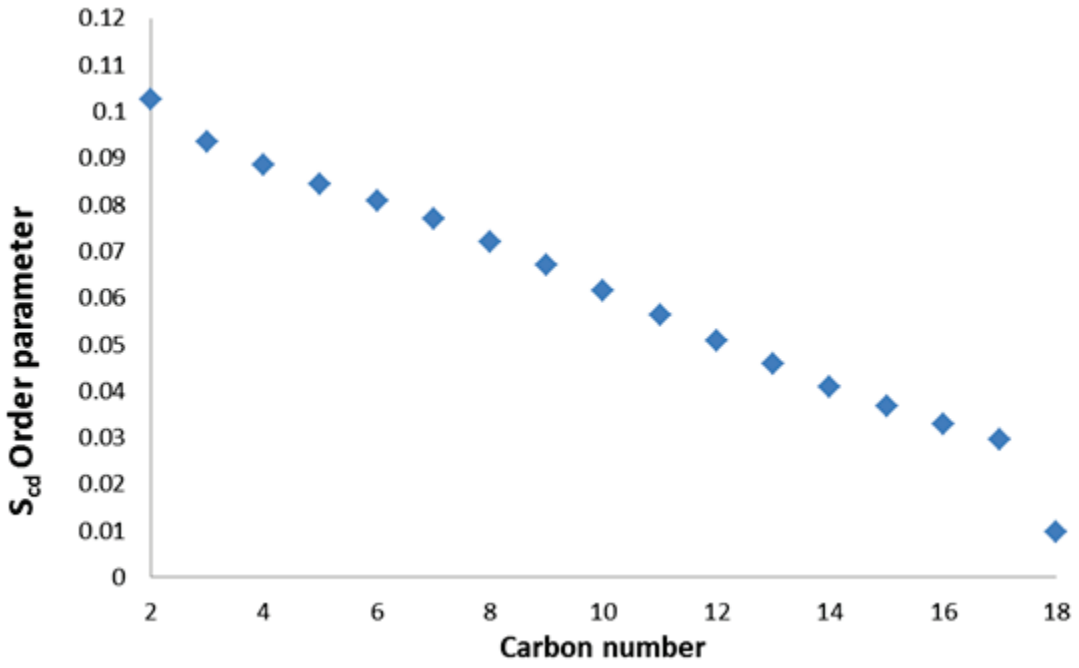

Figure 5.18. S_{CD} obtained from XTC2/DSPS-d70 at 312K pH 4.75 with 1M Na^+.

How does the H_{II} order parameter of XTC2/DSPS-d70 change with respect to temperature? As temperature increases, it is hypothesized that chains have more flexibility to move, thus we would predict obtaining smaller $\Delta\nu$ values. For example, a decrease in quadrupolar splitting was observed for the H_{II} phase of PLPE-d_{31}. Thurmond, et al (1993) reported a 1 kHz change over a 10 degree range. To investigate this, the quadrupolar splitting $\Delta\nu$ was measured by taking the width of the half height of the shoulder over a temperature range of 292K to 316K. All measurements were within the range of 11.21 kHz and 11.39 kHz. Thus the H_{II} phase order parameter is insensitive to temperature over this range. This suggests that the H_{II} phase formed has constant properties with regard to chain conformational freedom, which would in turn suggest that

the H_{II} phase formed has consistent properties with respect to composition and cylinder radius.

The order parameter profile for the H_{II} phase at high salt concentration shows a similar pattern to that at low salt concentration (Fig. 5.9). The largest S_{CD} is still 0.1, which proves that the structure of the acyl chains in the H_{II} phase stays stable with salt.

5.4.5. M_1 allows us to compare the phase behaviour of XTC2/DSPS-d70 for three salt concentrations

The effect on the average spectral width, $M_{1,}$ of increasing the Na^+ concentration from 0.25M to 1M on the XTC2/ DSPS-d70 system is investigated. High salt certainly stabilized the gel phase and made it harder to change to H_{II} phase completely. Therefore, at high salt concentration we observed a higher T_{BH} as shown in the M_1 vs. temperature plot (Fig. 5.19). In the 0.25M salt solution, the T_{BH} occurs near 289K, but in the 1M salt solution the T_{BH} of XTC2/DSPS-d70 occurs approximately at 308K with no clear start and end point of the transition. In conclusion, increasing the salt concentration results in an increase in the gel to H_{II} phase transition temperature; this is opposite to our original hypothesis.

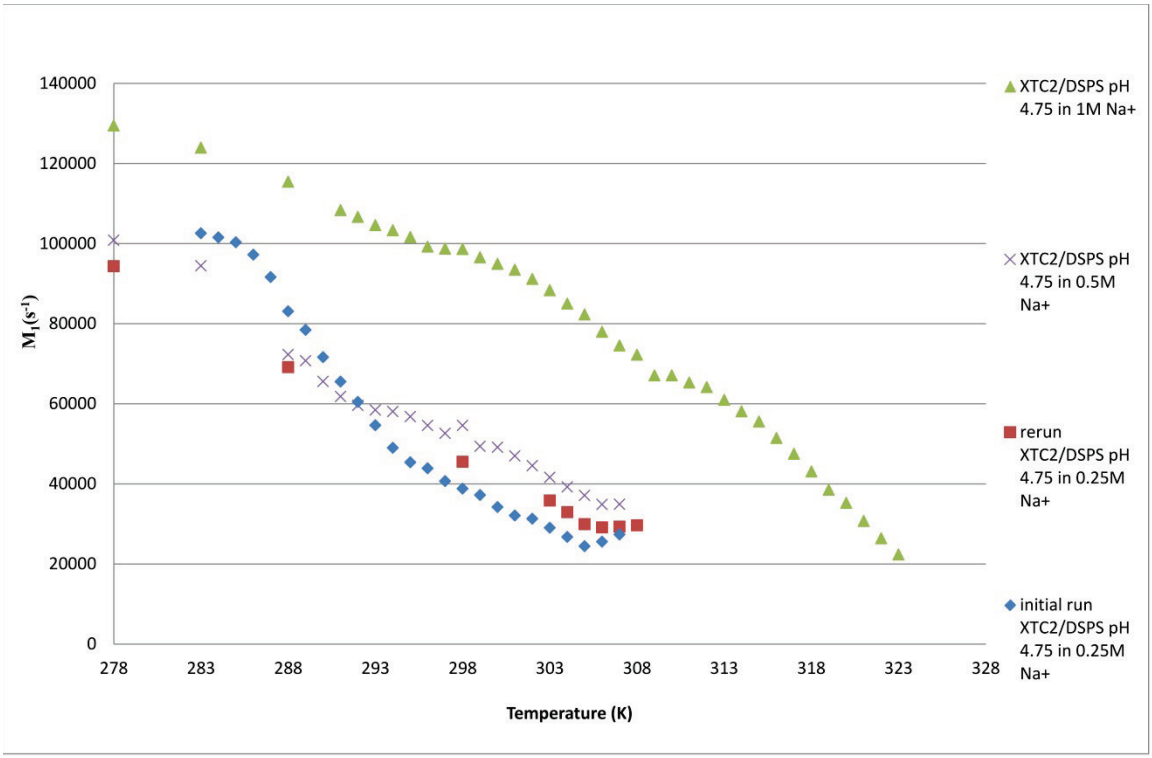

Figure 5.19. M_1 comparison for XTC2/DSPS-d70 at different [Na^+].
XTC2/DSPS-d70 model membrane at pH 4.75 in 0.25M, 0.5M and 1M Na^+ from 278 to 323K Between the initial data collection and the rerun of the 0.25M Na^+, sample was transferred to a 4 mm MAS tube for ^{31}P NMR experiments (results not shown) then transferred back to ^2H NMR tube with some sample lost.

Why are our results opposite from those of Scarzello et al (2005)? This may be because it is more complicated for our system in that we need to take into account that the PS has an ionisable headgroup while DOPE's is neutral. DOPE alone will form the H_{II} phase but the addition of the cationic SAINT-2 creates more volume in the headgroup region leading to bilayer morphology. Upon addition of salt, the electrostatic repulsion between SAINT-2 headgroups is screened, reducing the effective headgroup area and inducing the formation of the H_{II} phase.

Interestingly, salt stabilizing the bilayer with respect to temperature was also interpreted by Li & Schick (Li & Schick, 2001). Their calculation on the model system composed of permanently charged cationic lipid DODAC and anionic ionisable lipid cholesteryl hemisuccinate (CHEMS) agreed with experimental data (Hafez et al., 2000) and they further explicated the mechanism of the role of the counterions $H_9O_4^+$. A plausible explanation for the increase in T_{BH} is that the Na^+ shields the negative charge on DSPS. This results in a weaker interaction with the cationic lipid XTC2 which would

increase the spatial distance between the two lipids. For a similar reason, the chloride and the acetate anion can associate with the positively charged head group of XTC2. This reduces the coulomb interactions between the headgroup previously discussed in Chapter 5.3. The counterions also create more volume between the ion pair, making the headgroup region larger and the headgroup to chain area ratio close to one. This disrupts the favorable cone shape of the ion pair and makes it more cylindrical, favoring the bilayer shape shown in Fig.5.20.

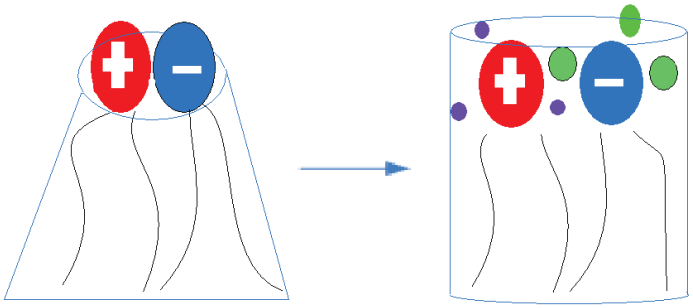

Figure 5.20. Proposed mechanism for higher T_{BH} at higher [Na^+].
The electrostatic interaction of the charged headgroup is interrupted by the counterion and the Coulomb interaction is weakened. The increase of the charge and size of the headgroup counts for effective volume. The area of the headgroup to area of the acyl chain ratio is increased. This cone shape is gradually turned in to cylindrical shape.

Chapter 6. Summary and Future Work

6.1. Summary of the XTC2/DSPS model system's phase behaviour

Membrane phase behaviour was closely examined by NMR spectral shape and order parameter profile using model membranes (Chapters 4 and 5). The DSPS model membrane was studied at various temperatures and the XTC2/DSPS model membrane was characterized under conditions of different pH, temperature and salt concentration by ^{31}P and ^{2}H NMR spectroscopy. The DSPS model membrane undergoes a gel to liquid crystalline phase transition at 338 K and remains in L_α phase to at least 343K. We also did not observe any H_{II} phase at pH 8.4 for the XTC2/DSPS model membrane. At low pH, however, the XTC2/DSPS model membrane exhibits a gel to inverse hexagonal phase transition. I showed that salt stabilizes the gel phase and increases the T_{BH} of XTC2/DSPS. The order parameter profiles show more flexibility of the DSPS-d70 acyl chains in the H_{II} phase than the bilayer phase, as expected. The H_{II} phase order parameter profile, though, was remarkably insensitive to temperature and salt concentration.

6.1.1. The Gel/L_α, Gel/H_{II}, H_{II}/Isotropic phase transitions temperatures are pH and salt concentration sensitive

As shown in Chapter 4, the ^{2}H NMR spectral line shape analysis showed that pure DSPS undergoes a gel to liquid crystalline phase transition with a midpoint of 336-337K. The DSPS-d70 transition temperature T_m was lower than the nondeuterated DSPS T_m, which was approximately 339K from the ^{31}P NMR spectroscopy. Attributed to Guard-Friar, et al (1985), the deuteron labelled chains are more disorderd than the non labelled chains.

The XTC2/DSPS model membrane phase behavior under conditions of different pH, temperature and salt concentration was shown in Chapter 5. At pH 8.4, the XTC2/DSPS model membrane undergoes gel to liquid crystalline phase transition at

328K by spectral shape analysis; no H_{II} phase was observed. When pH is lowered to 4.75, the XTC2/DSPS-d70 membrane undergoes a bilayer to H_{II} phase transition centered at 293K characterized by ^{31}P NMR. In comparison, the XTC2/DSPS-d70 system undergoes a gel to H_{II} phase transition at 289K at pH 4.75 characterized by ^{2}H NMR spectral shape analysis. This 4 degree lower T_{BH} must be due to the effect of chain deuteration as a similar reduction in T_m of the DSPS-d70 membrane was also observed. This can be rationalized using the molecular shape theory by Israelachvili, et al (1976) discussed in Chapter 5.3.

As shown in Figure 6.1 by a steep reduction in the average spectral width, introducing the neutral form of XTC2 into the DSPS-d70 model membrane dramatically lowers the T_m from 338K to 328K. By decreasing the salt concentration at from 1M to 0.5M to 0.25M Na^+ at pH 4.75, the gel to H_{II} transition temperature ranges are lowered from 303-313K to 293-303K, and to 283-293K respectively (The transition range for 0.5M salt can't be deduced from M_1 vs. T figure).

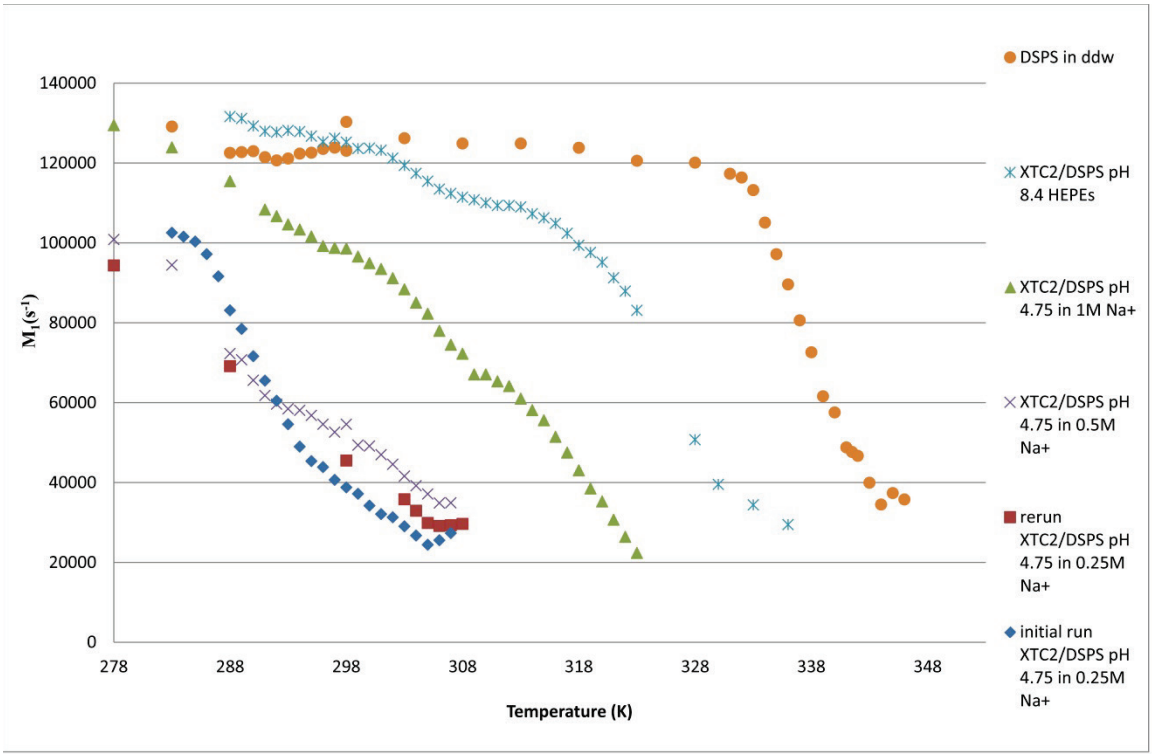

Figure 6.1. M_1 comparisons for DSPS, XTC2/DSPS-d70 without and with salt.
M_1 plots for DSPS-d70 and XTC2/DSPS-d70 model membranes at pH 8.4 and 4.75 and in different [Na^+] from 278 to 346K.

A summary of the T_m and T_{BH} obtained from Chapter 4 &5 were listed table 6.1.

Table 6.1. Summary of T_m and T_{BH} obtained from ^{31}P and ^{2}H NMR results.

Model Membrane	[Na+]	T_m (K)	T_{BH} (K)	Method	Figure
DSPS	0	339		^{31}P NMR	Fig 4.1
DSPS-d70	0	336-337		^{2}H NMR	Fig 4.2
XTC2/DSPS (pH 8.4)	0	NA		^{31}P NMR	Fig 5.1
XTC2/DSPS-d70 (pH 8.4)	0	328		^{2}H NMR	Fig 5.5
XTC2/DSPS (pH 4.75)	0.25M		293	^{31}P NMR	Fig 5.7
XTC2/DSPS-d70 (pH 4.75)	0.25M		289	^{2}H NMR	Fig 5.9
XTC2/DSPS-d70(pH 4.75)	1M		303-313	^{2}H NMR	Fig 5.13
XTC2/DSPS-d70(pH 4.75)	0.5M		293-303	^{2}H NMR	Fig 5.15

6.1.2. ^{2}H NMR reveals lipid chain packing information in L_a and H_{II} phase

The order parameter profile, S_{CD} vs. C#, shows that DSPS-d70 acyl chains have much more flexibility in H_{II} phase than in the bilayer phase. When the spectral shapes of the L_α phase and H_{II} are compared (Fig 6.2), the narrower plateau splitting for H_{II} phase spectrum indicates that the H_{II} phase acyl chain has looser packing and is therefore not as ordered as in the L_α phase. Due to the fact that lipids in the H_{II} phase have an additional axis of motional symmetry, the lateral diffusion around the cylinder leads to a reduction of the spectral width by half. The order parameter profiles illustrate this reduction: the maximum S_{CD} of the H_{II} phase is 0.1 while the maximum S_{CD} in the gel phase is 0.21(Fig 6.3a). The fact that the reduction is larger than expected from the extra rotational symmetry reflects the less ordered chain in the H_{II} phase. This additional reduction is least noticeable for the maximum order parameters; it becomes more evident as H_{II} phase and bilayer phase order parameters are compared along the chain. This pattern has also been seen in the PLPE-d_{31} study (Thurmond et al., 1993). It was rationalized by Thurmond et al that the smaller cross-sectional area results in an increase in the order parameter and the length of the plateau region of the order parameter profile in the bilayer phase.

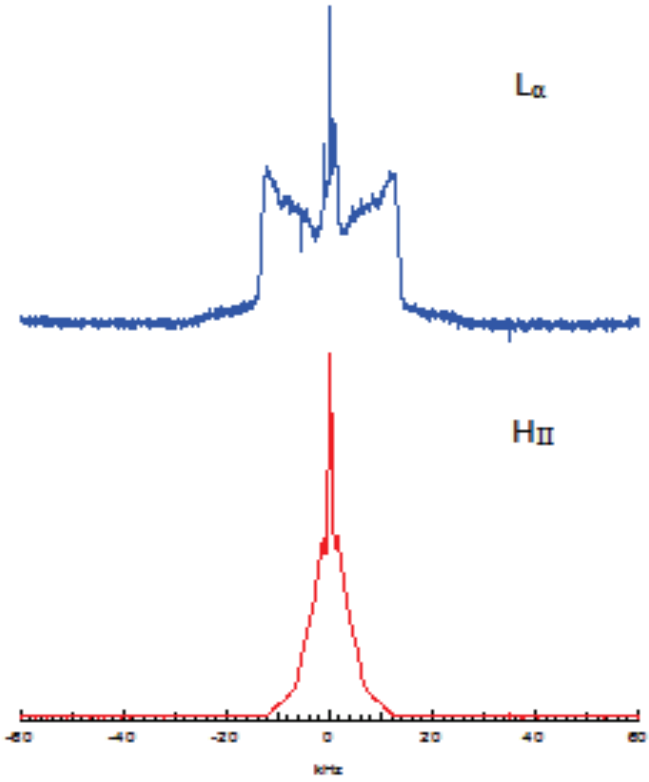

Figure 6.2. Spectral shape comparison for lamellar phase and H_{II} phase.
Top: ^2H NMR spectra of DSPS-d70 at 341.5K pH 8.4 in HEPES buffer (top). XTC2/DSPS-d70 at 307K and pH of 4.75 in sodium acetate buffer (bottom). The spectra were obtained with 5us dwell time 100000 scans.

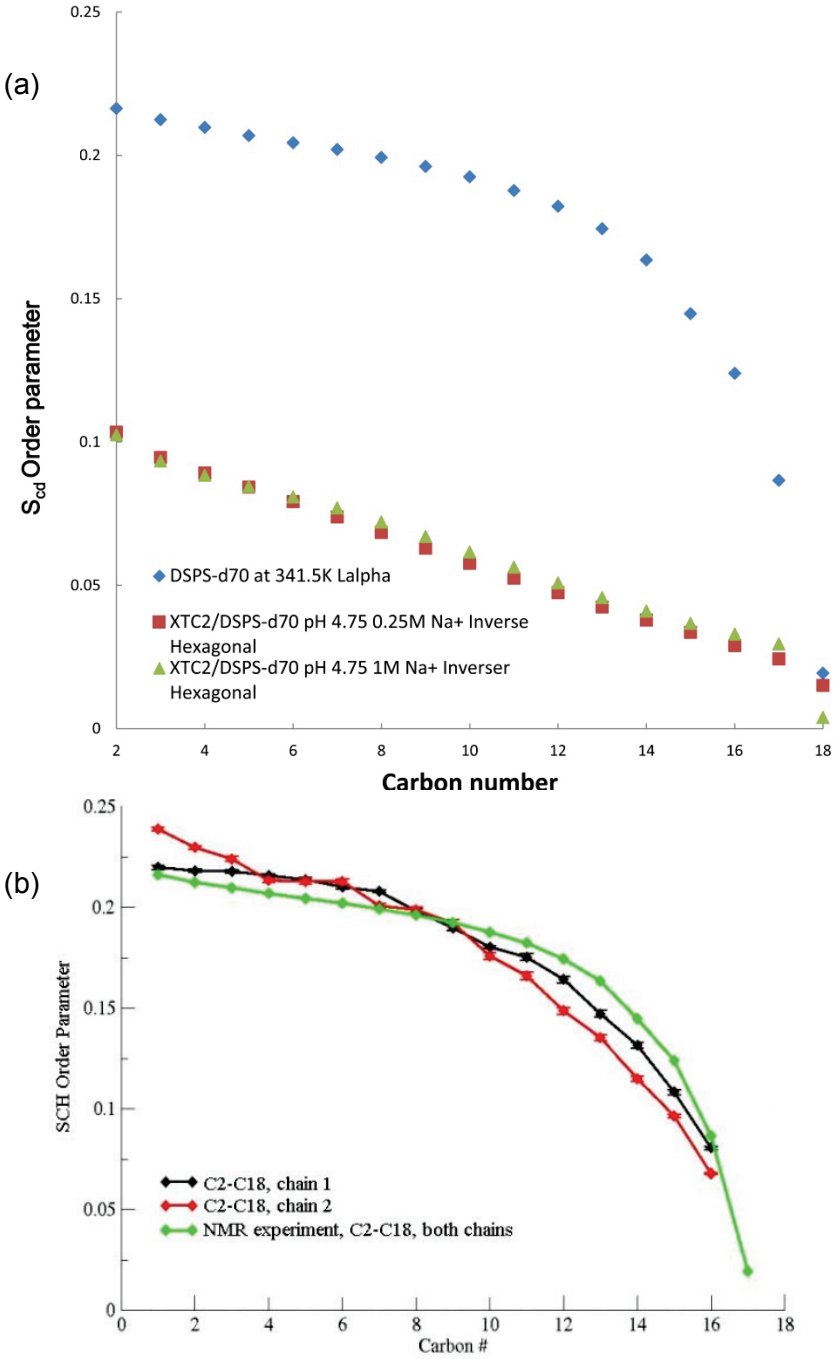

Figure 6.3 Comparison of experimental and simulated S_{CD} results.
S_{CD} obtained from DSPS-d70, XTC2/DSPS-d70 pH 4.75 and XTC2/DSPS-d70 pH 4.75 with 1M Na^+ (a). The simulated DSPS order parameter profile S_{CH} by Dr. Mo Ashtari and Dr.Peter Tieleman at the University of Calgary (b).

The simulated DSPS matches the experimental DSPS-d70 order parameter S_{CD} shown in Fig.6.3. Note that the experimental DSPS-d70 order parameter represents the average of both chains under the assumption that S_{CD} decreases monotonically from C2

to C18. The simulated order parameters overestimate S_{CD} in the plateau region and underestimate it towards the end of the acyl chain.

6.1.3. Increasing salt concentration stabilized the gel phase of XTC2/DSPS-d70

Previously it has been shown that T_{BH} decreases with increasing salt concentration, as seen for DSPE by Harolos and Eibl (1981). Salt was also shown to be inducing the bilayer to H_{II} phase transition for cationic pyridinium amphiphiles SAINT-2 and DOPE membrane by Scarzello et al. (Scarzello et al., 2005) Since the XTC2/DSPS model system resembles the SAINT-2/DOPE membrane, we hypothesized that the T_{BH} would decrease with an increasing salt concentration. However, as shown in Chapter 5 we observed the opposite. The XTC2/DSPS model membrane has a higher T_{BH} value when increasing salt was present in the buffer. Increasing salt concentration resulted in a significant increase in the gel to H_{II} phase transition temperature at pH 4.75. What makes the difference is that at higher salt concentration, the ions in solution compete with the lipid heagroup charges, reducing the driving force behind lipid headgroup ion pair formation (Li & Schick, 2001). This in turn increases the effective headgroup cross-sectional area, increasing the stability of the bilayer phase according to the molecular shape theory.

6.2. Conclusion and Future Work

In conclusion, we studied the phase behavior for DSPS and XTC2/DSPS model membranes under different pH and salt concentrations. At pH 8.4, the XTC2/DSPS-d70 model system is mainly in the gel phase with a small portion of the isotropic phase as temperature increases. At pH 4.75, the system is in H_{II} and gel coexisting phase at low temperature; pure H_{II} phase was observed at 307K. Salt stabilized the XTC2/DSPS system, observed by increasing T_{BH} values with increasing salt concentration. Order parameters S_{CD} obtained through de-Paked spectra gave acyl chain conformational information showing a more mobile arrangement of lipid chain in H_{II} phase. The detailed acyl chain order parameters measured in the H_{II} phase will provide an important test for models used to perform molecular dynamics simulations on this system. By studying the

model membrane phase behaviour, we get close to understanding the LNP and endosomal membrane disruption mechanism.

To better characterize the H_{II} phase structure, the experimental S_{CD} order parameter data may be used to estimate the hexagonal phase cylinder radius published by Lafleur et al (Lafleur et al., 1996). The experimental and the simulation results can be compared to gain insight into the H_{II} structure. The effect of cholesterol on the XTC2/DSPS model membrane may be investigated in the future. It has been showed that equimolar of cholesterol decrease the T_{BH} of synthetic DOPE membrane by 10°C (Cullis & de Kruijff, 1978). Moreover, Lafleur et al 1998 showed different percentage of cholesterol have different effects on T_{BH}, specifically 0-30% of cholesterol lowers the T_{BH} whereas higher than 30% of cholesterol increases T_{BH} (Pare & Lafleur, 1998). It was also found that high ergosterol concentrations (more than 40 mol percentage) significantly decrease L_{α} to H_{II} transition temperature and POPE-d_{31} chain order (Hsueh et al., 2010). Lysobisphosphatidic acid is found in the endosomal membrane lipid, it may be studied as the anionic species in the model membrane. As more is learned about the phase behaviour of LNP components from model systems, more effective LNPs can be designed.

References

Allen, T. M., & Cullis, P. R. (2013). Liposomal drug delivery systems: From concept to clinical applications. *Advanced Drug Delivery Reviews, 65*(1), 36-48.

Bangham, A. D., Standish, M. M., & Watkins, J. C. (1965). Diffusion of Univalent Ions across Lamellae of Swollen Phospholipids. *Journal of Molecular Biology, 13*(1), 238-&.

Browning, J. L., & Seelig, J. (1980). Bilayers of Phosphatidylserine - Deuterium and Phosphorus Nuclear Magnetic-Resonance Study. *Biochemistry, 19*(6), 1262-1270.

Cullis, P. R., & de Kruijff, B. (1978). The polymorphic phase behaviour of phosphatidylethanolamines of natural and synthetic origin. A 31P NMR study. *Biochimica Et Biophysica Acta, 513*(1), 31-42.

Cullis, P. R., & Dekruijff, B. (1979). Lipid Polymorphism and the Functional Roles of Lipids in Biological-Membranes. *Biochimica Et Biophysica Acta, 559*(4), 399-420.

Cullis, P. R., Hope, M. J., Bally, M. B., Madden, T. D., Mayer, L. D., & Fenske, D. B. (1997). Influence of pH gradients on the transbilayer transport of drugs, lipids, peptides and metal ions into large unilamellar vesicles. *Biochimica Et Biophysica Acta-Reviews on Biomembranes, 1331*(2), 187-211.

Cullis, P. R., Hope, M. J., & Tilcock, C. P. S. (1986). Lipid Polymorphism and the Roles of Lipids in Membranes. *Chemistry and Physics of Lipids, 40*(2-4), 127-144.

Finer, E. G. (1973). Interpretation of deuteron magnetic resonance spectroscopic studies of the hydration of macromolecules. *Journal of the Chemical Society, Faraday Transactions 2: Molecular and Chemical Physics, 69*(0), 1590-1600.

Gennis, R. B. (1989). *Biomembranes :molecular structure and function* (1st ed.). New York: Springer-Verlag,.

Gregoriadis, G., & Ryman, B. E. (1971). LIPOSOMES AS CARRIERS OF ENZYMES OR DRUGS - NEW APPROACH TO TREATMENT OF STORAGE DISEASES. *Biochemical Journal, 124*(5), P58-&.

Guard-Friar, D., Chen, C. H., & Engle, A. S. (1985). Deuterium isotope effect on the stability of molecules: phospholipids. *The Journal of Physical Chemistry, 89*(9), 1810-1813.

Hafez, I. M., Ansell, S. M., & Cullis, P. R. (2000). Construction and characterization of tunable pH sensing vesicles based on mixtures of anionic and cationic lipid. *Biophysical Journal, 78*(1), 396a-396a.

Harlos, K., & Eibl, H. (1981). Hexagonal phases in phospholipids with saturated chains: phosphatidylethanolamines and phosphatidic acids. *Biochemistry, 20*(10), 2888-2892.

Hope, M. J., Bally, M. B., Webb, G., & Cullis, P. R. (1985). Production of Large Unilamellar Vesicles by a Rapid Extrusion Procedure - Characterization of Size Distribution, Trapped Volume and Ability to Maintain a Membrane-Potential. *Biochimica Et Biophysica Acta, 812*(1), 55-65.

Hope, M. J., & Cullis, P. R. (1987). Lipid Asymmetry Induced by Transmembrane Ph Gradients in Large Unilamellar Vesicles. *Journal of Biological Chemistry, 262*(9), 4360-4366.

Hsueh, Y. W., Weng, C. J., Chen, M. T., Thewalt, J., & Zuckermann, M. (2010). Deuterium NMR Study of the Effect of Ergosterol on POPE Membranes. *Biophysical Journal, 98*(7), 1209-1217.

Israelachvili, J. N., Mitchell, D. J., & Ninham, B. W. (1976). Theory of Self-Assembly of Hydrocarbon Amphiphiles into Micelles and Bilayers. *Journal of the Chemical Society-Faraday Transactions Ii, 72*, 1525-1568.

Jayaraman, M., Ansell, S. M., Mui, B. L., Tam, Y. K., Chen, J. X., Du, X. Y., . . . Hope, M. J. (2012). Maximizing the Potency of siRNA Lipid Nanoparticles for Hepatic Gene Silencing In Vivo. *Angewandte Chemie-International Edition, 51*(34), 8529-8533.

Lafleur, M., Bloom, M., Eikenberry, E. F., Gruner, S. M., Han, Y. Q., & Cullis, P. R. (1996). Correlation between lipid plane curvature and lipid chain order. *Biophysical Journal, 70*(6), 2747-2757.

Leung, A. K. K., Hafez, I. M., Baoukina, S., Belliveau, N. M., Zhigaltsev, I. V., Afshinmanesh, E., . . . Cullis, P. R. (2012). Lipid Nanoparticles Containing siRNA Synthesized by Microfluidic Mixing Exhibit an Electron-Dense Nanostructured Core. *The Journal of Physical Chemistry C, 116*(34), 18440-18450.

Li, X.-j., & Schick, M. (2001). Theory of Tunable pH-Sensitive Vesicles of Anionic and Cationic Lipids or Anionic and Neutral Lipids. *Biophysical Journal, 80*(4), 1703-1711.

Macdonald, R. C., Simon, S. A., & Baer, E. (1976). Ionic Influences on Phase-Transition of Dipalmitoylphosphatidylserine. *Biochemistry, 15*(4), 885-891.

MacLachlan, I. (2006). Chapter 9. Liposomal Formulations for Nucleic Acid Delivery. In S. T. Crooke (Ed.), *Antisense drug technology: principles, strategies, and applications*: CRC Press.

Mahato, R. I. N., Ajit S. (2012). Pharmaceutical dosage forms and drug delivery /Ram I. Mahato, Ajit S. Narang.

Mayer, L. D., Bally, M. B., Hope, M. J., & Cullis, P. R. (1986). Techniques for Encapsulating Bioactive Agents into Liposomes. *Chemistry and Physics of Lipids, 40*(2-4), 333-345.

Moncelli, M. R., Becucci, L., & Guidelli, R. (1994). THE INTRINSIC PK(A), VALUES FOR PHOSPHATIDYLCHOLINE, PHOSPHATIDYLETHANOLAMINE, AND PHOSPHATIDYLSERINE IN MONOLAYERS DEPOSITED ON MERCURY-ELECTRODES. *Biophysical Journal, 66*(6), 1969-1980.

Olson, F., Hunt, C. A., Szoka, F. C., Vail, W. J., & Papahadjopoulos, D. (1979). Preparation of Liposomes of Defined Size Distribution by Extrusion through Polycarbonate Membranes. *Biochimica Et Biophysica Acta, 557*(1), 9-23.

Pare, C., & Lafleur, M. (1998). Polymorphism of POPE/cholesterol system: A H-2 nuclear magnetic resonance and infrared spectroscopic investigation. *Biophysical Journal, 74*(2), 899-909.

Poste, G., & Papahadjopoulos, D. (1976). Lipid Vesicles as Carriers for Introducing Materials into Cultured-Cells - Influence of Vesicle Lipid-Composition on Mechanism(S) of Vesicle Incorporation into Cells. *Proceedings of the National Academy of Sciences of the United States of America, 73*(5), 1603-1607.

Rowell, J. C., Phillips, W. D., Melby, L. R., & Panar, M. (1965). NMR Studies of Some Liquid Crystal Systems. *The Journal of Chemical Physics, 43*(10), 3442-3454.

Scarzello, M., Chupin, V., Wagenaar, A., Stuart, M. C. A., Engberts, J., & Hulst, R. (2005). Polymorphism of pyridinium amphiphiles for gene delivery: Influence of ionic strength, helper lipid content, and plasmid DNA complexation. *Biophysical Journal, 88*(3), 2104-2113.

Scarzello, M., Chupin, V., Wagenaar, A., Stuart, M. C. A., Engberts, J. B. F. N., & Hulst, R. (2005). Polymorphism of pyridinium amphiphiles for gene delivery: Influence of ionic strength, helper lipid content, and plasmid DNA complexation. *Biophysical Journal, 88*(3), 2104-2113.

Seelig, J. (1977). Deuterium Magnetic-Resonance - Theory and Application to Lipid-Membranes. *Quarterly Reviews of Biophysics, 10*(3), 353-418.

Seelig, J. (1978). P-31 Nuclear Magnetic-Resonance and Head Group Structure of Phospholipids in Membranes. *Biochimica Et Biophysica Acta, 515*(2), 105-140.

Semple, S. C., Akinc, A., Chen, J., Sandhu, A. P., Mui, B. L., Cho, C. K., . . . Hope, M. J. (2010). Rational design of cationic lipids for siRNA delivery. *Nat Biotechnol, 28*(2), 172-176.

Semple, S. C., Akinc, A., Chen, J. X., Sandhu, A. P., Mui, B. L., Cho, C. K., . . . Hope, M. J. (2010). Rational design of cationic lipids for siRNA delivery. *Nature Biotechnology, 28*(2), 172-U118.

Sessa, G., & Weissmann, G. (1968). Phospholipid spherules (liposomes) as a model for biological membranes. *Journal of Lipid Research, 9*(3), 310-318.

Sharma, A., & Sharma, U. S. (1997). Liposomes in drug delivery: Progress and limitations. *International Journal of Pharmaceutics, 154*(2), 123-140.

Tam, Y., Chen, S., & Cullis, P. (2013). Advances in Lipid Nanoparticles for siRNA Delivery. *Pharmaceutics, 5*(3), 498-507.

Thurmond, R. L., Lindblom, G., & Brown, M. F. (1993). Curvature, Order, and Dynamics of Lipid Hexagonal Phases Studied by Deuterium Nmr-Spectroscopy. *Biochemistry, 32*(20), 5394-5410.

Tsui, F. C., Ojcius, D. M., & Hubbell, W. L. (1986). The intrinsic pKa values for phosphatidylserine and phosphatidylethanolamine in phosphatidylcholine host bilayers. *Biophysical Journal, 49*(2), 459-468.

Wan, C., Allen, T. M., & Cullis, P. R. (2013). Lipid nanoparticle delivery systems for siRNA-based therapeutics. *Drug Delivery and Translational Research*, 1-10.

Yu, B., Lee, R. J., & Lee, L. J. (2009). Chapter 7 - Microfluidic Methods for Production of Liposomes. In D. Nejat (Ed.), *Methods in Enzymology* (Vol. Volume 465, pp. 129-141): Academic Press.